Enhancing CO_2 Mass Transfer in Algal Raceway Ponds through Wave Generation using Slopes

Frans van der Linde

In fulfilment of the requirements for the degree of Master of Science

Supervisors:
Prof Sue Harrison;
Dr Nodumo Zulu

Department of Chemical Engineering
Faculty of Engineering and the Built Environment
University of Cape Town

December 2023

University of Cape Town

The copyright of this thesis vests in the author. No quotation from it or information derived from it is to be published without full acknowledgement of the source. The thesis is to be used for private study or non-commercial research purposes only.

Published by the University of Cape Town (UCT) in terms of the non-exclusive license granted to UCT by the author.

University of Cape Town

Plagiarism Declaration

1. I know the meaning of plagiarism and declare that all the work in the document, save for that which is properly acknowledged, is my own.
2. I have used the Harvard system for citation and referencing. Each significant contribution to, and quotation in, this report from the work, or works, of other people has been attributed, and has been cited and referenced.
3. This thesis/dissertation has been submitted to the Turnitin module

Signed by candidate

Signature

Abstract

Microalgae possess great potential to mitigate the growing energy, environmental and food-related challenges of our time. The large scale cultivation of microalgae is currently mostly done using raceway ponds. These ponds however suffer from low algal productivities compared to closed photobioreactors, in part due to inadequate CO_2 mass transfer into the culture. A previous study at the University of Cape Town explored a method to improve the transfer of atmospheric CO_2 into the pond through surface turbulence created by inserting a sloping structure into the pond. This showed promise as a less energy and resource intensive alternative to CO_2 gas sparging. Depending on the design, the slope can either act like a beach, to mimic the formation of shoaling ocean waves, or act like a weir to create a hydraulic jump. This study aimed to shed light on the effect of different slope parameters on the CO_2 mass transfer rate, hydrodynamics and energy demand of a lab scale raceway pond, and through this improve on the previous slope designs.

For the weir-like slope designs, a 2^{4-1} fractional factorial design of experiments (DOE) was performed to evaluate the effects of the different slope parameters. The DOE considered the upslope angle (25 ° and 54 °), downslope angle (10 ° and 39 °), slope height (9 cm and 10 cm) and paddlewheel rpm (19.8 and 28.9). The measured responses included the fluid hydrodynamics, CO_2 mass transfer rate and energy demand. These responses were also measured for a slope that was designed to create waves similar to shoaling ocean waves. This design had set parameters, selected based on theoretical calculations. The new slope designs were compared to a control without a slope, as well as the previous best performing slope designs. Based on the results of the DOE, three slope configurations were selected and compared to a control in terms of the algal productivity, where *Scenedesmus* sp. was cultivated. To potentially further decrease the energy demand of the raceway, a propeller system was investigated as an alternative to the paddlewheel, since a propeller is thought to be a more energy efficient fluid driving device.

The experiments were performed in an indoor lab scale raceway pond with a 62 L working volume operated at a fluid depth of 12 cm, with no gas sparging. The hydrodynamics were quantified through conductivity tracer experiments and photographic imagery. The CO_2 mass transfer rate was measured using a pH method, which monitored the decrease in the fluid pH as CO_2 transferred into the pond. The CO_2 mass transfer coefficient, k_La, was primarily used to assess the gas mass transfer rate. To quantify the energy demand, theoretical calculations were performed and the actual energy input was measured using a power meter.

With the slope designed to imitate ocean waves it was not possible to create breaking waves, likely due to the dominating effects of surface tension on this small scale. As a result, the k_La was not improved compared to the control. However, the mixing time was decreased by 18 % while the fluid velocity was not altered. The weir-like slopes on the other hand led to an increase in k_La compared to the control due to adequate surface turbulence from the hydraulic jump. The factorial DOE however revealed that this increase was independent on the different slope parameters (in the range of values tested). This meant that variation in the slope parameters could not further improve on the k_La compared to the previous slope designs. The average increase in k_La compared to the control ran at the same rpm was 12 ± 2 % at 19.8 rpm and 16 ± 5 % at 28.9 rpm. In this case, the choice in selecting the ideal slope parameters should therefore be based on the resulting hydrodynamics and energy demand.

Compared to the previous slope designs, when using the same rpm, it was possible to increase the fluid velocity from 6.4 ± 0.1 cm s^{-1} to 10.0 ± 0.3 cm s^{-1} and decrease the mixing from 142 ± 1 s to 112 ± 0 s. This was primarily due to a lower slope height, indicating that it is the most important slope parameter to optimize. The weir-like slopes however led to a considerable increase in the energy demand of the system, which was incorporated in the algal productivity for comparative purposes. The slopes led to an increase in algal productivity of up to 10 % at the same rpm as the control. This increase in algal productivity due to the slope was closely related to the increase in k_La, which suggested that the culture was CO_2 limited. The control however had the highest productivity per unit of theoretical energy requirement (0.67 ± 0.02 g L^{-1} day^{-1} W^{-1} compared to the highest of 0.42 g L^{-1}

day^{-1} W^{-1} achieved with a slope). These results suggested that on this scale a slope might not be required, as a similar effect could be achieved by simply increasing the paddlewheel rpm.

The energy demand of the raceway could further be reduced by using a propeller, which showed a reduction of 56 % in the actual energy input compared to the paddlewheel. The propeller was however not as good of a gas mass transfer device. The k_La measured with the propeller system was 28 % lower compared to the paddlewheel, but the k_La per unit of actual energy input was 58 % higher. The motor for the paddlewheel was however oversized, which contributed to a higher actual energy input for the paddlewheel system. On a larger scale, however, the overall mixing and gas mass transfer in raceway ponds are less dominated by the paddlewheel, meaning that the effects of the propeller, as well as the slopes, could be more significant when scaled up.

These results have shown the need to evaluate the slopes on a larger scale, where additional factors come into play. With the slope that imitates a beach, it could be possible to successfully create breaking waves due to a less dominating effect of surface tension. These slopes can then potentially improve the gas mass transfer without a significant negative effect on the fluid velocity and energy demand. It was also shown that the slopes greatly improved the mixing in the pond, which would play a more important role on a larger scale with the presence of temperature gradients and varying light. The results of this study could be used to guide the design of the slopes for a larger scale. The large scale designs should be compared to a gas sparging system on the same scale, to adequately show that the slopes are a more cost and resource effective alternative to gas sparging.

Acknowledgements

I wish to acknowledge the financial assistance of the South African Research Chairs Initiative (SARChI) towards this research. Any opinions raised or conclusions drawn in this work are those of the author and not necessarily attributed to SARChI.

Furthermore, I am extremely thankful for:

- My supervisors, Prof Sue Harrison and Dr Nodumo Zulu. Thank you for the exceptional insights, motivations, support and commitment.
- The Department of Chemical Engineering's Electronics Workshop along with the Mechanical Workshop for assisting in the construction of equipment.
- The members of the Algae Research Discussion Group, with special thanks to Dr Mariette Smart, Gordon Dodge and Tarryn Terry, for answers to questions, thought provoking discussion and assistance in the lab.
- Laboratory friends who made working in a laboratory far less laborious: James Hockey, Catherine Edward, Gordon Dodge, Tarryn Terry, Elina Chen, Obakeng Jona and Sarah Fernandez.

You are all greatly appreciated!

Table of Contents

List of Figures

List of Tables

Symbols and Acronyms

γ_b	Breaker depth index (-)
λ_∞	Wave steepness (-)
A	Area (m^2)
A_T	Total Alkalinity (mmol L^{-1})
C	Concentration (mol L^{-1})
c_D	Drag coefficient (-)
D	Diffusivity coefficient (m^2 s^{-1})
D_h	Hydraulic diameter (m)
DOE	Design of experiments
DoF	Degrees of Freedom
E	Normalized concentration (-)
F_D	Friction drag (kg m s^{-2})
Fr	Froude number (-)
F_{x1}	First Gran function (-)
g	Gravitational acceleration (m s^{-2})
h	Height (m)
c_H	Henry's law constant (-)
H_c	Concentrated head loss (m)
H_d	Distributed head loss (m)
I_s	Irradiance (µmol m^{-2} s^{-1})
J	Mass transport flux (mol s^{-1} m^{-2})
k	Mass transfer coefficient (m h^{-1})
K	Overall mass transfer coefficient (m h^{-1})
k_b	Bend loss coefficient (-)
k_La	Volumetric mass transfer coefficient (h^{-1})
L	Length (m)
m	Beach slope (-)
p	Productivity (g L^{-1} day^{-1})
P	Power (W)
Pe	Peclet number (-)
Q	Volumetric flow rate (m^3 s^{-1})
Re	Reynolds number (-)
rpm	Rotations per minute
RSS	Residual Sum of Squares
s	Level of submergence (-)
t	Time (s)
v	Fluid velocity (m s^{-1})
V	Volume (m^3)

y	Fluid depth (m)
ΔC	Concentration gradient (mol L^{-1})
ΔH	Head loss (m)
η	Efficiency (%)
θ	Reduced time (-)
μ	Specific growth rate (day^{-1})
ρ	Density (kg m^{-3})
δ	Film thickness (m)
ε	Roughness coefficient (-)
λ	Friction coefficient (-)
ξ	Iribarren number (-)

1 Introduction

1.1 Background and context

Microalgae are unicellular, photosynthetic organisms that show great versatility in their use. Although microalgae have been utilized as a food source for thousands of years, their commercial use in biotechnology is relatively new, dating back to the 1950's and 60's (Blackburn and Volkman, 2012; Hallman, 2007). Microalgae are classified as a renewable and potentially sustainable source of a wide variety of bioproducts (Khan et al., 2018). These products include pigments, pharmaceuticals, nutraceuticals, feeds and biofuels. Numerous pigments can be extracted from algae, such as β-carotene, astaxanthin and phycocyanin (unique to algae) which are used in the medical and food industries (Pulz and Gross, 2004). Due to their high lipid content they are also used as biomass feed for the production of biodiesel and residual biomass can be utilised in anaerobic digestion to create biomethane (Ansari et al., 2017). Certain microalgae can also have a high protein content and contain desired essential fatty acids, which makes for an excellent source of food and feed supplements, for both human and animal consumption (Packer et al., 2016).

There are several advantages that deem microalgal biomass superior to terrestrial crops. For example, it can be cultivated continuously, which allows for constant processing, unlike the seasonal variations associated with terrestrial crop (Packer et al., 2016). Algal productivity can however become lower during winter times with suboptimal cultivation conditions. It can also be cultivated on non-arable land (Ansari et al., 2017) or utilize ocean water, when considering marine species. On top of this there are additional applications of microalgae in conjunction to the production of bioproducts. For example, cultivating microalgae can offer a less energy intensive method of waste water treatment (Oswald, 2003). Here the growth of algae promotes the removal of organic carbon, nitrogen and phosphorus, which are macro nutrients for algae. Microalgae also facilitate the biosorption of heavy metals (such as gold, copper, nickel and lead), where the metals can either adsorb onto the surface of the cells or absorb into intracellular ligands (Mehta and Gaur, 2005). Since microalgae also utilise CO_2 through photosynthesis it allows for application in CO_2 sequestering, either from the atmosphere or from flue gas produced from industrial processes (Klinthong et al., 2015).

With microalgae being fairly new in their commercial use, there is still much room for development and improvement in the field (Pulz and Gross, 2004). The commercial production of numerous bioproducts from microalgae is often hindered by low economic feasibility compared to other feedstocks. A prime example of this is the biofuels industry, where the commercialization of biodiesel from microalgae has not yet been fully realized due to the high costs associated with the production process (Borowitzka, 2013). In general, large scale cultivation is seen as one of the bottlenecks in the overall production process due to low areal productivities in combination with the low biomass concentrations achieved (Gifuni et al., 2019; Zhang et al., 2016). This is in reference to raceway ponds, which are currently the most viable method for the large scale production of microalgae, and are utilized by the strong majority of commercial production facilities (Grobbelaar, 2012; Kumar et al., 2015). Their frequent use stems from their scalability, relatively low energy demand and ease of operation (Ansari et al., 2017).

The primary factors contributing to the lower productivities in raceway ponds are poor gas exchange between the fluid and the atmosphere as well as limitations on light penetration and mixing inside the pond (Benedetti et al., 2018; Molina-Grima, 1999). For raceways, CO_2 mass transfer from the atmosphere through the surface of the pond is typically not sufficient by itself to maintain the desired growth rates (Chisti, 2016). Sparging CO_2 into the system is a method often used to enhance the CO_2 mass transfer rate and has proven to increase algal productivities (Mendoza et al., 2013b; Putt et al., 2011; Zheng et al., 2018). The disadvantage of this approach in raceway ponds, however, is the low bubble retention time due to the shallow depth of the ponds (Kumar et al., 2015). The loss of CO_2 is undesired, as the costs can be considerable. A techno-economic assessment by the National Renewable Energy Laboratory (Davis et al., 2016) attributed the cost of CO_2 to roughly 63 % of the

variable operating costs of an algae production plant (roughly 20 km^2 of cultivation area in raceway ponds). Flue gas has been shown to be an effective alternative to CO_2, although its use is dependent on the gas composition (in terms of CO_2 as well as contaminant concentration) and puts a limitation on where algal farms can be constructed (de Godos et al., 2014; Mendoza et al., 2013b).

This study explored a method to enhance the CO_2 mass transfer into a raceway without relying on gas sparging, potentially providing a more cost effective approach. This approach seeks to create surface turbulence in the form of waves and draws inspiration from nature. In the ocean, shoaling waves on a beach greatly enhances gas-liquid mass transfer by creating turbulence at the ocean surface accompanied by air entrainment (Melville, 1996). Surface waves are also present in rivers and streams in the form of a hydraulic jump, which can be created by a weir or an obstacle in the field of flow. These waves can be replicated in a raceway by adding a slope to the channel which could either imitate a beach or act like a weir to create a hydraulic jump. Using a slope to create surface turbulence in raceway ponds is not presented in published literature. Previous work at the University of Cape Town (Burke, 2016) has however shown the potential of using this method. Burke (2016) evaluated a number of slope designs with varying lengths and heights that showed significant improvement in the mixing and gas-liquid mass transfer in the raceway pond. However, the study does not address the relative importance of the different slope parameters. Further, the slopes did not properly mimic shoaling ocean waves as originally intended. This study aimed to build on the work performed by Burke (2016) to improve on the slope designs and demonstrate the value of these improvements on the cultivation of microalgae.

1.2 Scope and constraints

In this study, two different approaches to surface wave formation in a raceway pond were evaluated: using a slope to imitate a beach and create shoaling ocean breakers and using a weir-like slope to create a hydraulic jump. The slope designs of Burke (2016) fall within the latter approach. The main focus of this work was on the weir-like slope designs. This study builds on the work of Burke (2016) by getting a better understanding of how the different slope parameters affect the hydrodynamics, CO_2 mass transfer rate, energy demand and resulting algal productivity and through this improve on the slope designs. This was done by performing a fractional factorial design of experiments (DOE) which evaluated four different factors: the upslope angle, the downslope angle, the slope height and the paddlewheel rpm. The responses monitored in the DOE were the hydrodynamics, CO_2 mass transfer rate, energy demand and CO_2 mass transfer per unit of energy required. The hydrodynamics under investigation were the fluid velocity, mixing time, the Peclet number, the size of the recirculation zone after the slope and the height of the surface wave created. The abovementioned variables were quantified through experimental work and the results were compared to the best performing designs of Burke (2016) and a control without any slope.

The experiments were performed using a lab scale raceway pond (with a working volume of 62 L) identical to the raceway used by Burke (2016). While scale-up for these small scale studies were not within scope, the potential implications on a larger scale raceway are discussed. The results of Burke (2016) were used as an additional guide in designing the new slopes. Based on the results of the DOE, with regards to the energy input, hydrodynamics and gas-liquid mass transfer, three different slope configurations were chosen and compared to a control without any slope in terms of the algal productivity. Due to the increase in energy demand brought about by adding a slope into the raceway channel, a propeller was also investigated as a more energy efficient fluid driving device compared to a paddlewheel, which is typically used in raceway ponds. Its impact was considered in terms of the energy input, hydrodynamics and gas-liquid mass transfer. Cultivation experiments were not performed using the propeller system due to the small motor of the propeller. The motor overheated easily and was not fit to operate continuously for days on end, as is required for cultivation experiments.

1.3 Structure of thesis

A literature review was conducted to obtain a better understanding of both the raceway pond and how the slopes could improve the CO_2 mass transfer rate. The review is presented in Chapter 2, and covers topics related to photosynthesis and CO_2 assimilation (Section 2.1.1), algal productivity (Section 2.1.2), , the limitations of raceway ponds (Section 2.1.3), theory of gas mass transfer (Section 2.2), shoaling waves in the ocean (Section 2.3), lab scale wave formation (Section 2.4.1), the work performed by Burke (2016) (Section 2.4.2), hydraulic jumps (Section 2.4.3), other internal structures used in raceway ponds (Section 2.5) and alternative fluid driving systems (Section 2.6). Based on the review of the literature, two hypotheses were formulated along with key questions that needed to be addressed to test the hypotheses. These are presented in Section 2.8.

Chapter 3 covers the approach to the experimental work. This section details the experiments that were performed, the equipment used as well as the methods and analytical approaches followed to obtain all the necessary data to answer the key questions.

Chapter 4 centres on the results and discussion, which are presented together. This chapter starts with the results of the previous slope designs (Section 4.1), followed by the slope designed to create breaking ocean waves (Section 4.2), the factorial DOE for the weir-like slopes (Section 4.3), algal cultivation experiments (Section 4.4), the propeller system (Section 4.5) and finally, considerations for scale-up (Section 4.6). Chapter 5 contains the conclusions based on the results and provides recommendations for future work.

2 Literature Review

2.1 Microalgae Cultivation

For successful cultivation, microalgae require a few basic necessities. Algae are typically photo autotrophs, meaning they use light to carry out photosynthesis, whereby carbon is fixed from CO_2. The transfer of CO_2 to the algal cell is primarily governed by gas-liquid mass transfer. Additionally, for optimum growth sufficient nutrients are required along with ideal temperatures. When cultures are at their optimum temperature, light utilization is enhanced and they are less likely to become photoinhibited (discussed in further detail in Section 2.1.3) (Borowitzka and Moheimani, 2013).

2.1.1 Photosynthesis and CO_2 assimilation

Photosynthesis is a biochemical reaction that occurs in the chloroplasts of algal cells. Light is used as an energy source to convert CO_2 and water into carbohydrates, releasing oxygen and excess heat as by-products (Masojídek et al., 2021):

$$CO_2 + 2H_2O + Photons \rightarrow [CH_2O] + H_2O + O_2 + Waste\ Heat \quad \text{Equation 2-1}$$

The process involves two subsequent phases: the light reactions and dark reactions (Simon et al., 2019). The light reactions are responsible for converting light energy into chemical energy in the form of adenosine triphosphate (ATP) and also supply the chemical reductant $NADPH_2$. The chemical energy is then used in the dark reactions (also known as the Calvin-Benson cycle) to fix CO_2 into organic molecules.

The conversion of light energy relies on two pigment-protein systems located on the thylakoid membranes inside the chloroplasts (Janssen, 2016). These systems are known as Photosystem II, involved in the generation of ATP, and Photosystem I, involved in the generation of $NADPH_2$. Light energy is captured by Photosystem II and energizes electrons in pigment molecules (of which the chlorophylls are the most abundant) (Masojídek et al., 2021). The energized electrons then enter an electron transport chain where carrier molecules transfer the electrons to Photosystem I. With each transfer between molecules, the electrons enter a lower energy state and release small amounts of energy (and heat) (Simon et al., 2019). This energy is ultimately used to produce ATP. Absorbed light energy in Photosystem II is also used to split H_2O molecules into electrons, protons and O_2 (released as by-product) (Janssen, 2016). The electrons from this reaction are used to replace those originally lost by the pigment molecules. The release of protons establishes a proton gradient across the thylakoid membrane. The flow of protons across the membrane (and through ATP synthase) is responsible for the production of ATP from adenosine diphosphate and phosphate molecules (Simon et al., 2019). In Photosystem I, similar to Photosystem II, light energy is absorbed and excites electrons in pigment molecules. The electrons then enter an electron transport chain, and the electrons from Photosystem II replace the electrons lost by the pigment molecules. $NADP^+$ is the final electron acceptor, and gets reduced to $NADPH_2$ (Simon et al., 2019).

The Calvin-Benson cycle involves four distinct steps, and the overall reaction is depicted as follows (Masojídek et al., 2021):

$$CO_2 + 4H^+ + 4e^- \xrightarrow{2NADPH_2+3ATP} [CH_2O] + H_2O \quad \text{Equation 2-2}$$

The initial step in the cycle is a carboxylation reaction, where CO_2 is attached to ribulose bisphosphate (Masojídek et al., 2021). This reaction is catalysed by the enzyme ribulose bisphosphate carboxylase/oxygenase (Rubisco). Rubisco has a low affinity to CO_2, which possibly stems from the relatively high atmospheric CO_2 concentrations when it first evolved (Moroney and

Somanchi, 1999). In response to the changing environment, microalgae developed methods to enhance Rubisco activity, such as the carbon-concentration-mechanism (Moroney and Somanchi, 1999; Wang et al., 2015).

Carbon-concentration-mechanism

The carbon-concentration-mechanism (CCM) refers to the adaptation that microalgae have evolved to survive in a CO_2 limited environment (Price et al., 2008). The function of the CCM is to accumulate inorganic carbon near the site of Rubisco to improve photosynthetic efficiency (Moroney and Somanchi, 1999; Wang et al., 2015). The CCM relies on numerous inorganic carbon uptake systems, which allows for both the uptake of CO_2 and HCO_3^- from the environment (Price et al., 2008; Wang et al., 2015). Internally, however, HCO_3^- is the preferred form of inorganic carbon due to the greater permeability of CO_2 through lipid membranes (which can result in leakage and loss of CO_2) (Price et al., 2008). Internal CO_2 is therefore converted into HCO_3^- through a carbonic anhydrase (Wang et al., 2015).

However, CO_2 (as opposed to HCO_3^-) is required in the Calvin cycle, where Rubisco catalyses the carboxylation reaction of ribulose bisphosphate (Masojídek et al., 2021). Another carbonic anhydrase therefore converts internal HCO_3^- back into CO_2 at the sites where Rubisco is concentrated (Moroney and Somanchi, 1999). The conversion of HCO_3^- into CO_2 leads to OH^- in the algal cells, which needs to be neutralized by the uptake of H^+ from the environment (Chi et al., 2011). This uptake of H^+ ultimately results in an overall increase in the pH of the environment during photosynthesis. During algal cultivation, CO_2 is typically supplied to improve the algal productivity and control the pH of the environment (Chisti, 2016).

2.1.2 Factors Affecting Productivity

The objective of the large scale production of algae is to maximise the amount of algal biomass (or a specific product) over a minimal period of time (Grobbelaar, 2012), which can be quantified with the algal productivity. The productivity can be defined as the product of the biomass concentration (C) and the specific growth rate (μ) (Borowitzka and Moheimani, 2013; Griffiths and Harrison, 2009):

$$p = \mu C \qquad \text{Equation 2-3}$$

There are many factors that affect algal productivity, some being interlinked and convoluted. Figure 2-1 illustrates a simplified diagram showing the relations.

The specific growth rate is affected by the cultivation temperature, gas-liquid mass transfer and light (Fernandez et al., 2012). The latter can be divided into the light regime and profile. The light regime refers to the time cells spend in light and dark zones as well as the frequency at which they move between them (Fernandez et al., 2012). Increased growth rates are accompanied by an increase in the biomass concentration. This in turn affects the light profile by decreasing the depth to which the light penetrates. Furthermore, the light regime is affected by the fluid dynamics, which also influences the gas mass transfer and temperature profile. Mixing and turbulence effects the time the cells spend in the light and dark zones, removes gradients in the temperature or concentration of the media and improves gas mass transfer (Borowitzka and Moheimani, 2013; Molina-Grima, 1999). Gas-liquid mass transfer plays a role in supplying sufficient quantities of CO_2 to the culture but also removes O_2. Photosynthesis leads to an increased concentration of O_2 in the culture. This can result in photorespiration, which inhibits photosynthesis and significantly reduces algal productivity (Borowitzka and Moheimani, 2013). The interactions between these factors are present in all phototrophic cultivation systems although different reactor designs have different limitations with respect to each factor.

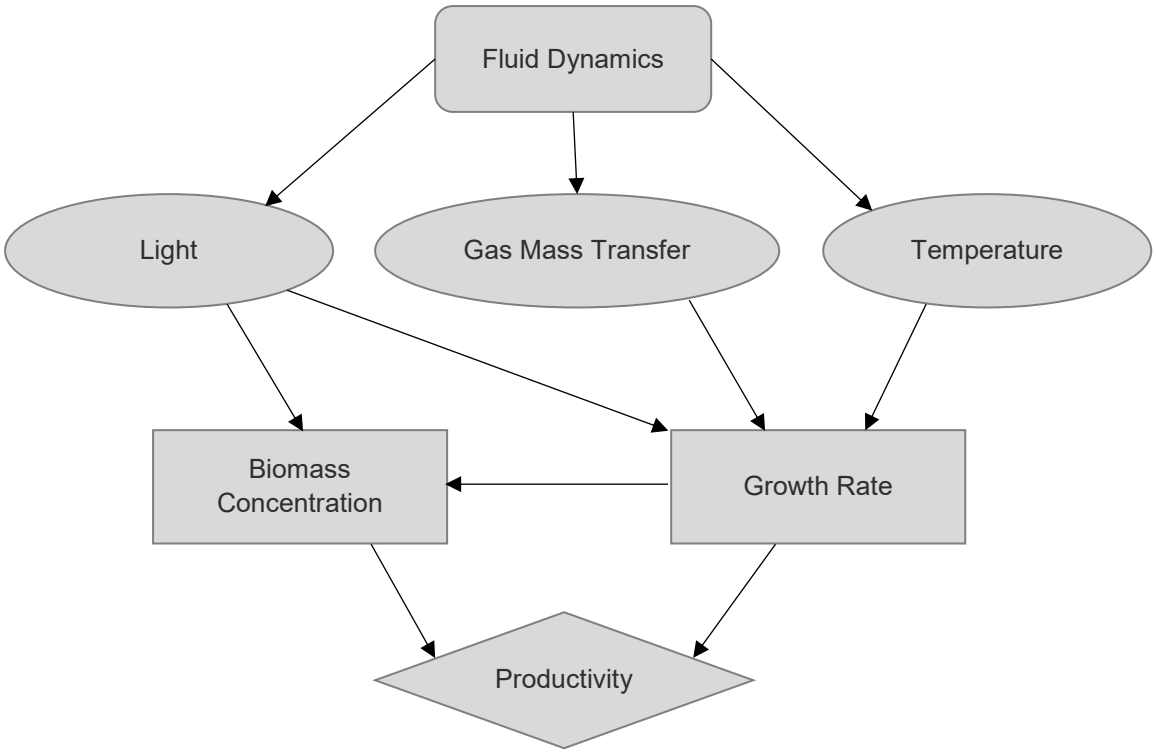

Figure 2-1: Simplified diagram of the factors affecting algal productivity. Adapted from Molina-Grima (1999)

2.1.3 The Raceway Pond and its Limitations

There are numerous ways in which microalgae can be cultivated, the primary methods being open ponds and closed photobioreactors. Open ponds operate at low cell densities but have large volumes, while closed photobioreactors offer a more controlled system with a reduced volume, but can achieve higher algal concentrations (Molina-Grima, 1999). Raceway ponds are known to achieve comparatively low algal productivities due to limitations regarding light penetration, gas mass transfer, and mixing.

Raceway ponds are usually elliptical in shape with a baffle in the centre allowing for the fluid to be recirculated in a closed loop using a paddlewheel (Chisti, 2016). Ponds typically operate at a depth of 15-30 cm (Ansari et al., 2017; Benedetti et al., 2018; Chisti, 2016). This shallow depth is required to alleviate the limitation of light penetration inside the pond. A decrease in pond depth however decreases the aerial productivity of the pond. Due to the shallow configuration, scale-up of the ponds are done by increasing its area (Kumar et al., 2015), often in a modular fashion. Raceways therefore typically stretch over large areas, but they will rarely be larger than 5000 m^2 (1000 - 1500 m^3) (Chisti, 2016). In general, average fluid velocities range between 15 and 30 cm s^{-1} (Chiaramonti et al., 2013; Hreiz et al., 2014; Molina-Grima, 1999), as velocities lower than 10 cm s^{-1} could lead to algal sedimentation (Becker, 1994; Dodd, 1986). The degree of sedimentation is however species dependent due to varying morphologies of the algae (some species have flagella, as an example, meaning the algae can stay afloat even at very low fluid velocities). A minimum velocity of 10 cm s^{-1} is a good guideline although some researchers go as far as using this velocity as a threshold to identify dead zones in raceway ponds (Hadiyanto et al., 2013; Huang et al., 2015; Sompech et al., 2012).

Long term productivities obtained in raceways are generally lower than 20 g m^{-2} day^{-1} (Benedetti et al., 2018; López et al., 2019; Olaizola, 2000), with Chisti (2016) stating that an average annual productivity of 25 g m^{-2} day^{-1} is achievable for well operated systems. These numbers are about ten times less than the productivities achievable in closed photobioreactors (Benedetti et al., 2018). As

mentioned, the lower algal productivities are primarily due to limitations on light penetration, poor gas exchange between the fluid and the atmosphere and mixing inside the pond (Benedetti et al., 2018; Molina-Grima, 1999). On top of this, paddlewheels have been reported to have low efficiencies (Chiaramonti et al., 2013), with respect to how effective the rotational motor shaft energy is transformed into the fluid. This opens up the possibility to improve the energy demand of the system with a more energy efficient fluid driving device. These limitations observed with raceway ponds are discussed in more detail below.

Paddlewheels

Paddlewheels are the most used propulsion device in raceway ponds (Becker, 1994). Their suitability for raceways stems from the ability to drive large volumes of fluid at the low head difference requirements in the pond (Musgrave, 2017). Additional advantages include low shear flow, which does not damage algae, as well as its mechanical simplicity (Musgrave, 2017).

Chiaramonti et al. (2013) reported a paddlewheel efficiency of 10 % for their setup, while Borowitzka (2005) reported typical efficiencies of 17 %. Many design factors affect the efficiency of the paddlewheel, including the rotational speed, radius of the paddlewheel, difference in head across the paddlewheel, the number of blades and clearance between the blades and channel wall (Chiaramonti et al., 2013; Li et al., 2014; Musgrave, 2017). Increasing the difference in head across the paddlewheel results in more backflow which ultimately reduces the paddlewheel efficiency (Musgrave, 2017). To relieve these effects, one blade should be immersed in the fluid at all times. Eight bladed paddlewheels are therefore preferred (Borowitzka and Moheimani, 2013). Naturally the clearance between the blades and channel wall could increase the reverse flow and should be kept at a minimum. Due to the multitude of factors that affect the paddlewheel efficiency, it is a complex parameter to determine (Chiaramonti et al., 2013).

The efficiency of the paddlewheel is typically estimated from knowledge on the theoretical energy requirements, the actual energy input and the efficiency of all other components in the fluid driving system (Chiaramonti et al., 2013). From the theoretical energy requirements (P_{Theo}) and actual energy input (P_{Act}), the overall efficiency can be determined (Equation 2-4). The overall efficiency is also the product of the efficiencies of all the components in the drive system (Equation 2-5) (Chiaramonti et al., 2013). In Equation 2-5 an example is given of a drive system consisting of a motor (η_e), worm drive (η_{t1}), timing belt (η_{t2}) and paddlewheel (η_{pw}). With knowledge of the actual energy input, theoretical energy demand and the efficiency of all other components in the drive system, the paddlewheel efficiency can be determined.

$$\eta_{tot} = \frac{P_{Theo}}{P_{Act}} \qquad \text{Equation 2-4}$$

$$\eta_{tot} = \prod_{i=1}^{n} \eta_i = \eta_e \cdot \eta_{t1} \cdot \eta_{t2} \cdot \eta_{pw} \qquad \text{Equation 2-5}$$

Light Penetration in Raceway Ponds

The density of the culture affects the depth at which the light penetrates, with a rapid decline in irradiance as the depth of the culture increases (Chisti, 2016). Photosynthesis is highly dependent on light, although optimal performance can be limited by both excessive or inadequate levels thereof (Carvalho et al., 2011). In raceway ponds only the surface of the pond is illuminated, resulting in a photic zone. The majority of photons from the sun are absorbed by algae that reside in the photic zone, leading to a phenomenon known as mutual shading (Lee, 2016). Cells in the bottom of the pond are photolimited and, in a stratified pond, will consume themselves through respiration (Chisti, 2016). During peak hours on sunlight however, high irradiance levels can lead to photo-inhibition of the cells at the surface (Borowitzka and Moheimani, 2013). Photo-inhibition is the decrease in the rate of photosynthesis due to excessive levels of irradiance (Masojidek et al., 2004). Photosynthesis

saturates once a tolerable photon flux is achieved in the pond (Gordon and Polle, 2007). A plot of the photosynthetic rate against the irradiance therefore results in three distinct regions (Carvalho et al., 2011), illustrated in Figure 2-2.

The photosynthetic rate will saturate at a certain irradiance, I_s. This amount varies between 200 – 400 µmol m^{-2} s^{-1} (Carvalho et al., 2011; Grobbelaar, 2009). Below this value, the photosynthetic rate increases linearly with increasing irradiance and becomes less efficient until it reaches saturation. At an irradiance of I_h the algae will become photo-inhibited, corresponding to a decrease in the rate of photosynthesis. The irradiance at which this happens is species dependent (Borowitzka and Moheimani, 2013).

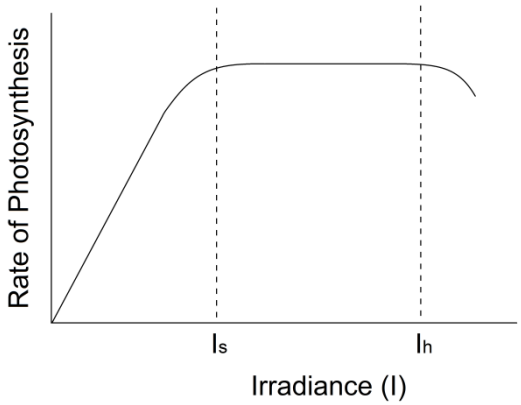

Figure 2-2: Photosynthetic rate as a function of irradiance, showing a point where the rate becomes saturated (I_s) before decreasing due to photo-inhibition at an irradiance above I_h

The saturation level of 200 – 400 µmol m^{-2} s^{-1} is however not an absolute limit (Carvalho et al., 2011). Instantaneous photon flux values of 2000 – 5000 µmol m^{-2} s^{-1} without saturation have been demonstrated (Gordon and Polle, 2007). This is achievable through the flashing light effect, where a pulse of high irradiance light is flashed at a high frequency. When correctly executed, the flashing light effect can result in increased algal productivity (Grobbelaar et al., 1996 as found in Abu-Ghosh et al., 2016). This effect however is mainly introduced using LED's that create ligh/dark cycles of very high frequencies ranging between 10 and 100 Hz (Abu-Ghosh et al., 2016). Potential applications of this effect in raceways are further discussed in Section 2.4.4. The importance of vertical mixing however is clear: algae needs to be transported between the dark zones and the photic zones as to prevent photo-inhibition or photolimitation.

Mixing and Gas Mass Transfer in Raceway Ponds

Mixing in raceway ponds is typically limited by laminar flow and the occurrence of dead zones (Grobbelaar, 2012). Dead zones reduce fluid mixing, promote algal sedimentation and increase energy losses (Chisti, 2013). These zones can occur at the inner channel walls after the bends as a result of flow separation (Chisti, 2013; Liffman et al., 2013). Flow separation can be defined as the phenomena where the boundary layer (the layer of liquid in contact with a surface) separates from the surface due to an adverse pressure gradient (Cengel and Cimbala, 2014; White, 2015). Vane baffles (or flow deflectors) can be installed in the bends, which promote the uniformity of the flow and alleviate the dead zones (Chisti, 2013). Alternatively, the raceway geometry can be altered to fill in the dead zones with the side walls (Chisti, 2013; Sompech et al., 2012). Increasing the channel length could also decrease the volume ratio of the dead zones (Hadiyanto et al., 2013).

Vertical mixing in raceways is very limited, although secondary flow does occur. At the bends, fluid is driven towards the outer wall through a centrifugal force creating a tilt in the water surface. This however brings about a pressure gradient along the cross section of the channel, pushing the fluid towards the inner wall. These two opposing forces drive the formation of secondary flow, also known

as flow of Prandtl's first kind (Bai et al., 2019). Secondary flow of Prandtl's second kind occurs in straight channels and arises due to turbulence (Yang et al., 2012). Mixing in the straight channels is however far less dominant than the mixing around the bends (Leman et al., 2018). The primary mixing occurs at the paddlewheel and areas of greater mixing bring about enhanced gas mass transfer. Mixing and mass transfer also naturally increase with an increase in fluid velocity, although this is at the expense of an increased energy demand (Mendoza et al., 2013b).

To achieve high productivities in raceway ponds, CO_2 gas needs to be supplied to improve the gas-liquid mass transfer rate (Chisti, 2013). Introducing CO_2 into the raceway is a challenge, as the bubbles have a very low residence time due to the shallow nature of the ponds. Different strategies to introduce the CO_2 into the culture are therefore utilized. A common method is to use a sump in the raceway channel, which increases the gas-liquid contact time (de Godos et al., 2014; Mendoza et al., 2013b; Musgrove and Heaven, 2014). Weissman et al. (1989) reported on CO_2 transfer efficiencies between 32 and 65 % for a carbonation sump with a centre baffle, which allowed for counter current injection of the gas. This meant that up to 68 % of the CO_2 was lost to the atmosphere. The low transfer efficiencies were however attributed to low algal productivities during winter months and is additionally dependent on the pH (Weissman et al., 1989). The sump naturally also increases the energy demand of the system by contributing to the head loss throughout the raceway, which was up to 25 % of the total head loss (Weissman et al., 1989). A more recent study by de Godos et al. (2014) showed that, with an optimized system, the CO_2 lost to the atmosphere can be as little as 6 %, although only 66 % of the CO_2 was utilized by the algae. The remaining dissolved inorganic carbon was present in the harvested stream.

Another approach that has been explored is the use of an external carbonation column, which led to CO_2 transfer efficiencies up to 83 %, far higher than the 37 % reported for the control with sparging directly into the straight channel (Putt et al., 2011). The additional energy associated with the pumping requirements was however not investigated. A possible method to further increase the CO_2 transfer efficiency is to utilize microbubbles, as this increases the residence time and surface area, although this is at the expense of an increase in the energy demand (Zheng et al., 2018). CO_2 injection remains a significant portion of the overall operating costs of the production process. In general, there is very little focus on improving the CO_2 mass transfer through non-sparging methods.

2.2 Theory of Gas/Liquid Mass Transfer

A number of models exist which describe gas-liquid mass transfer. The most commonly used and well documented theory is the two-film theory (Clarke, 2013), which will therefore be discussed in this text. While recognised to not be an exact description of the process, it provides a robust prediction of mass transfer. The transportation of a soluble gas into a fluid is visualised in Figure 2-3. According to the two-film theory, the gas travels across a stagnant gaseous film before crossing the gas/liquid interface followed by traversing a stagnant liquid film. It is assumed that the bulk fluids are well mixed and that all the resistance to the mass transfer resides in the stagnant films, meaning there is also no resistance to the transfer through the gas-liquid interface itself (Clarke, 2013).

Gas mass transfer through the stagnant films is governed by molecular diffusion, based on Fick's Law, which describes the molar flux of gas per unit area (J) as follows (Chisti, 2007; Clarke, 2013):

$$J = \frac{D}{\delta}\Delta C \qquad \text{Equation 2-6}$$

where D is the diffusivity coefficient of the gas, δ is the thickness of the film and ΔC the concentration gradient of the gas across the film. $\frac{D}{\delta}$ is related to the inverse of the resistance to diffusion and is known as the mass transfer coefficient, k (Chisti, 2007).

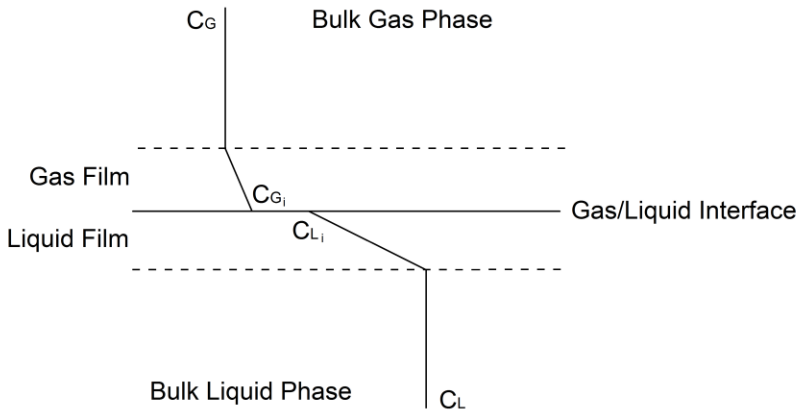

Figure 2-3: Gas mass transfer across the stagnant gas and liquid film on either side of the interface. Redrawn from Chisti (2007).

At steady-state the molar flux is the same through both stagnant films, meaning Equation 2-6 can be written for both the stagnant liquid film and the stagnant gas films as follows (Chisti, 2007; Richardson et al., 2002):

$$J = k_G\left(C_G - C_{G_i}\right) = k_L(C_{L_i} - C_L) \qquad \text{Equation 2-7}$$

Here k_G and k_L are the mass transfer coefficients for the gas and liquid films, respectively. Due to a gas having a high diffusivity in the gas phase and low solubility in the liquid phase, the liquid film dominates the resistance to mass transfer and the transfer through the liquid film becomes the rate controlling step (Clarke, 2013). The overall mass transfer can then be described as (Chisti, 2007):

$$J = K_L(C^{sat} - C_L) \qquad \text{Equation 2-8}$$

where K_L is the overall mass transfer coefficient and C^{sat} refers to the concentration of the gas in the liquid at the interface that would be in equilibrium with the gas in the stagnant gas film, in other words: the highest possible concentration. C^{sat} is related to C_G through Henry's Law (Clarke, 2013):

$$C_G = c_H C^{sat} \qquad \text{Equation 2-9}$$

where c_H is the Henry's constant, a dimensionless number that is specific to each compound and dependent on temperature (Chisti, 2007). K_L in actuality relates to both the individual mass transfer coefficients as follows (Chisti, 2007):

$$\frac{1}{K_L} = \frac{1}{k_L} + \frac{1}{c_H k_G} \qquad \text{Equation 2-10}$$

Since the liquid film resistance is the rate limiting step, the contribution of the gas phase resistance is therefore taken as being negligible and $K_L = k_L$.

The mass transport flux (J) is per unit of gas/liquid interfacial area, which is often difficult to measure (Clarke, 2013). Equation 2-8 can be rewritten as a transfer rate, in which k_L and α_L (the gas-liquid interfacial area per unit volume of the liquid) are lumped together:

$$\frac{dC_L}{dt} = k_L a_L (C^{sat} - C_L)$$ Equation 2-11

$k_L a_L$ is known as the overall volumetric mass transfer coefficient and for simplicity is referred to as the mass transfer coefficient or $k_L a$, throughout this text. $k_L a$ is dependent on the fluid properties and hydrodynamics of the flow. Enhancing fluid turbulence can decrease the resistance to mass transfer (through a decrease in the film thickness) and increase the interfacial area, thereby increasing $k_L a$ (Clarke, 2013). The fluid properties that influence $k_L a$ include the temperature, ionic strength, viscosity and surface tension (Chisti, 2007). Increasing temperature decreases the solubility of a gas in a liquid but increases its diffusivity (Elhajj et al., 2014). An increased diffusivity increases $k_L a$. Other fluid properties can affect bubble stability and reduce bubble coalescence, such as salinity or surface tension (Rivas-Interián et al., 2019). Small bubbles that do not coalesce are favourable as this increases the interfacial surface area and thus increases $k_L a$. These effects are less applicable to a raceway pond without gas sparging, since bubble formation is very limited. Increasing the liquid viscosity and surface tension regardless affect $k_L a$ adversely when considering mass transfer through the free surface only (Bin, 1984; Scargiali et al., 2013).

The second component affecting the overall mass transfer is the driving force, $(C^{sat} - C_L)$. The driving force for mass transfer reflects the tendency of the concentration difference between the gas and liquid phase to reach equilibrium (de Godos et al., 2014). The driving force is dependent on the solubility of the gas in the liquid, which is a function of its partial pressure in the gas phase as well as the temperature (Clarke, 2013).

Typically the $k_L a$ for CO_2 is determined by measuring the $k_L a$ for O_2 (through the dynamic gassing out method) and applying a correction factor based on the difference in diffusivity (Clarke, 2013). This method does not capture the complex reactions that gaseous CO_2 undergoes as it dissolves into water. The dissolution of CO_2 into water involves the following reactions:

$$CO_{2\,(g)} \leftrightarrow CO_{2\,(aq)}$$ Equation 2-12

$$CO_{2\,(aq)} + H_2O \leftrightarrow H_2CO_3$$ Equation 2-13

$$H_2CO_3 \leftrightarrow H^+ + HCO_3^-$$ Equation 2-14

$$HCO_3^- \leftrightarrow H^+ + CO_3^{2-}$$ Equation 2-15

Aqueous $CO_{2(aq)}$ and H_2CO_3 are chemically inseparable and cannot be differentiated from another (Zeebe and Wolf-Gladrow, 2001). These two species are therefore often lumped together into a single term, designated as CO_2^* from here on out. The above equilibrium reactions can be portrayed using the equilibrium constants in the following equations (Millero, 1995; Zeebe and Wolf-Gladrow, 2001):

$$K_0 = \frac{CO_2^*}{p_{CO2}}$$ Equation 2-16

$$K_1 = \frac{H^+ \cdot HCO_3^-}{CO_2^*}$$ Equation 2-17

$$K_2 = \frac{H^+ \cdot CO_3^-}{HCO_3^-}$$ Equation 2-18

$$K_w = OH^- \cdot H^+$$ Equation 2-19

Where Equation 2-16 describes the equilibrium between gaseous CO_2 and CO_2^* and Equation 2-19 describes the self-ionisation of water. The equilibrium constants are a function of temperature and salinity and are described through empirical equations (Millero, 1995) (https://figshare.com/s/00ec7e5192c6be962de8, Raceway 2).

A method to directly measure the k_La of CO_2 was developed by Burke (2016) which relies on measurement of the alkalinity and change in pH of the liquid. Rewriting Equation 2-11 for CO_2:

$$\frac{dC_T}{dt} = k_L a(CO_2^{sat} - CO_2^*) \quad \text{Equation 2-20}$$

Here CO_2^{sat} refers to the concentration of the CO_2 in equilibrium with the gaseous CO_2 in the atmosphere. CO_2^{sat} is determined through Equation 2-16, using a calculated equilibrium constant and the known partial pressure of CO_2 in the atmosphere.

The total inorganic carbon concentration (C_T) consists of the sum of all carbon species present: CO_2^*, HCO_3^- and CO_3^-. To quantify these concentrations, knowledge on the total alkalinity and change in pH of the fluid is required. At each time point the concentrations are simultaneously solved through use of the CO_2 equilibrium reactions (Equation 2-17 to Equation 2-19), pH data and the total alkalinity (A_T) described in Equation 2-21 (Zeebe and Wolf-Gladrow, 2001).

$$A_T = HCO_3^- + 2CO_3^- + OH^- - H^+ \quad \text{Equation 2-21}$$

dC_T/dt then corresponds to the slope of a graph describing the change in C_T over time. To determine the k_La for CO_2, dC_T/dt is divided by the mass transfer driving force.

The tactic of sparging CO_2 into a raceway focusses on increasing k_La by increasing the interfacial surface area through bubble formation and increasing the driving force by supplying a high partial pressure of CO_2 in the gas phase. Without sparging, the CO_2 mass transfer through the surface of a raceway pond is restricted by the lack of turbulence, vertical mixing and air entrainment. In the case of raceway ponds, the little vertical mixing in the straight channel sections could naturally lead to a CO_2 concentration gradient along the depth of the channel. Vertical mixing could therefore enhance the mass transfer driving force by replenishing the fluid close to the interface with 'fresh' fluid of a lower CO_2 concentration. Surface turbulence could then further enhance mass transfer by increasing k_La through a decrease in the liquid film thickness. An example of extreme surface turbulence can be found in the ocean, where breaking waves significantly increase gas-liquid mass transfer through not only surface turbulence but also air entrainment.

2.3 Ocean Waves and Air-Sea Interaction

The ocean and atmosphere are connected through mass, heat and momentum transfer (Veron et al., 2009). The transfer of gases across this coupling is an important aspect of numerous processes such as the carbon cycle and marine photosynthesis (Csanady, 2001). The resistance to diffusion of gas particles mainly resides in the water layer. This is because of the low solubility of many gasses in the ocean (Csanady, 2001). Breaking ocean waves enhance the turbulence in the surface layer of water and are therefore an important aspect in promoting the gas mass transfer, as it enhances the surface renewal, air entrainment and affects the liquid film thickness across which the mass transfer occurs.

2.3.1 The Breaking of Ocean Waves

Considering an ideal case with calm water, particles in ocean waves experience circular motions, as depicted in Figure 2-4. At the surface of the wave the diameter of the orbital corresponds to the wave height (Russell and MacMillan, 1954). This diameter decreases along the depth of the water until it completely dissipates. In the ocean, the depth at which the particles do not experience any motion related to the wave corresponds to roughly one wave length (Russell and MacMillan, 1954).

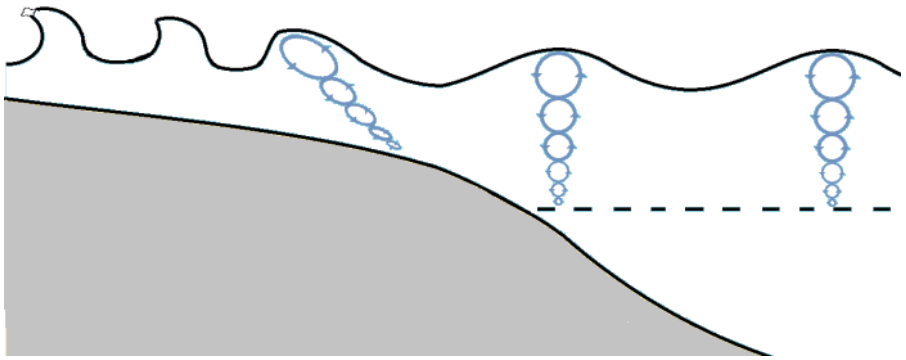

Figure 2-4: The circular motion of particles in the ocean as waves pass through them. A sloping beach causes waves to break as they increase in steepness and destabilize. Redrawn from Webb (2019)

As the wave approaches a sloping beach the surface of the beach affects the wave through friction: the height of the wave increases while the wavelength gets shorter. This increases the wave steepness (defined as the wave height divided by the wave length), which results in a less stable wave that ultimately topples over (Bascom, 1980). Waves break at a certain depth along the sloping beach. The breaker depth index (γ_b) is defined as the height of the wave at breaking divided by the depth at which it breaks (Battjes, 1974; Chella et al., 2015):

$$\gamma_b = \frac{H_b}{d_b} \quad \text{Equation 2-22}$$

Equation 2-22 can be used to give an estimate of the depth at which a wave will break on a slope. Calculation of the breaker depth index is usually done through empirical studies. Several formulas have been proposed (Battjes, 1974; Kraus et al., 1990; Weggel, 2015) and a general consensus is that γ_b is primarily dependent on the wave steepness and the slope of the beach. Camenen and Larson (2007) proposed a formula derived from data of 22 different sources. Their formula is applicable to a large variation in the slope angle (up to 22 °) and wave steepness (up to 0.14) and is described below.

$$\gamma_b = \frac{0.284}{\sqrt{\lambda_\infty}} tanh[f_*(m, \lambda_\infty)\pi\sqrt{\lambda_\infty}] \quad \text{Equation 2-23}$$

with

$$f_*(m, \lambda_\infty) = A_1 + A_2 \, sin\left[\frac{\pi}{2}\left(\frac{m}{m_{max}}\right)^{\varphi}\right] \quad \text{Equation 2-24}$$

$$m_{max} = 0.1 + 1.6\lambda_\infty \quad \text{Equation 2-25}$$

$$\varphi = 1 + 14\lambda_\infty \;\; if \; m \leq m_{max} \quad \text{Equation 2-26}$$

$$\varphi = -(1 + 20\lambda_\infty) \;\; if \; m > m_{max} \quad \text{Equation 2-27}$$

$$A_1 = 0.87 \quad \text{Equation 2-28}$$

$$A_2 = 0.32 + 14\lambda_\infty \quad \text{Equation 2-29}$$

where λ_∞ is the wave steepness and m is the beach slope, related to the slope angle. Equation 2-23 will however only apply if the properties of the waves are within the range applicable to the empirical equation.

Breaking waves can be categorized in four different types: spilling, plunging, collapsing and surging (Battjes, 1974; Sunamura and Okazaki, 1996). Spilling waves are characterised by turbulence created at the crest of the wave (Figure 2-5 a). These breakers have a slow rate of energy transfer from the wave into turbulence (Ting and Kirby, 1996). At a specific wave steepness and slope angle, the wave crest will topple over and form a plunging breaker (Figure 2-5 b). Collapsing and surging breakers (Figure 2-5 c) are very similar and are characterised by rapid movement of the base of the wave, which does not allow for the wave crest to develop properly. For collapsing breakers the base of the wave collapses, whereas surging breakers merely slide up the slope, creating little foam and turbulence (Sunamura and Okazaki, 1996).

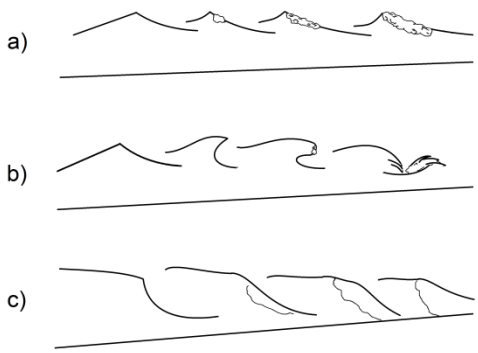

Figure 2-5: There are mainly four different types of waves: a) spilling, b) plunging, c) collapsing and surging. The type of wave which forms on a beach is dependent on the beach slope and the wave steepness.

Plunging breakers result in the most air entrainment (Cokelet, 1977). The air entrainment process occurs on two levels: the entry point of the jet that plunges into the water in front of the propagating wave as well as the pocket of air entrapped as the wave overturns, illustrated in Figure 2-6. The pocket of air is then broken down into smaller bubbles (Deane et al., 1999).

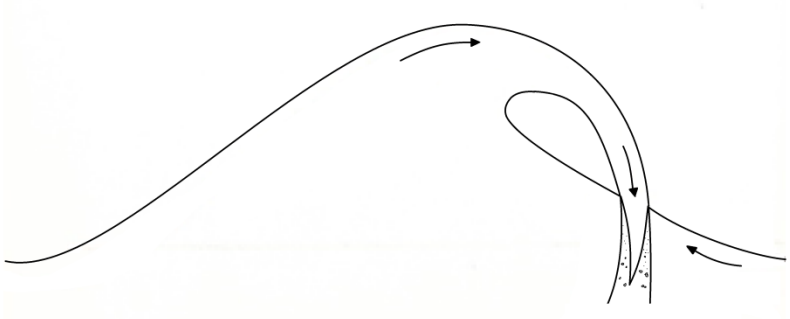

Figure 2-6: Plunging breaker, illustrating the pocket of air that gets entrapped and the jet that plunges into the water in front of the wave. Adapted and redrawn from Chanson and Jaw-Fang (1997)

The type of breaker which will form can be predicted by the Iribarren number (ξ) (Battjes, 1974; Holthuijsen, 2007):

$$\xi = \frac{tan(\alpha)}{\sqrt{\lambda_\infty}} \qquad \text{Equation 2-30}$$

which is depended on the beach slope angle (α) and the wave steepness (λ_∞). The beach slope (m) mentioned earlier is in fact equivalent to $tan(a)$. Table 2-1 depicts the values of ξ for each different type of wave (Holthuijsen, 2007). The transition from one type to the next is gradual however (Battjes, 1974). The ranges therefore only serve as approximations. Knowledge on the wave properties can

therefore be used to design a slope angle to form a specific breaker according to Equation 2-30 and the ranges in Table 2-1.

Table 2-1: Range of values of the Iribarren number corresponding to each type of breaker

Breaker Type	Range
Spilling	$\xi < 0.5$
Plunging	$0.5 < \xi < 3.3$
Collapsing/Surging	$3.3 < \xi$

2.4 Inducing waves through use of a slope

2.4.1 Lab scale wave formation on a slope

Studying ocean waves is a difficult task, since the ocean is an uncontrolled environment. Researchers therefore recreate waves on a lab scale to study them more effectively. Table 2-2 gives a summary of numerous studies that evaluated breaking waves. In these studies, the height of the wave approaching the slope varied between 3 and 15 cm. Slope angles of 1.6 to 6 ° were used. This gives an indication of the typical scale at which these experiments are performed and breaking waves are successfully created.

Table 2-2: Wave and slope properties of numerous lab scale experiments involving breaking wave formation

Wave Height (cm)	Wave Steepness	Slope	Angle (°)	Wave Type	Source
12.5	0.020	1:35	1.64	Spilling	Ting and Kirby (1996)
3	0.023	1:20	2.86	Spilling	Huang et al.(2009)
12.2	0.062	1:9.5	6	Spilling	Hoque and Aoki (2005)
45.5	0.028	1:9.5	6	Plunging	Hoque and Aoki (2005)
12	-	1:20	2.86	Plunging	Mukaro et al. (2013)
5.9	-	1:14	4.09	Plunging	Sumer et al. (2013)

In a raceway setting, the waves approaching the slope are created due to the motion induced by the paddlewheel blades. Blades that are about to exit the water scoop the liquid in an upwards direction but at the same time there is reverse flow beneath the blade due to the difference in head across the wheel. This creates a circular fluid motion which advances along with the bulk liquid through the raceway (Musgrave, 2017). Figure 2-7 illustrates the motion.

There is however a limit to the wave height of this pulse. Waves created by a small paddlewheel system should have a considerably smaller height than the waves indicated in Table 2-2. This would especially be true at a lower paddlewheel rpm since this reduces the energy transferred into the water to create the wave. For smaller waves, surface tension effects dominate, meaning the waves are more stable and less likely to break. Literature could not be found on the formation of breaking waves with a smaller height than indicated in Table 2-2. It is therefore not possible to say whether the waves will indeed break on a much smaller scale, indicating a potential problem for using this method to create breaking waves on a small scale.

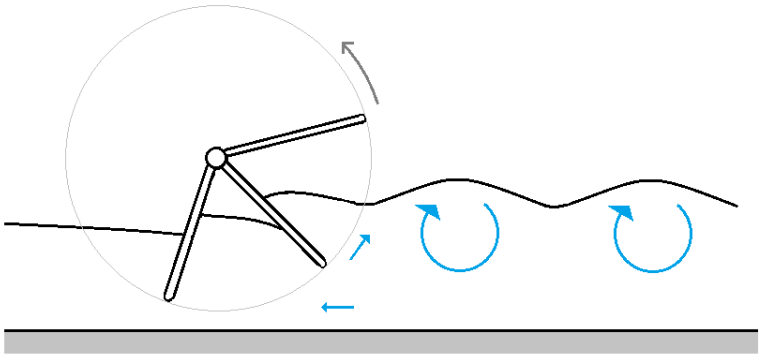

Figure 2-7: Circular fluid motion created by the paddlewheel, leading to a wave traveling through the raceway. Adapted and redrawn from Musgrave (2017)

2.4.2 Previous work on enhancing CO_2 mass transfer through wave generation

At the University of Cape Town, Burke (2016) designed and tested a number of slopes with the aim of creating hydraulic jumps and waves similar to shoaling waves found in the ocean (as discussed in Section 2.3.1). The surface aeration brought about by the slopes was compared to a number of sparging techniques in terms of mass transfer and energy requirements. All experiments were performed in an indoor lab scale raceway pond operating at a pond depth of 12 cm and a paddlewheel rpm of 19.8. The dimensions of the slopes that were evaluated are summarized in Table 2-3. Slope 1, 2, 5 and 6 had a height of 10 cm while Slope 3 and 4 had a height of 12 cm, equal to the depth of the fluid.

A single slope was equipped in the straight channel opposite the paddlewheel. It was expected that a wave would form and break on the slope, but this flow pattern was not observed with any of the slopes (Burke, 2016). Instead, only a standing wave in the form of a hydraulic jump was produced after the slope, similar to the flow described over weirs (discussed in detail in Section 2.4.3) (Burke, 2016). Figure 2-8 is an example of the observed flow pattern, visualized using a phenolphthalein solution along with an acid/alkali tracer. The tracer experiments also revealed the formation of a recirculation zone after the slope, where reverse flow occurred.

Figure 2-8: Flow pattern observed over the slope with a 20 cm horizontal and 10 cm vertical section using a phenolphthalein solution (Burke, 2016). A recirculation zone was also observed after the slope.

As discussed earlier, the paddlewheel creates a pulse that travels through the raceway. The pulse approaching the slopes had a height of 7 mm (Burke, 2016). The properties of this approaching wave were a lot different than typical waves studied on a lab scale, as mentioned in Section 2.4.1. Given the height and steepness of the approaching wave, it is likely that the surface of the slopes were too

deep to affect the formation of a breaking wave on the slope. The implications of such small waves are not clear. As mentioned, it is possible that breaking waves on the slope will not be able to form on this scale.

Table 2-3: Illustrations and dimensions of slopes assessed by Burke (2016)

Slope	Illustration	α (°)	H (cm)	L_1 (cm)	L_2 (cm)
1	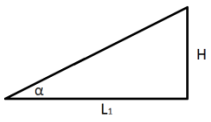	27	10	20	-
2	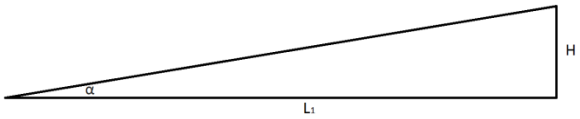	7	10	80	-
3	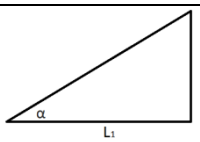	31	12	20	-
4	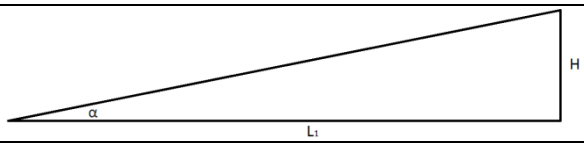	9	12	80	-
5	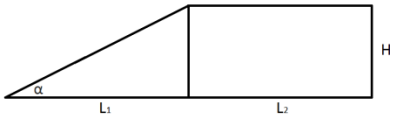	27	10	20	20
6	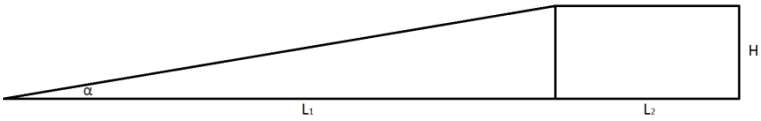	7	10	80	20

Mass transfer experiments were performed in growth media. The addition of the slopes did indeed increase the CO_2 mass transfer coefficient compared to a control without any slopes. This was due to enhanced mixing and turbulence provided by the slope (Burke, 2016). Slope 1 and 2 were the two best performing slopes, with an increase in k_La of 56 % and 80 %, respectively, when compared to the control (Burke, 2016). Using the data of Burke (2016) the error in k_La was propagated to the percentage increase in k_La. The uncertainty in terms of standard error was 56 ± 17 % and 80 ± 25 % (https://figshare.com/s/00ec7e5192c6be962de8, Raceway 2). Table 2-4 shows the percentage increase in k_La compared to the control as well as the circulation time and mixing time for each of the six slopes.

A recirculation zone formed after every slope except Slope 2, which gave the highest k_La. Burke (2016) concluded that this zone contributed to a decrease in the k_La due to a decrease in turbulence and in the surface renewal rate. It was speculated that the longer horizontal section of Slope 2 decreased the velocity of the fluid sufficiently through frictional forces to allow it not to overshoot the edge of the slope (Burke, 2016). Using the data of Burke (2016), the mean k_La of Slope 1 and 2 were compared. At a 95 % confidence level, one cannot however conclude that there was a significant difference in the observed k_La ($p = 0.28$). The same is true for Slope 2 and Slope 5 ($p = 0.21$). It is also interesting to note that Slope 6 did have a recirculation zone. This slope should experience similar frictional forces as Slope 2. The increase in k_La of Slope 6 (6 ±14 %, showing standard error) was also low compared to the increase produced by Slope 2 even though Slopes 1, 2, 5 and 6 had a very similar mixing time and circulation time. It is clear however that the slopes with a height equal to

the liquid depth (Slope 3 and 4) were not ideal as they reduced the k_La, mixing time and velocity to a great extent.

Table 2-4: Percentage increase in k_La compared to the control for each slope, along with the circulation time and mixing time (Burke, 2016). The standard error is also shown.

Slope	Percentage Increase in k_La (%)	Circulation Time (s)	Mixing Time (s)
1	58 ± 18	47 ± 2	118 ± 1
2	80 ± 25	46 ± 2	111 ± 2
3	-9 ± 10	218 ± 9	465 ± 5
4	-36 ± 10	234 ± 3	516 ± 6
5	49 ± 19	46 ± 0	116 ± 1
6	6 ± 14	45 ± 2	122 ± 0

The effects of the recirculation zone were however backed by experiments which involved a slope and sparging of air right after the slope. This removed the recirculation zone after Slope 1 (Burke, 2016). The percentage increase in k_La for Slope 1 and 2 with sparging is depicted in Table 2-5. The significant jump in k_La of Slope 1 with sparging was attributed to the removal of the recirculation zone, while Slope 2 did not experience a significant increase since the recirculation zone was not present without sparging (Burke, 2016). It is therefore difficult to conclude whether the recirculation zone did in fact affect the CO_2 mass transfer. Removing the recirculation zone could nonetheless be advantageous from a cultivation point of view, since algae could potentially settle in the area right after the slope and decrease algal productivity.

Table 2-5: Percentage increase in k_La compared to the control (without sparging) for Slope 1 and 2 with sparging after the slope, as assessed by Burke (2016)

Slope	Percentage Increase in k_La (%)	Circulation Time (s)	Mixing Time (s)
1	109 ± 22	49 ± 0	118 ± 1
2	90 ± 19	47 ± 1	114 ± 2

Another configuration worth discussing is a wave-cover combination, which combined the effects of sparging under a cover and creating a surface wave. The cover had the same angle as Slope 2 and started 4 cm above the channel bottom, allowing fluid to flow below the cover. This resulted in a lower volumetric flow over the top of the cover, reducing the hydraulic jump and surface effects (Burke, 2016). This configuration had only a 36 % increase in k_La compared to the control without sparging (Burke, 2016). Propagating the error in k_La to the percentage increase gives 36 ± 15 %. Fluid flow under the slope therefore reduces the surface turbulence through a smaller hydraulic jump.

The slopes were also assessed based on mass transfer per unit of energy required. Table 2-6 indicates the calculated theoretical power required along with two methods used to assess the mass transfer per unit of energy required (Burke, 2016).

Table 2-6: Mass transfer rate per unit of energy input, as calculated by Burke (2016), also showing the Control with no slopes.

Configuration	Maximum Mass Transfer Rate per Unit Theoretical Power Required (mol L^{-1} s^{-1} W^{-1} $x10^{10}$)	Improvement in Maximum Mass Transfer Rate per Unit Theoretical Power Required (mol L^{-1} s^{-1} W^{-1} $x10^{10}$)
Control	18	0
Slope 1	16	59
Slope 2	13	56
Slope 3	48	-50
Slope 4	26	-147
Slope 5	14	45
Slope 6	6.8	4

The maximum mass transfer rate per unit of theoretical power required showed that Slope 3 and 4 performed the best. The theoretical power required is depended on the fluid velocity and the volumetric flow rate, which was the lowest for Slope 3 and 4, which led to an extremely low theoretical power requirement and as a result the highest mass transfer per unit of energy (Burke, 2016). Burke (2016) deemed this comparison to be non-conclusive since Slope 3 and 4 performed worse than the control when other factors were considered, such as the mixing. The slopes were then compared in terms of the improvement in maximum mass transfer per unit of theoretical power required, which is the increase in mass transfer compared to the control divided by the theoretical energy requirement for the specific slope configuration. These calculations however never incorporate the power consumption of the control. It therefore only serves as a comparison between the slopes and never addresses whether the control has the best mass transfer per energy requirement. Also, in practice, one might expect Slope 3 and 4 to have the highest actual power requirement (which incorporates the efficiency of the fluid driving system). This is because these slopes provide the greatest resistance to the flow as they have a height of 12 cm as opposed to the height of 10 cm. The greater force exerted on the fluid should decrease the fluid velocity and increase the fluid height upstream of the slope. The increased height creates a greater difference in head across the paddlewheel, also allowing more liquid to seep through the clearance between the blades and channel walls. As discussed in Section 2.1.3, a greater difference in head across the paddlewheel would decrease the paddlewheel efficiency and likely increase the actual power requirement compared to the other slopes. In terms of k_La per unit of theoretical power required, the slopes did however perform better than any of the sparging systems that were evaluated (Burke, 2016).

Burke (2016) also evaluated whether the addition of a slope (Slope 2) in the raceway increased the algal productivity compared to a control. Similar productivities were however found (Burke, 2016). The increase in CO_2 mass transfer did not reflect in the algal productivity. Since Spirulina was cultivated, the pH of the culture was maintained at 10 through the addition of sodium bicarbonate. Less sodium bicarbonate was required for the raceway fitted with the slope (Burke, 2016). To draw better comparisons to the control, it would once again be fitting to not only asses the productivity but also the productivity per unit of energy required.

Overall these results showed the importance of the slope height on the mixing time and mass transfer and also indicated that the recirculation zone potentially impacts the mass transfer negatively. Flow below the slope negatively impacts the k_La by reducing the surface turbulence. Also, to address the mass transfer per unit of energy, the actual energy input could give a clearer view as the theoretical energy input does not incorporate the paddlewheel efficiency. The increased energy requirement for the slopes is partly due to the energy lost in the hydraulic jump and recirculation zone created by the slopes. A more energy efficient slope design could potentially improve on the k_La per unit of energy required.

2.4.3 The hydraulic jump caused by weirs

A weir is a hydraulic structure placed in an open channel used to control the fluid flow and level while additionally acting as a flow measurement device (Chanson, 2004). The structure usually spans the entire width of the channel and raises the upstream water level. Weirs are often used to induce a hydraulic jump with the aim of dissipating energy, mixing chemicals or acting as aeration devices (Chaudhry, 2008). Flow in an open channel has an associated Froude number (Fr) (Chanson, 2004; Massey, 2006):

$$Fr = \frac{v}{\sqrt{gy}} \qquad \text{Equation 2-31}$$

Where v is the fluid velocity (m s^{-1}), g is the gravitational acceleration (m s^{-2}) and y the fluid depth (m). For Fr =1, the flow is said to be critical whereas Fr < 1 corresponds to subcritical flow and Fr > 1 is supercritical. At the appropriate height, a weir can allow the flow to transform from supercritical/critical into subcritical. Accompanying this transformation is a hydraulic jump or surface disturbance (Wood, 2018). The hydraulic jump is brought about by the dissipation of energy, when the liquid at critical conditions enters a subcritical state (Chanson, 2011). The energy is transformed into turbulence and surface waves which can results in air entrainment (Chanson, 2004). The required height of a weir to ensure critical flow above it can be determined by applying the Bernoulli equation to a point before and on the weir (Munson et al., 2009), with reference to Figure 2-9:

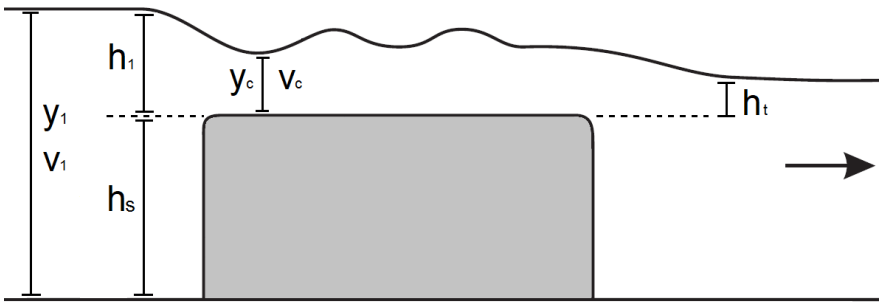

Figure 2-9: Defining sketch for critical flow over a weir resulting in a standing wave. Adapted from Chanson (2004)

$$y_1 + \frac{v_1^2}{2g} = y_c + h_s + \frac{v_c^2}{2g} \qquad \text{Equation 2-32}$$

where y_1 is the upstream fluid depth, v_1 is the approaching fluid velocity, h_s is the height of the weir and v_c the critical velocity corresponding to critical flow. The critical depth y_c is calculated through Equation 2-33 (Massey, 2006; Munson et al., 2009):

$$y_c = \left(\frac{Q^2}{gw^2}\right)^{1/3} \qquad \text{Equation 2-33}$$

Where Q is the volumetric flow rate and w the width of the channel. The corresponding critical velocity (v_c) is determined by:

$$v_c = \frac{Q}{y_c w} \qquad \text{Equation 2-34}$$

Flow over a weir can be described as either free flow or submerged flow (Azimi et al., 2014). Free flow is characterized by a low downstream depth and this depth does not affect the upstream flow (Hakim and Azimi, 2017). Once the downstream depth reaches approximately the depth of the weir

height, the flow is described as being submerged (Wu and Rajaratnam, 1996). The submergence of a weir is defined as:

$$S = \frac{h_t}{h_1}$$ Equation 2-35

Air entrainment increases as the submergence decreases (Fritz and Hager, 1998), in other words, free flow conditions are preferred if the weir is used as an aerator. However, due to the design of a raceway pond, submerged flow is the most applicable when a slope is equipped in the channel. For free flow conditions, the fluid depth downstream of the slope would need to be much lower than the upstream depth. Free flow conditions might be obtained with a difference in the elevation of the channel floor but this entails a redesign of the raceway geometry. The level of submergence could however be influenced by the head loss across the slope as this influences the downstream depth in relation to the upstream depth. Factors such as the paddlewheel rpm or the slope height could be considered.

Wu and Rajaratnam (1996) found that the level of submergence primarily governs the flow pattern associated with a submerged hydraulic jump. They studied the different flow patterns for submerged flow over sharp crested weirs. The flow was divided into four categories, which were brought about from different levels of submergence. These were impinging jets, breaking waves (surface jump), surface waves (undular jump) and surface jets. With the impinging jet regime (Figure 2-10 a), a submerged water jet plunges over the weir into the channel bottom, creating a recirculation zone at the surface after the weir, with little surface disturbance (Wu and Rajaratnam, 1996). As the tailwater depth increases the surface jump (Figure 2-10 b) turns into a number of undulating surface waves (Figure 2-10 c) which gradually fade out until the surface is horizontal (Hakim and Azimi, 2017), as in the case of the surface jet (Figure 2-10 d). As opposed to the impinging jet, surface flow regimes (Figure 2-10 b – d) result in a bottom recirculation zone (Fritz and Hager, 1998; Wu and Rajaratnam, 1996).

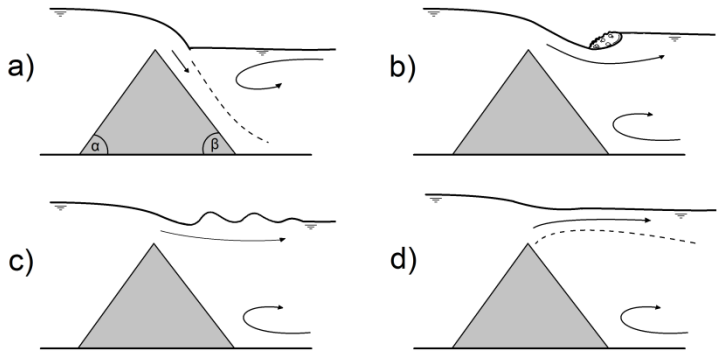

Figure 2-10: Four categories of submerged flow over a weir. a) Impinging jet; b) Surface jump; c) Undular jump; d) Surface jet, occurring in order as the level of submergence is increased. Redrawn from Wu and Rajaratnam (1996). The indicated angles α and β refer to the upstream slope angle and downstream slope angle, respectively.

Fritz and Hager (1998) evaluated the hydraulics of embankment weirs (broad crested weirs with both an upstream and downstream slope) and showed that the length of the bottom recirculation zone was a function of the upstream depth above the weir and the level of submergence. They did however not change the downstream slope angle (which was fixed at 26 °). The sudden expansion after a weir leads to a deceleration of the fluid velocity. A lower velocity translates to an increase in the pressure, meaning an adverse pressure gradient is created. The adverse pressure gradient, if strong enough, leads to reverse flow and a recirculation zone. The addition of a downwards slope decreases the size of the recirculation zone and can completely remove it at a sufficiently low angle (Ali, 2013). Energy losses also occur in the recirculation zone (Ali, 2013), meaning a weir with a lower downslope angle

could decrease the head loss along with the energy requirements. A popular weir design with a low downstream angle is a Crump weir, which has an upstream slope of 1:2 and a downstream slope of 1:5 (Crump, 1952). The intent of the design was to create a weir that could accurately measure flow under both free flow and more drowned conditions where the 1:5 downslope serves the purpose of maintaining a more stable tailwater flow (Crump, 1952; White, 2015). This weir design could therefore potentially serve the purpose of flow measurement in a raceway pond (without redesigning the raceway geometry).

The flow patterns observed by Burke (2016) resembled typical undular hydraulic jumps. The characteristics of the undular jump is determined by the inflow Froude number and the corresponding aspect ratio (y_c/W) at that point (Ohtsu et al., 2001). For flow with Froude numbers close to one, the wave height is proportional to the Froude number (Chanson and Montes, 1995). Undular jumps have an upper limit of the Froude number, after which the jump turns into a weak hydraulic jump without the surface undulations (Chanson and Montes, 1995). The undular jump profile could also be affected by the upstream angle of the weir. Madadi et al. (2013) studied the effect of upstream slope angle and the curvature of the top edge on the formation of undular waves above broad-crested weirs. Free flow conditions were used. They found that increasing the angle of the upstream slope from 21 ° to 90 ° increased the wave height formed above the weir. Increasing the curvature of the inflow corner decreased the wave height. The aspect ratio on the other hand affects the undular jump through a dampening effect that the channel walls have on the flow pattern (Chanson and Montes, 1995). The aspect ratio decreases as the channel width gets increased, to a point where the walls have no effect on the flow. The wave height increases with a decrease in the aspect ratio (Chanson and Montes, 1995).

In a raceway setting, major changes to the aspect ratio can likely only be brought about by changes in the channel width, although the slope height could affect it. The wave height could further be manipulated by the upstream Froude number and the upslope angle. As shown in the types of undular jumps, increasing the Froude number increases the turbulence which should improve the mixing and surface disturbances.

2.4.4 Revisiting light penetration and the light/dark cycles

Slopes also contribute to vertical mixing, bringing the algae from the bottom dark zone into the top light zone, reducing the time of a light/dark cycle. This is somewhat similar to the flashing light effect mentioned in Section 2.1.3. Some researchers have tried to exploit this effect in raceway ponds, adding baffles and up-down chutes to the pond.

Cheng et al. (2015) included two pairs of up-down chutes in a lab scale raceway, in conjunction with gas sparging. They found that this decreased the light/dark cycle time along with an increase in the O_2 mass transfer coefficient by 25 % and biomass yield by 32.6 %. They did not specify the increase in energy demand due to the chutes. In a study by Zang et al. (2015), 26 wing baffles were added to a 4 m^2 pond. The light/dark cycle period was decreased from 14.0 s to 4.4 s and the final biomass concentration increased by 30.1 %.

Demory et al. (2018) however points out that in many studies, no clear evidence between the effects of mixing and shorter light/dark cycles are ever distinguished. These two variables are interconnected when considering the use of chutes or slopes in raceway ponds. According to them the effects of frequent fluctuations in light are not yet fully understood. Sutherland et al. (2015) also argues that the flashing light effect is less conclusive on medium scale frequencies of seconds to minutes, as observed in raceways. Light/dark cycles should ideally be on a millisecond time scale (Grobbelaar, 2009). It is therefore difficult to argue increases in algal productivity purely from a light cycle perspective.

2.4.5 Statistical methods to evaluate slope parameters

Based on Sections 2.4.2 - 2.4.4, it is clear that the combination of different slope parameters show intricate trade-offs. Without the aid of intensive computational fluid dynamics, it is difficult to use theoretical calculation to predict which parameters affect the hydrodynamics and mass transfer the most and what the preferred value of each parameter would be. To capture the complexity of these trade-offs, a factorial design of experiments (DOE) could be formulated. A factorial DOE has an advantage over the typical approach of varying one factor at a time through the ability to identify interactions between factors. The factorial DOE evaluates all possible combinations of factors at a number of predetermined levels. For example, a 2^4 design contains four factors with two levels each, leading to 16 possible combinations (or treatments). It is possible to further reduce the number of treatments with a fractional factorial design, which comes with limitations, however.

Limitations of the fractional factorial design

Fractional factorial designs have a trade-off between the amount of experiments performed (which relates to time and resources) and the amount of information one obtains from the results. These designs do not include all the combinations of factor levels. For example, the 2^{4-1} fractional design only requires 8 combinations of factors. This leads to what is known as aliasing or confounding and the concept of design resolution (Montgomery, 2013). Since the 2^{4-1} design has less treatment combinations, less data is available to estimate the effects of factors and interactions, meaning the same data is sometimes used to estimate different effects. Two effects are said to be confounded when the same data was used to estimate the effect. The effects of confounded pairs cannot be distinguished from another. For example, if the interaction AB from Factor A and Factor B is confounded with the interaction CD from Factor C and Factor D, both interactions would have the same effect on the response, but it is not possible to determine if this effect is from only AB, only CD or a combination of AB and CD. The design resolution gives an indication of how much the effects are confounded with one another, or how clearly the effects can be separated from each other, and is denoted by a roman numeral (III, IV, V etc).

One limitation of the design used in this study was that the 2^{4-1} fractional factorial is a resolution IV design, meaning the main effects are confounded with the three-factor interactions while the two-factor interactions are confounded with each other. An additional limitation of this DOE is that only two levels of each factor are tested. This does not test for curvature in the responses, meaning that the ideal values of each factor couldn't be obtained if a response varies non-linearly with the changes in each factor. This design does however still serve the purpose of identifying how each factor (and the interactions) affects the responses and which factors had the greatest effect on the responses.

Analysing the fractional factorial DOE

The design and analysis of the results are performed using statistical software. The effects of factors and their interactions can be presented using a Pareto chart. The Pareto chart shows the relative magnitude of the effect estimates as well as its direction. A higher magnitude therefore indicates that a factor or interaction plays a more dominant role in the measured response. The direction (indicated by the sign of the magnitude) shows whether the value of the response increases or decreases if the level of the factor is increased from the low to the high value. A positive effect estimate therefore indicates that the response increases if the level of the factor is increased.

Both the standardized effect estimates and the effect estimates can be plotted. The standardized effect estimates are the effects divided by their respective standard errors, and this Pareto chart also shows whether the effect is significant. Figure 2-11 is a sample of a Pareto chart showing the standardized effect estimates. Effects in which the standardized estimate extends beyond the p = 0.05 line (in red) can be considered statistically significant (at a 95 % confidence level).

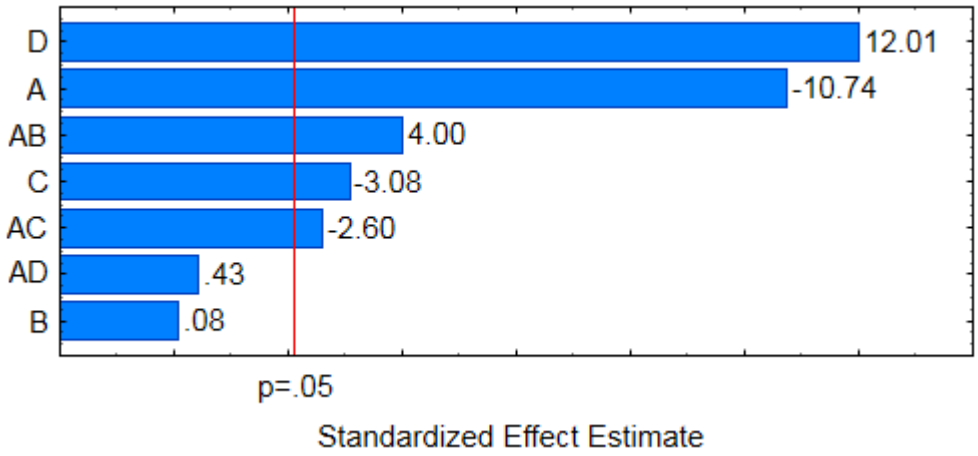

Figure 2-11: Sample of a Pareto chart, showing the standardized effects estimates of four factors (A, B, C and D) and their interaction on a response. Effect estimates beyond the p = 0.05 line are considered significant at a 95 % confidence interval.

Only three two-factor interactions are ever shown, as the two-factor interactions are confounded with one another. Any specific two-factor interaction is confounded with the complimentary two-factor interaction. For example, in Figure 2-11, the AB interaction is confounded with the CD interaction. Likewise the AC interaction is confounded with the DB interaction. An attempt can be made to determine which of the confounding pairs better describe the response. To do this, principles such as effect heredity are used, along with experimental validation of the models. Effect heredity considers the significance of an interaction based on the significance of the main effects in that interaction. An interaction is said to have a strong heredity if both main effects have a significant effect on the response and a weak heredity when the main effects have an insignificant effect on the response (Montgomery, 2013). Interactions with strong heredity are more likely to occur than interactions with weak heredity. For example, in Figure 2-11, the AB and CD confounded pair has a standardized effect estimate of 4.00. The CD interaction has strong heredity whereas the AB interaction has weak heredity (since the main effect of B had an insignificant effect on the response). It is therefore more likely that this effect estimate is from the CD interaction (or at least that the CD interaction has a dominating contribution to the effect estimate). It should be noted however that in this design it is not possible to confirm this with certainty.

If the experimental treatments are replicated a total of three times, it is possible to determine the pure error, which refers to the error due entirely to variability in the measurement of the response. The pure error is utilized in determining whether an effect can be considered significant (indicated in the Pareto chart showing the standardized effect estimates). Given enough degrees of freedom (DoF), one can estimate the lack of fit of a model, which addresses the residual error (any remaining variability that cannot be accounted for by the factors and interactions in the model). A model with significant lack of fit indicates that there is variability which cannot be explained by the current model and that additional considerations need to be included in the model. This means that there are likely higher order interactions that need to be included in the model, or that the confounded pairs need to be separated, in order to paint a clearer picture of the effects. For a 2^{4-1} design, the total available degrees of freedom are $2^{4-1}n-1$ (Montgomery, 2013), where n is the number of independent replicates (n = 3). The total degrees of freedom in this case is therefore 23. The degrees of freedom associated with an effect can be viewed as the number of pieces of data used to determine the effect. The degrees of freedom associated with a main effect A is (a – 1), where a is the number of levels for factor A (Montgomery, 2013). A breakdown of the degrees of freedom is presented in Table 2-7.

Table 2-7: Summary of the degrees of freedom for a 2^{4-1} fractional factorial design with factors A, B, C and D. Lower case letters refer to the number of levels of the associated uppercase letter (in this case, always 2). n refers to the number of independent replicates of each treatment.

Effect	Calculating DoF	Degrees of Freedom
A	a - 1	1
B	b - 1	1
C	c - 1	1
D	d - 1	1
A by B	(a -1)(b - 1)	1
A by C	(a – 1)(c – 1)	1
A by D	(a – 1)(d – 1)	1
Pure Error	½abcd(n-1)	16
Total	½abcdn-1	23

Table 2-7 shows that a model which includes all four main effects and all three confounded two-factor interactions satisfies all the degrees of freedom, leaving no room to determine the lack of fit. It is only when some effects are removed from the model that there is enough degrees of freedom to calculate the lack of fit.

2.5 Other internal structures in raceways used to enhance CO_2 mass transfer

Using structures inside raceway channels to enhance gas mass transfer has seen some traction in recent years. These structures aim to improve mixing as well as increase bubble retention time and decrease bubble size, in the case of gas sparging. Table 2-8 below summarises different designs and their effects on the mass transfer coefficient and mixing time compared to a control. In all instances where sparging is present, the structure was compared to a control that also incorporated sparging. The values depicted under the percentage increase in k_La and mixing time are the highest values obtained by varying the parameters mentioned in the Variables column. The majority of the designs were evaluated on a lab scale.

The majority of the structures summarized in Table 2-8 were used in conjunction with gas sparging and were designed to affect the sparged bubbles. The focus was not on creating surface turbulence, which is an important characteristic when gas sparging is not utilised since the gas mass transfer then only occurs at the free surface interface. Leman et al. (2018) equipped the raceway channel floor with semi-circular and triangular bars (longitudinally along the channel) with the aim of improving vertical mixing and gas transfer at the free surface. The bars varied between 9 and 21 mm in height. With variations in the fluid depth between 9.5 and 38 cm, it was observed that the addition of the bars had a negligible effect on the gas transfer velocity at the free surface. It was speculated that the flow structure created by the bars did not reach the free surface and therefore did not contribute to the gas transfer (Leman et al., 2018). Also considering the wave-cover combination tested by Burke (2016) (discussed in Section 2.4.2), raising the slope to allow fluid flow beneath it had a negative impact on the free surface turbulence (and mixing time) since critical fluid flow was no longer achieved over the slope. These results show the importance of slope height and position along the vertical plain if the aim is to produce surface turbulence.

In general, the literature assessed had little focus on the additional power requirements involved in adding the structures to the raceway (which would also need to incorporate the energy of the gas

sparging if applicable). These structures contribute some drag force against the flow of the fluid and would require an increase in power to overcome these forces. It is important to incorporate the increase in energy alongside the increase in k_La to draw better comparisons to the controls. Huang et al. (2015) incorporated the energy demand due to up-down sloping baffles, which were used to promote mixing in a 20 m^2 raceway. Although the effects on gas mass transfer were not addressed, the algal productivity per unit of energy input was determined. The addition of the up-down baffles, along with flow deflectors around the bends, resulted in an average algal productivity per energy input of 0.65 g W^{-1} d^{-1} compared to the 0.51 g W^{-1} d^{-1} observed for the control without the baffles and flow deflectors. Although CO_2 was still supplied through sparging, this nonetheless shows the value that these baffles could add. The power requirements however only incorporated the power expended by the paddlewheel and did not include the power associated with the gas sparging.

It is however difficult to draw direct comparisons between all these studies to identify the superior structure designs, especially considering the lack of reporting on the energy requirements. The difference in scale used in the experiments also complicates the matter. The decrease in mixing time for example is dependent on the ratio between the area affected by the structures and the total area of the raceway. Many of the designs also require upscaling to address the effects on a larger scale, since raceways are predominantly used on a larger scale. Since including structures in a raceway also contributes to an increase in the energy demand, replacing the paddlewheel with a more energy efficient device is even more desired.

2.6 Propellers as alternative fluid driving devices

The low efficiency of paddlewheels was discussed in Section 2.1.3. Alternative fluid driving devices such as propellers have been proposed, although the literature on comparisons between a propeller and paddlewheel driven raceway pond is quite scarce. Chiaramonti et al. (2013) did a study where they aimed to redesign the traditional pond system to relieve its energy demand by substituting the paddlewheel with a propeller. A single propeller was used, equipped in the centre of the pond, with a narrowing of the channel which diverted the fluid into it. Their results indicated that the redesigned system was less energy intensive. The propeller system had a 65 % reduction in energy demand for a 5 m^2 pond and a 60 % reduction when comparing a theoretical scale-up to a 500 m^2 pond. The redesigned ponds however also included baffles in the curve sections of the pond. It was not stated to what extent the baffles and the propeller contributed to the reduction in energy. Similar algal productivities were obtained in the paddlewheel driven and propeller driven ponds.

In another study, Laws and Berning (1991) compared a paddlewheel with a propeller system in terms of its energy demand and influence on algal productivities. 24 m^2 raceways ponds were used but with a different setup compared to Chiaramonti et al. (2013). On the one side of the pond a manifold was installed, with three PVC pipes connected into and out of it. Each PVC pipe in the inlet was equipped with a propeller. On the paddlewheel driven rig, the paddlewheel was installed just downstream of the manifold outlet. Their results however contradicted the study of Chiaramonti et al. (2013). The propeller system demanded 26 % more energy than the paddlewheel system. This finding was never explained throughout the text. The resulting algal productivities for each system were comparable.

A key element in utilising a propeller system appears to be its setup. Similar to the paddlewheel system, the clearance around the propeller, which allows for back-flow, needs to be minimal. The setup of Chiaramonti et al. (2013) has a lower capital cost compared to that of Laws and Berning (1991), since a single propeller was used. Care however must be given to the design of the narrowing and expansion of the channel at the propeller. A sharp narrowing and expansion of the channel can lead to fluid recirculation and dead zones (Musgrave, 2017). A slower rate of change in the channel width is therefore required.

Table 2-8: Summary of different structures in raceway ponds that have been explored to improve mixing and mass transfer

Illustration	Description	Variables	Scale	Sparging	Percentage increase in k_La (%)	Percentage decrease in mixing time (%)	Notes	Source
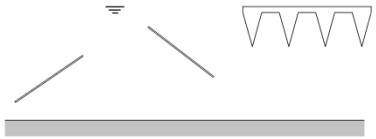	Up-Down baffle followed by an inverted oscillating baffle to trap bubbles	Fluid velocity and pond depth	0.39 m^2 (62-108 L)	No	12	-	k_ia does not increase below velocity of 30 cm/s, attributed to the inverted baffle reducing the surface area	Yang et al. (2016)
				Yes	130	33	Sharp increase in k_La due to inverted baffle increasing bubble retention time	
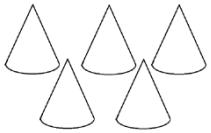	Conical baffles to create vortex flow fields	Cone spacing and height	1.2 m^2	Yes	21	24	Vortex flow field increased bubble retention time	Cheng et al. (2018)
	Helical Baffle	Pitch length and diameter	0.12 m^2 (6 L)	Yes	62	41	Very small scale. Experiments performed in duplicate	Kubar et al. (2020)
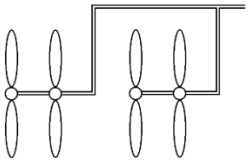	Self-rotatory propellers	Propeller blade number and diameter	0.12 m^2 (8.4 L)	Yes	84	67	Spargers placed below propeller. Propellers reduce bubble size and increase retention time through vortex flow field	Kumar et al. (2019)
	Bars that stretch longitudinally in the channel to create secondary flow fields	Bar shape, size, quantity and spacing as well as fluid depth	16.6 m^2	No	0	-	Lack of increase in k_La was attributed to the secondary currents created by the bars not reaching the free surface of the fluid	Leman et al. (2018)

2.7 Summary of literature review

Raceway ponds suffer from low algal productivities, partly due to limited mixing and CO_2 mass transfer from the atmosphere. Numerous methods that aim to improve gas mass transfer exist, but rely heavily on gas sparging. The method of using a slope in a raceway pond to create surface turbulence that enhances the CO_2 mass transfer does not rely on CO_2 sparging and its potential has been shown in a previous study at UCT by Burke (2016). Although a large focus of this method was to mimic shoaling waves in the ocean, these waves were never observed with the slope designs. This is possibly due to the surface of the slope being too deep to affect the small waves created by the paddlewheel. The slopes however created hydraulic jumps which greatly enhanced the CO_2 mass transfer.

In the ocean, breaking waves will form when a wave approaches a sloping beach and a certain depth below the wave is reached. The depth at which a wave will break is dependent on the steepness of the approaching wave as well as the slope angle and can be calculated based on empirical equations. These two variables also govern which type of breaking wave will form and plunging breakers are desired as they create more turbulence and air entrainment compared to spilling breakers. The scale used in oceanography studies however is larger than the scale of the observed waves in the lab scale raceway pond used by Burke (2016). This opens up the question of whether breaking waves can be formed on this smaller scale.

The slope designs of Burke (2016) resembled weirs. The transition from critical flow over a weir into subcritical flow results in the formation of a hydraulic jump or standing wave due to energy dissipation. This occurs at a certain weir height. For submerged flow conditions, different surface flow patterns could arise due to the level of submergence. These flow patterns include the formation of a recirculation zone brought about by an adverse pressure gradient across the weir. From the study by Burke (2016) the slope height had a significant effect on the gas mass transfer observed. The effect of the recirculation zone on the gas mass transfer however is still unclear. The addition of a downstream slope angle can decrease the size of the recirculation zone after the weir and could also potentially be considered as a more energy efficient weir since the recirculation zone is associated with a loss of energy. Additionally, to create more surface turbulence, the surface wave height could be increased by increasing the upstream Froude number or upslope angle. Adding a slope in the raceway however increases the energy demand of the system. Paddlewheels are known to have low efficiencies and could potentially be replaced by a more energy efficient fluid driving device such as a propeller. Literature on the use of propellers is however scarce and shows mixed results.

2.8 Defining the research project

The slope designs of Burke (2016) showed promise as a means to enhance the atmospheric CO_2 mass transfer rate into the pond. The main aim of this study was to improve on the previous slope designs evaluated by Burke (2016), with the focus on enhancing the mixing and CO_2 mass transfer rate due to the slope. Objectives for the research were set, along with hypotheses and key questions that needed to be answered.

2.8.1 Objectives

The following objectives were formulated:

- Re-evaluate the best performing slope designs of Burke (2016)

Evaluate the two best performing slope designs tested by Burke (2016) in terms of their effect on the hydrodynamics, the CO_2 mass transfer and energy requirement. The operating conditions of the pond are to be kept the same as used by Burke (2016).

- Improve on the slope designs

Get a better understanding on how the slope parameters affect the hydrodynamics, mass transfer and energy requirement and through this attempt to improve on the slope designs. The improvements aim to enhance the mixing and achieve a higher CO_2 mass transfer rate from the atmosphere into the pond. Assess whether these effects translate to an increase in algal productivity compared to a control.

- Compare a propeller to a paddlewheel as the fluid driving device in the raceway

To assess the viability of using a propeller in a raceway pond, compare a propeller driven raceway with a paddlewheel driven raceway in terms of the effects on the hydrodynamics, CO_2 mass transfer and energy requirement.

2.8.2 Research hypothesis and key questions

Hypotheses

Two hypotheses were formulated:

1. The addition of a slope in the raceway pond will increase the algal productivity due to enhanced mixing and CO_2 mass transfer from the atmosphere. The enhanced gas mass transfer is achieved through the formation of surface turbulence in the form of waves.

2. The increase in CO_2 mass transfer through the addition of a slope can be enhanced by creating standing waves with a larger wave height and by reducing the recirculation zone after the slope. Larger waves are related to more surface turbulence and enhance mixing and surface renewal in the pond. Reducing the size of the recirculation zone improves surface renewal and increases the mass transfer driving force.

Key Research Questions

To validate the hypotheses, the following key questions need to be addressed:

- What is the effect of the upstream slope angle, downstream slope angle and slope height on the resulting wave height?
- What is the effect of the recirculation zone on the CO_2 mass transfer rate?
- Are breaking waves on the surface of the slope (similar to shoaling ocean breakers) possible on a small scale?
- How do the slope parameters affect the mixing inside the raceway?
- How does the propeller system affect the mixing in the raceway?
- How do the slope parameters affect the CO_2 mass transfer in the raceway?
- How do the slope parameters affect the CO_2 mass transfer per unit of energy required?
- Does the implementation of a propeller system reduce the energy demand compared to a paddlewheel?
- Does the addition of a slope improve the algal productivity compared to a control without a slope?

3 Project Approach and Methodology

3.1 Research methodology

This research was quantitative in nature and followed a deductive approach. Data collected from experiments were used to answer key questions and ultimately test the hypotheses presented in Section 2.8.2. Changes in algal productivity are brought about by differences in hydrodynamics and gas mass transfer. The mass transfer is also ultimately dependent on the hydrodynamics. Improvements in the gas mass transfer or hydrodynamics however typically arise at the expense of energy. These four elements (hydrodynamics, gas mass transfer, energy requirements and algal productivity) therefore had to be quantified to successfully answer the key questions and test the hypotheses.

Inserting a slope in the raceway channel affects the hydrodynamics through changes in the fluid velocity, mixing and surface disturbances (which leads to enhanced CO_2 mass transfer). The surface disturbances were quantified by measuring the size of the wave formed. The wave amplitude is a variable that could easily be measured through photographic imagery and was assumed to be proportional to the surface turbulence. The fluid velocity and mixing time were obtained through tracer experiments. Data from a tracer experiment also allows for the determination of the Peclet number. The Peclet number is a dimensionless number that relates fluid transport phenomena and can give an indication of back-mixing in the raceway as oppose to plug flow conditions. A conductivity tracer was used as opposed to a pH tracer since CO_2 mass transfer also affects changes in pH (which could potentially distort the data). A weir-like slope also typically creates a recirculation zone after the crest. The recirculation zone was visualized using a colour based tracer which allowed for the size of the recirculation zone to be estimated. A phenolphthalein solution was used, which changes colour based on pH. A pulse of a strong acid or base was therefore utilized to change the colour of the fluid in the raceway. Using a phenolphthalein solution as opposed to a dye tracer is advantageous as the colour of the solution can be changed an indefinite amount of times. The methods followed to quantify these variables are outline in Section 3.3.1.

To quantify the CO_2 mass transfer rate, a pH-alkalinity method was used. This method allows for the k_La of CO_2 to be measured directly as opposed to measuring the k_La for O_2 through the typical dynamic gassing out method and then using a conversion factor to obtain the k_La for CO_2. The pH-alkalinity method involves increasing the pH of the fluid and monitoring the decrease in pH as gaseous CO_2 dissolves into the fluid. A thorough derivation of the method can be found in Burke (2016), although an outline of the theory is given in Section 2.2. This method gives more accurate results compared to the dynamic gassing out method. This is because CO_2 undergoes a series of reversible reactions upon its dissolution into water. The equilibrium of this reactive system is captured in the pH-alkalinity method.

Adding a slope to the channel also increases the head loss throughout the raceway. The increased depth of fluid upstream of the slope adds to the hydrostatic pressure pushing against the paddlewheel blades - thereby increasing the energy demand of the system. To draw a clearer comparison between the slopes, the energy requirements needed to be considered. A more detailed comparison of the slopes and the control was obtained by assessing not only the k_La and productivity but also addressing these variables in relation to the energy requirement of the system. The energy demand was assessed on two levels: the actual energy input, measured using a power meter, and the theoretical energy requirement. The theoretical energy was obtained through calculations. The calculations relied on knowledge of the fluid velocity and fluid depth at certain locations in the channel. The velocity was obtained from the tracer experiments while the fluid depth was measured using photographic imagery. The methods followed to quantify the energy requirements are discussed in Section 3.3.2.

The effect of the change in the hydrodynamics and k_La on the algal productivity was also evaluated. Increasing the algal productivity in an energy efficient way is the primary goal of incorporating a slope in the raceway. Cultivation experiments were therefore performed to quantify the algal productivity.

3.2 Equipment and Materials

3.2.1 The laboratory scale raceway pond

The experiments were performed in a 100 L indoor lab scale raceway pond. The raceway was consistently operated at a fluid depth of 12 cm, which corresponded to a working volume of 62 L for the control. An illustration of the raceway, along with its dimensions in centimetres, is depicted in Figure 3-1. This is the exact same raceway design used by Burke (2016). The raceway was constructed of clear Perspex and consisted of sheets joined by thermoplastic weldings which protruded about 1 mm into the channel (positions depicted in Figure 3-1). The weldings are numbered since reference will be made to the positions throughout the text.

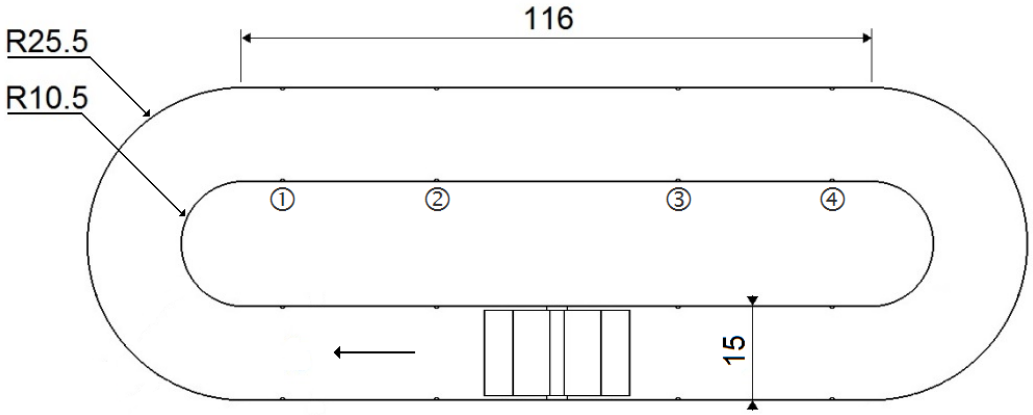

Figure 3-1: Lab scale raceway pond with dimensions in centimetres. The weldings along the straight channel section opposite the paddlewheel are numbered for referencing throughout the text.

The paddlewheel had 6 blades each with a length and width of 11.5 cm and 13.5 cm, respectively. The blades were connected to a central hub with a 4 cm diameter giving the paddlewheel an overall diameter of 27 cm. The clearance between the channel and blades were 0.8 cm on each side and 2.5 cm below. A 0.37 kW Bonfiglioli motor with a S2U Bonfiglioli variable frequency drive (VFD) was used to drive the paddlewheel.

For the purpose of algae cultivation the raceway was illuminated by several fluorescent lights. Cool White Osram 58 W bulbs were used throughout. Two 1.5 m bulbs spanned each outer wall of the raceway, along with three 0.6 m bulbs on the inner walls, positioned at the centre of the channel. An additional two 1.5 m bulbs illuminated the straight channel opposite the paddle wheel from below. Details on the cultivation conditions are described in Section 3.3.4.

3.2.2 Slope designs inserted into the raceway

Numerous slope designs were evaluated, including the two best performing slope designs of Burke (2016), new weir-like slope designs and a slope designed to create breaking waves similar to shoaling ocean waves. Details of the thought process behind the design of the new slopes are discussed in Section 4.2.1 and 4.3.1.

Best performing slope designs of Burke (2016)

Table 3-1 depicts the two best performing slope designs of Burke (2016), as well as their dimensions. Both slopes had a height of 10 cm. The length however varied, giving rise to two different upslope angles. The one slope had a length of 20 cm, referred to as the 20 cm slope, whereas the 80 cm slope had a length of 80 cm. These two slopes were constructed by the Department of Chemical Engineering's Mechanical Workshop and made of PVC with a stainless steel surface. The crest of each slope was positioned roughly 10 cm after Welding 3 (Figure 3-1) in the raceway pond to match the position used by Burke (2016). The spacing between the slope edges and the raceway channel walls were sealed off using clear tape. This was a quick and easy method that prevented the spacing from disrupting the flow pattern over the slope and also held the slope in position. The tape however did not create a perfect seal, meaning this method was only used for the hydrodynamic and mass transfer experiments, ad not the cultivation experiments.

Table 3-1: Parameters of the two best performing slope designs of Burke (2016). Fluid flow occurs from left to right.

Slope	Illustration	RPM	α (°)	H (cm)	L (cm)
20 cm	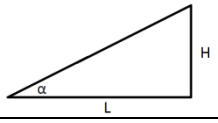	19.8	27	10	20
80 cm	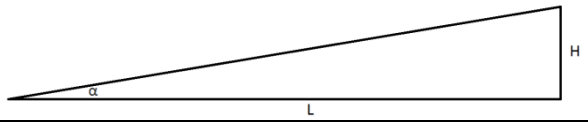	19.8	7	10	80

New weir-like slope designs

The new weir-like slopes were evaluated in a 2^{4-1} fractional factorial DOE. A summary of the DOE is presented in Table 3-2. The Slope column indicates the naming convention used for the slope configurations, which consisted of a four letter code referring to the level of each factor (being either L for low or H for high). The first letter refers to the paddlewheel RPM whereas the remaining letters refer to the slope parameters. The second letter refers to the upslope angle, followed by the downslope angle and then the slope height. For example, configuration LHLH is slope HLH operated at the low paddlewheel RPM. Details of the though process behind the slope designs and selected levels are discussed in Section 4.3.1.

The new slope designs were constructed by a different manufacturer (Clear Designs, Cape Town). These were entirely made of clear Perspex, similar to the slopes used by Burke (2016). The components of the slopes were modular, where each slope configuration was made by combining different up and down slopes and stacking these slopes on platforms to change the height. The crest of each slope was positioned 2 cm after Welding 2 (Figure 3-1). The slopes were positioned close to the start of the straight channel to accommodate space for the down slopes. In this instance the surface turbulence due to the slope also occurred roughly at the centre of the straight channel section, which is normally an area where very little mixing occurs.

Table 3-2: Dimensions of the slopes evaluated in the fractional factorial DOE. These slope designs aim to create a hydraulic jump. Fluid flow occurs from left to right.

Slope	Illustration	RPM	α (°)	β (°)	H (cm)
LLLL	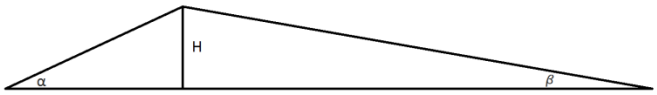	19.8	25	10	9
LHLH	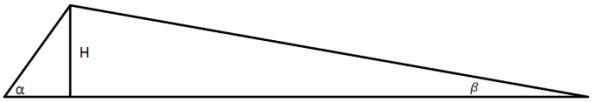	19.8	54	10	10
LLHH	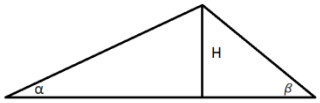	19.8	25	39	10
LHHL	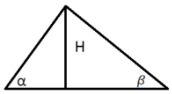	19.8	54	39	9
HLLH	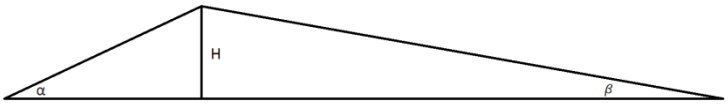	28.9	25	10	10
HHLL	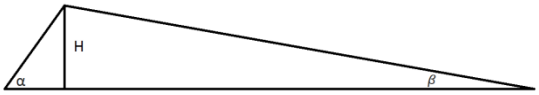	28.9	54	10	9
HLHL	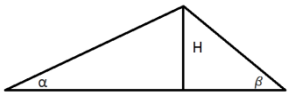	28.9	25	39	9
HHHH	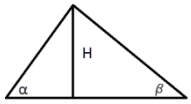	28.9	54	39	10

Progressive wave slope

The new slope design (slope PW), which was based on the principles of ocean breakers, is illustrated in Table 3-3, along with its dimensions. The platform that was used as slope PW was initially used in the designs of the weir-like slopes, which had a predetermined length. Slope PW therefore had a thickness of 1 cm, a length of 56 cm and its leading edge had an angle of 10 °. The crest of Slope PW was positioned 10 cm after Welding 3 (Figure 3-1). Details of the thought process and calculations behind the design are discussed in Section 4.2.1.

Table 3-3: Parameters of the new slope design which aimed to create progressive breaking waves similar to those found in the ocean. Fluid flow occurs from left to right.

Slope	Illustration	RPM	α (°)	H (cm)	L (cm)
PW	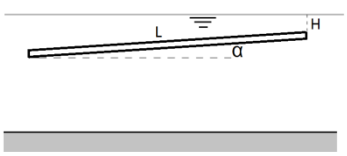	19.8	2	0.85	56

3.2.3 Propeller system

The propeller system utilized a combination of readily available components (which included the motor and propeller) and additional components bought online to construct the drive system and remaining electronics required for the motor. These included a suitable power supply, on/off switch, a timing belt, bearings and motor speed controller. The propeller system is illustrated in Figure 3-2. A framework was designed to secure the propeller axis in position (in the T-section), hold the motor in a motor bracket, and mount the system to the raceway. The T-section was designed to position the propeller axis in the centre of the cross-sectional area of the channel (at a depth of 6 cm). The design for the frame was drawn in SolidWorks (Appendix A) and sent to Clear Designs, Cape Town, for construction (out of Perspex). All the electronic components were positioned on the platform of the framework and housed in a plastic container as a safety measure against splashing water. The framework was mounted at the position where the paddlewheel would've been. One downside of this framework design was that it was fit for purpose and specific for the operating conditions of a fluid depth of 12 cm. It would therefore not be ideal to evaluate lower fluid depths (since the propeller axis would not be in the centre of the channel) but might be possible to evaluate higher depths if the entire framework is raised by an equivalent amount.

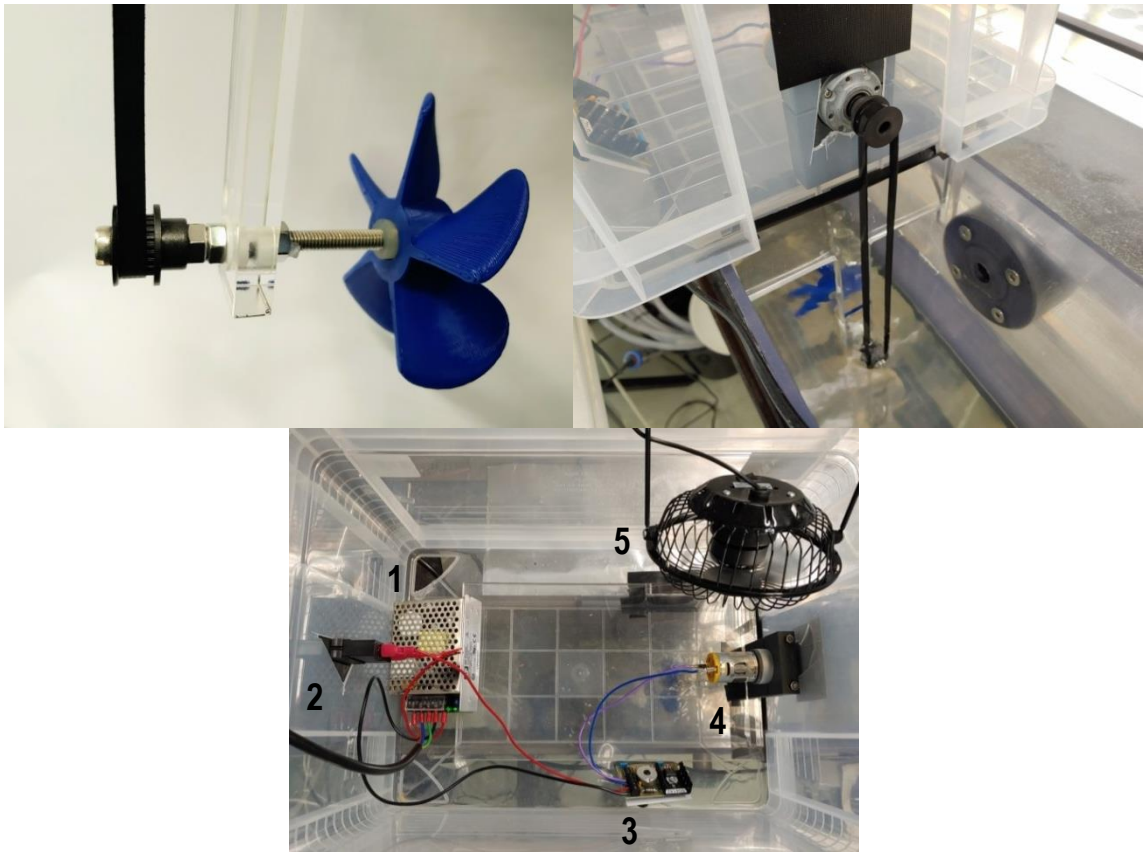

Figure 3-2: Propeller system showing the timing belt mechanism to drive the propeller as well as a top view which illustrates the electric components. The system consisted of a power supply (1) connected to an on/off switch (2), a motor speed controller (3) and a small gear motor (4). A fan (5) was included to prevent the motor from overheating.

The electronic components consisted of an RS Pro 12 V brushed DC gear motor connected to a motor speed controller (6 to 15 V), on/off switch and XP Power 50 W power supply. A fan was directed onto the motor to prevent it from overheating. The wiring for the system was done by the Chemical Engineering Department's Electronics Workshop. The axis and drive system was self-designed and assembled and consisted of a 6 mm diameter stainless steel screw that rested on two

plastic ball bearings that were attached to the T-section of the framework. The screw was secured in place by adding two nuts on either side of the ball bearings. The screw also allowed for the propeller to be screwed off and easily switched. The propeller axis was directly connected to the motor with a timing belt. The propeller had five blades with an outer diameter of 8 cm.

3.2.4 Microalgae strain and media

The freshwater alga *Scenedesmus* sp., sourced from the CeBER culture library, was used for the cultivation experiments. The algae were grown in 3N-BBM growth media, of which the composition is presented in Table 3-4.

Table 3-4: Composition of 3N-BBM used in the cultivation of *Scenedesmus* sp.

Component	Concentration (g L^{-1})
$NaNO_3$	0.75
$CaCl_23H_2O$	0.025
$MgSO_47H_2O$	0.075
$K_2HPO_43H_2O$	0.075
KH_2PO_4	0.175
NaCl	0.025
Na_2EDTA	0.0045
$FeCl_36H_2O$	5.82×10^{-5}
$MnCl_24H_2O$	2.46×10^{-5}
$ZnCl_2$	3.00×10^{-5}
$CoCl_26H_2O$	1.20×10^{-5}
$Na_2MoO_42H_2O$	2.40×10^{-5}
Vitamin B1	1.20×10^{-3}
Vitamin B12	1.00×10^{-6}

Concentrated stock solutions of each media component were made. These stock solutions were autoclaved at 121 °C for 20 min. To create the media, the appropriate amount of each component was diluted into water and topped up to the desired volume of the media. Deionised water was used for the pre-inoculum of the culture (and the media was then autoclaved at 121 °C for 20 min) while un-autoclaved tap water was used in the raceway.

3.3 Methods

3.3.1 Hydrodynamics

All hydrodynamic experiments were performed in tap water at a fluid depth of 12 cm. The fluid temperature was also kept constant at 25 ± 0.2 °C to keep the properties of the water the same as in the gas mass transfer experiments. This was achieved by using two aquarium heaters (DoPhin 150 W submersible) attached diagonally to the outer side wall before the paddlewheel.

Wave size

The size of the hydraulic jump was measured through photographic imaging and image processing using ImageJ software. The amplitude of the first wave was used as a means to quantify the size. An LG V20 smartphone mounted onto a tripod was used to capture the images. The camera lens was aligned with the first wave after the crest of the slope and placed 35 cm from the side of the raceway. A ruler with 1 mm accuracy was attached to the raceway to provide a scale for use in the software.

The waves changed in size due to a staggered flow pattern created by the paddlewheel. It is this staggered flow that creates the pulse that travels throughout the raceway. Only the maximum wave size was considered – which was when the pulse from the paddlewheel overlapped with the hydraulic jump. The raceway was illuminated from the bottom and back to light up the meniscus of the water (Figure 3-3). Measurements were made from the centre point of the meniscus. An example is illustrated in Figure 3-3. Final measurements were rounded to the nearest millimetre since this corresponded to the accuracy of the ruler used.

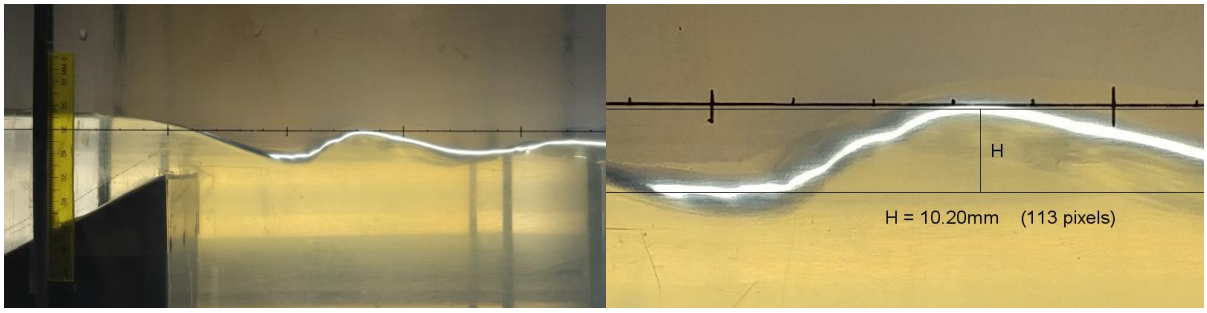

Figure 3-3: The meniscus of the water was lit up using the fluorescent lights on the side and bottom of the raceway. The wave size was measure in ImageJ using the center of the meniscus. The ruler attached to the side of the raceway was used to set the scale in ImageJ, giving an accuracy of 1 mm.

Images such as the above were obtained by taking a long burst shot of the flow pattern. Three images (where the pulse from the paddlewheel overlapped the hydraulic jump) were selected from the series of images from one burst shot and sized using ImageJ. Two such burst shots were taken on independent occasions: once after a gas mass transfer experiment and once more after another replicate of the mass transfer experiment.

Recirculation zone size

The size of the recirculation zone was a measured using image processing. The recirculation zone was visually observed using a phenolphthalein solution. Phenolphthalein turns bright pink in alkaline solutions, beyond a pH of roughly 8.3 (Kapoor, 2019), and is clear in neutral to acidic solutions. 60 mL of a 1 g L^{-1} phenolphthalein solution (phenolphthalein dissolved in 50 % EtOH) was added to the raceway (which was filled with tap water) and thoroughly mixed. The pH was increased to 9.5 using 6 M NaOH, creating a bright pink colour. Colour changes from pink to clear and vice versa were achieved by repeatedly injecting a pulse of 6 M HCl and 6 M NaOH into the raceway. The recirculation zone was best observed with a colour change from clear to bright pink. For these runs a 2 mL pulse of 6 M NaOH was injected just after the paddlewheel. This was followed by a 2 mL pulse of 6 M HCl. The pH was allowed to reach steady state between each pulse and a total of 3 NaOH pulses were recorded. The chosen injection position led to the clearest visual flow pattern after the slope.

For each slope configuration, the colour tracer experiments were performed directly after the conductivity tracer experiments, meaning the same solution was used in both tracer experiments. Phenolphthalein was therefore present in the fluid used in the conductivity tracer experiments, at a concentration of roughly 1 mg L^{-1}. It was assumed that this low concentration would not affect the

hydrodynamics through changes in the properties of the fluid. This also meant that the salinity of the solution was typically higher than the normal tap water, since the conductivity tracer, as well as the NaOH and HCl, increased the salinity. The solution was replaced after every second slope configuration tested. The effects of the increased salinity on the properties of the solution were assumed to be negligible. A 5 % increase in the viscosity would only be observed once the molarity of the NaCl reached about 0.5 M inside the raceway (from data in Goldsack and Franchetto (1977)). This would only occur after well over a 100 pulses each of NaOH and HCl.

The video footage of the flow patterns were taken using an LG V20 smart phone mounted to a tripod. The camera lens was positioned 35 cm from the side of the raceway. The footage was then processed using ImageJ and Shotcut (a free video editing software). This was done by firstly using Shotcut to create a series of still frames from the video. The images were then imported to ImageJ as a stack. An illustration of the recirculation zone is depicted in Figure 3-4. Naturally the recirculation zone also turns pink after a short period of time when the fluid gets mixed properly. The frame in which the pink fluid first touched the channel bottom (and in which reverse flow could be identified) was used to size the recirculation zone.

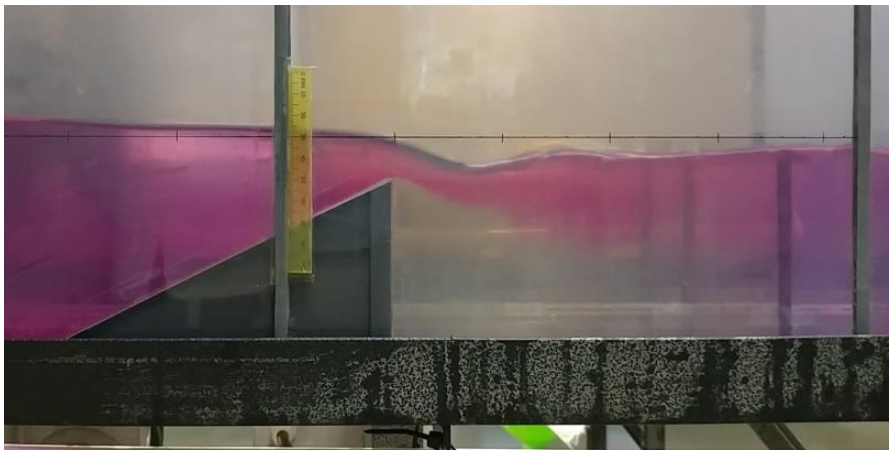

Figure 3-4: The recirculation zone after the 20 cm slope visualized using the phenolphthalein tracer

ImageJ was used to distinguish between the clear recirculation zone and the pink forward moving fluid. A colour threshold was chosen to create a clear border between these two zones. Figure 3-5 (a) depicts the range in properties (hue, brightness and saturation) of the threshold colour. The specific range was obtained through trial and error to get the clearest distinction between the two zones. This threshold was used throughout all runs. To obtain a final image in black and white, a second grey scale threshold was applied after the initial colour threshold. This was done by converting the image into greyscale and applying the threshold depicted in Figure 3-5 (b).

Figure 3-6 depicts the final image. From the black and white image, an area was selected that bordered the recirculation zone. ImageJ was used to calculate the white area in the total area selected. The raceway however had a side rail which obstructed the view of the actual channel bottom. The area of the recirculation zone was extrapolated into the side rail. The known slope height was used as a reference to obtain the actual bottom of the raceway. This area is highlighted in red in Figure 3-6. The total area was the sum of the white zone and the highlighted red zone. The area was then multiplied by the channel width (15 cm) to obtain an estimate of the recirculation zone volume. The volume can only be considered as rough estimates due to the uncertainty in the area of the extrapolated zones.

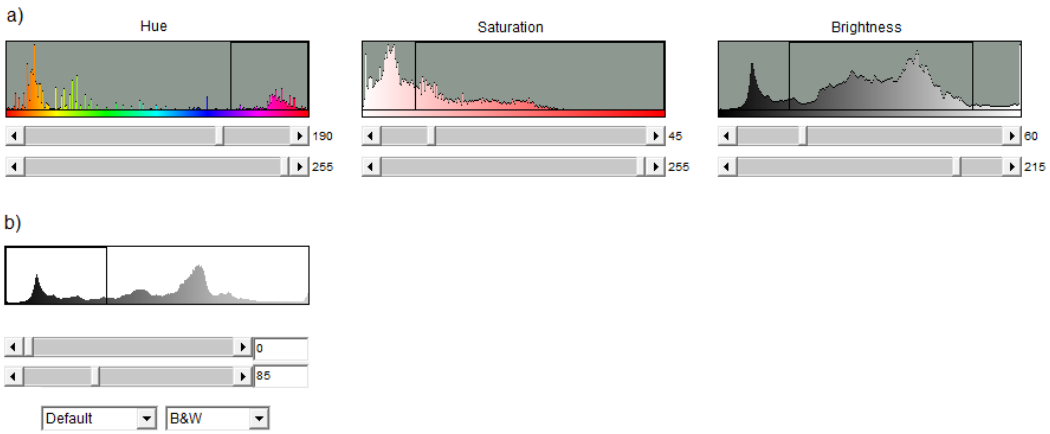

Figure 3-5: Colour thresholds applied in ImageJ used to size the recirculation zone. a) Colour threshold indicating the applicable range in hue, saturation and brightness. b) Greyscale threshold used to obtain a final image in black and white

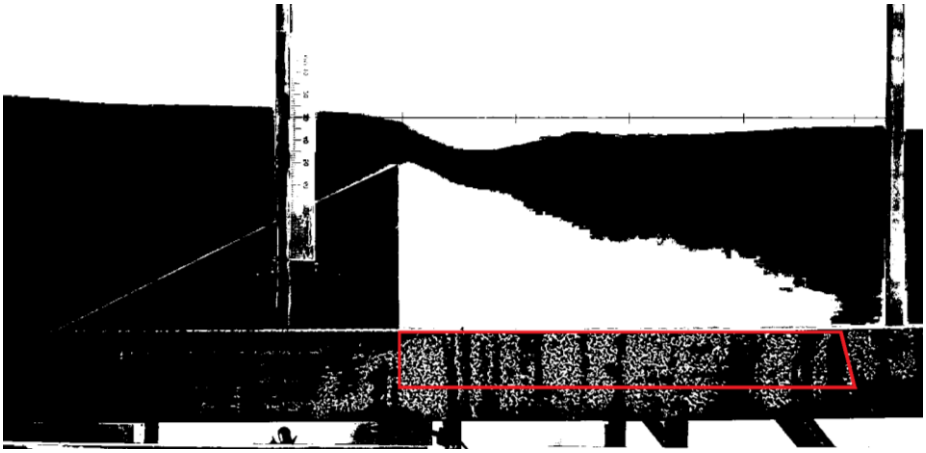

Figure 3-6: Final black and white image used to size the recirculation zone. The highlighted red area depicts the extrapolated recirculation zone, since the side railing of the raceway obstructed the view of the channel bottom.

Mixing and circulation times

Mixing and circulation times were obtained using a conductivity tracer. Figure 3-7 illustrates an example of a typical response observed when a conductivity tracer is injected into a closed loop system such as a raceway. The circulation time corresponds to the time between each peak. An estimate of the average fluid velocity was obtained using this information along with the average length around the raceway pond (3.46 m), measured along the centre of the channel. Changes in this length due to the slopes were assumed to be negligible. The mixing time was defined as the time it took for the response to reach 95 % of its steady state value. The two black lines in Figure 3-7 indicate the zone in which the conductivity is within this limit. The mixing time was therefore taken as the time between the first peak and the time where the conductivity first enters this zone without leaving it again.

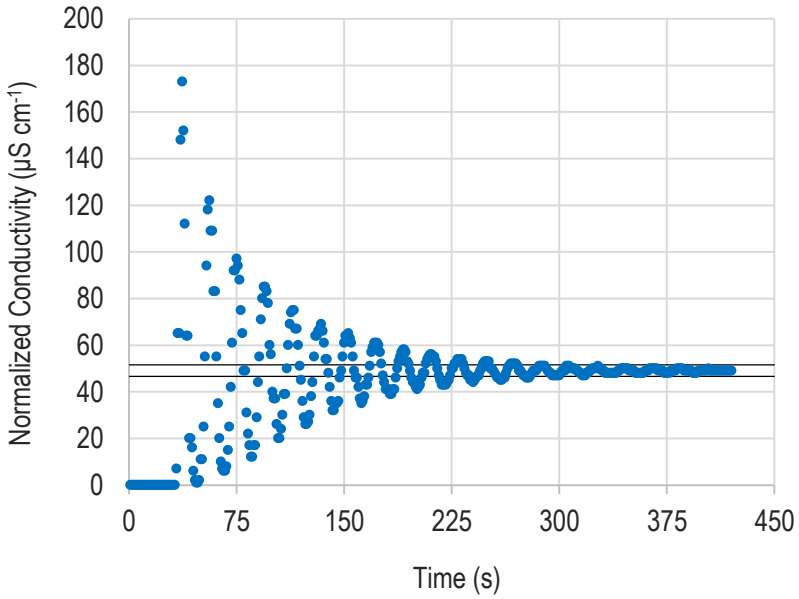

Figure 3-7: Example of the conductivity tracer response over time for the raceway control. The two black lines indicate the zone where the conductivity reaches 95 % of its final steady state value.

For these experiments a Hanna HI98194 portable conductivity meter was used, with the probe positioned in the centre of the channel at Welding 1 (Figure 3-1) at a depth of 6 cm. A 5 mL pulse of 5 M NaCl was injected in the centre of the channel just upstream of the probe, three quarters around the bend. Conductivity data was logged at an interval of 1 s to measure the response. For each pulse response, the first three peaks were used to obtain two estimates of the circulation time. Three pulses were performed for each experimental condition. The three pulses were performed in succession and the conductivity was allowed to stabilize between each pulse. As previously mentioned, for each slope these experiments were performed before the phenolphthalein experiments, using the same liquid.

Mixing was further characterised by determining the Peclet number (Pe). The Peclet number puts the convective transportation of the fluid in the axial direction in relation to the dispersive transportation, depicted in the following equation (Davis and Davis, 2003):

$$Pe = \frac{vL}{D} = \frac{Convective\ Flow}{Dispersive\ Flow} \qquad \text{Equation 3-1}$$

Where v is the velocity measured in the axial direction (m s^{-}), L the characteristic length (in this case the average length around the raceway, measured in meters) and D the axial dispersion coefficient (m^2 s^{-1}). Following the mixing specifications used by Mendoza (2013a) for raceway ponds, plug flow occurs when Pe >100 whereas a Pe of 0 corresponds to perfectly mixed conditions with complete back-mixing. The Peclet number was determined using the methods described by Hreiz (2014). The response to the conductivity tracer was modelled using Equation 3-2 (https://figshare.com/s/00ec7e5192c6be962de8, Raceway 1), which describes the change in the normalised concentration of the tracer pulse (E) over the change in the reduced time (θ). The normalised concentration is defined as the concentration at each specific time point divided by the final steady state concentration (Equation 3-3) and is related to the conductivity data over time. The reduced time is defined as the specific time point divided by the circulation time (Equation 3-4).

$$E(\theta) = \frac{1}{2}\sqrt{\frac{Pe}{\pi\theta}}\sum_{j=0}^{\infty} exp\left[-\frac{Pe}{4\theta}\ (j-\theta)^2\right] \qquad \text{Equation 3-2}$$

$$E(\theta) = \frac{C(\theta)}{C_\infty} \qquad \text{Equation 3-3}$$

$$\theta = \frac{t}{t_{circ}}$$ Equation 3-4

From the model, the Peclet number and circulation time were determined through the method of least squares. Although this gives an additional estimate of the circulation time, the circulation time determined between the peaks of the response (as described before) was used instead. An example of the response describing the normalised concentration observed for the 20 cm slope is depicted in Figure 3-8, along with the model data obtained using Equation 3-2 .

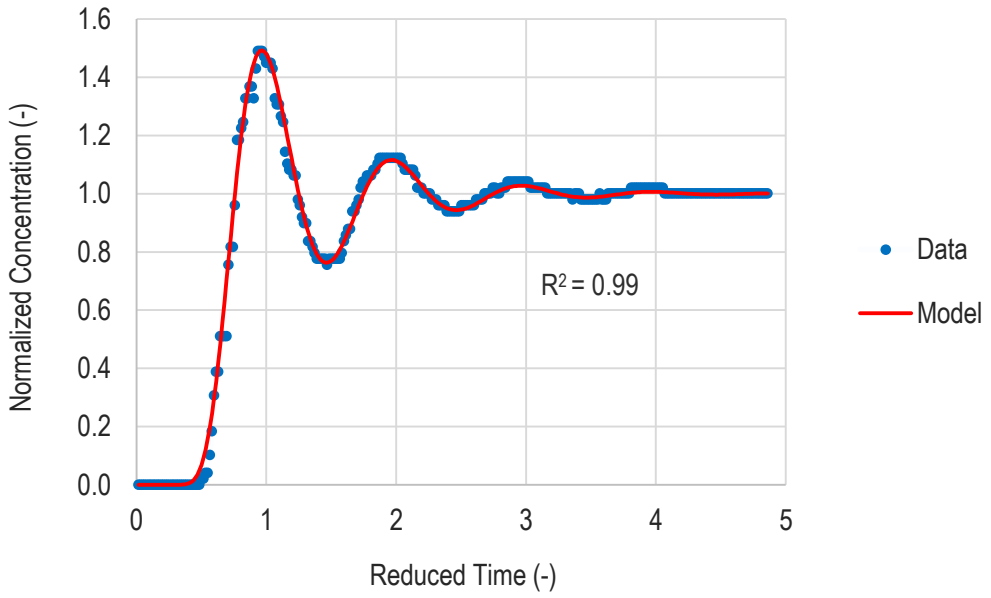

Figure 3-8: Example of the normalized concentration against the reduced time for the 20 cm slope. The actual data obtained from the conductivity tracer is depicted in blue, while the solid red line depicts the model data obtained using Equation 3-2.

3.3.2 Mass transfer experiments

The k_La for CO_2 was directly measured using a pH-alkalinity method (described in Section 2.2). Scilab code to calculate the k_La was provided and is documented in the CeBER Methods Manual (https://figshare.com/s/00ec7e5192c6be962de8, Raceway 2). Data measured during a run (temperature, alkalinity, salinity and the change in pH) are used as input in the code, which calculated the k_La for CO_2 based on the method outlined in Section 2.2 (Equation 2-16 to Equation 2-21). The k_La was determined in triplicate for each experimental condition.

Data measurements during a run

The change in pH was recorded using a Mettler Toledo InPro 3250/120/PI1000 pH probe with a built in temperature sensor. The probe was positioned in the centre of the raceway channel at Welding 1 (Figure 3-1) and the tip immersed to a depth of 6 cm. A Mettler Toledo M300 Transmitter, with the accompanied software, was used to log the pH at intervals of 5 s. pH measurements were reported to three decimal places. Before each run the pH probe was calibrated with a pH 7.00 and 9.21 buffer. A calibration slope of 95 – 102 % was considered acceptable. The probe was cleaned on a weekly basis with an acidic pH electrode cleaning solution to ensure quick and accurate pH measurements. The relative humidity in the lab typically varied between 40 and 60 % and this difference was assumed to have a negligible effect on the mass transfer.

The alkalinity of the fluid was determined through a Gran titration, broadly following the method outlined in Lahav et al. (2001). This method is suitable for low alkalinity waters (such as tap water) and is independent on knowledge of the titration end-point (Lahav et al., 2001). Total alkalinity (A_T) was calculated using the following equation (Lahav et al., 2001):

$$A_T = \frac{V_e C_a}{V_s}$$ Equation 3-5

Here V_e is the volume of acid (mL) required to reach the equivalence point of carbonic acid, C_a is the normality of the acid used in the titration (mol L^{-1}) and V_s refers to the volume of the sample used (mL). To obtain V_e, the first Gran function (F_{x1}) was solved through Equation 3-6 over a range of titration data points for a pH between 4 and 3.5 (Lahav et al., 2001).

$$F_{x1} = -10^{-pH_x}(V_s + V_x)$$ Equation 3-6

V_x refers to the volume of acid added to obtain a corresponding pH of pH_x. Plotting F_{x1} against V_x results in a linear slope from which V_e can be obtained at the y-intercept ($F_{x1} = 0$). The total alkalinity is not affected by the CO_2 mass transfer. This is because the dissolution of CO_2 leads to an equal concentration of positive and negative ionic species (Equation 2-14 and Equation 2-15). From Equation 2-21, one can see that the net effect on the total alkalinity would be zero. Measuring the alkalinity was therefore performed anytime during the course of the run.

A 20 mL sample was titrated with a 0.01 M H_2SO_4 solution using a micropipette. A micropipette was used instead of a burette to achieve greater accuracy in the results. The sample was placed in a 25 mL glass beaker and magnetically stirred during the titration. The 0.01 M H_2SO_4 was added until a pH of roughly 4 was reached – noting the volume required to do so. Six data points were then obtained in the pH range of 4 down to roughly 3.5 by repeatedly adding 50 µL of the acid. A Jenway 3510 pH meter was used to measure the pH. To verify the procedure the alkalinity of a standard 96.5 mg L^{-1} $NaHCO_3$ solution was measured (which is a standard used by Lahav et al. (2001)). This standard solution should result in a total alkalinity of 1.15 mmol L^{-1} (or 57.5 mg L^{-1} as $CaCO_3$). The standard alkalinity solution was also used as a measure to ensure that the molarity of the acid used remained consistent. For each run the alkalinity was measured in triplicate. Due to a high precision of the measurements (typically a relative standard deviation below 2 %), the variability in the alkalinity was assumed to be negligible and was not incorporated into the variability in the k_La measured for the specific run.

The temperature of the water inside the raceway was manually maintained using two aquarium heaters (DoPhin 150 W submersible). These were positioned diagonally on the outer wall of the raceway before the paddlewheel. The temperature was measured using the temperature sensor of the pH probe and kept constant at 25 ± 0.5 °C. This accuracy does not incorporate the accuracy of the probe sensor itself, but reflects how much the measured temperature varied. Three 10 mL samples were taken from the raceway to measure the salinity of the water during the run. An AZ 86555 benchtop conductivity meter was used. The conductivity meter was calibrated weekly with an 84 µS cm^{-1} conductivity standard.

Initiating a run

Mass transfer experiments were performed in tap water. Tap water was used as opposed to growth media as the media required the use of large quantities of chemicals which would go to waste. Fresh tap water was used for each new run. The raceway was filled to a depth of 12 cm and operated for ± 18 hrs at 19.8 RPM before each run. This was done to allow for the water to equilibrate with the local atmospheric conditions and to remove any chlorine gas in the liquid. During this time the tap water inside the raceway was characterised in terms of total alkalinity, salinity, conductivity and pH to monitor its consistency between runs. Average properties of the water were as follows: alkalinity of 7.6 ± 2.1 mg L^{-1} as CaCO3, salinity of 0.06 ± 0.00 g L^{-1}, conductivity of 146 ± 8 µS cm^{-1}, pH of 7.2 ± 0.2.

For each run the change in pH was recorded from 10 down to 9.5. Once the temperature in the raceway reached 25 °C the pH was increased to just above 10 by adding 6 M NaOH. Upon stabilization of the pH, the data logging was commenced. During the course of the run the salinity and alkalinity of the water was measured in triplicate. The high pH values resembled an uncontrolled algae cultivation system that experiences a high pH due to the utilization of CO_2 during photosynthesis. During the cultivation experiments, the pH of the culture typically peaked between 10.5 and 11.

3.3.3 Energy demand

The power consumption of the raceway was assessed on two levels: the theoretical power required to move the fluid in the raceway and the actual power input – which incorporates the overall efficiency of the fluid driving system. The theoretical hydraulic power required was calculated using the following equation (Chiaramonti et al., 2013):

$$P_{Theo} = \rho Q g \Delta H \qquad \text{Equation 3-7}$$

Here ρ refers to the fluid density (kg m^{-3}), Q is the volumetric flow rate (m^3 s^{-1}), g is the gravitational acceleration (m s^{-2}) and ΔH is the total head loss throughout the raceway (m). The total head loss consisted of the concentrated head losses at the raceway bends, the head loss experienced in the straight channel sections due to friction (distributed head loss) and the head loss due to the slope (if applicable).

The concentrated head loss is dependent on the bend loss coefficient (k_b) as follows (Chiaramonti et al., 2015):

$$H_c = k_b \frac{v^2}{2g} \qquad \text{Equation 3-8}$$

where v is the velocity of the fluid (m s^{-1}). The bend loss coefficient typically varies between 1.5 and 4 for raceway ponds (Chiaramonti et al., 2013). The value is however dependent on the channel and bend geometry as well as the fluid velocity (Shukry, 1950). Since the geometry of the raceway used in these experiments was not typical to large scale ponds, the bend loss coefficient was determined through empirical curves created by Shukry (1950), instead of assuming a value from literature. The empirical curves take into account the fluid depth, channel width, radius of curvature, degrees of the bend and the Reynolds number. The validity of the curves was tested by calculating the k_b for a large scale raceway design which falls within the range of values tested by Shukry and comparing the result to typical literature values for k_b (https://figshare.com/s/00ec7e5192c6be962de8, Raceway 2). For the raceway pond in this study, it was assumed that the fluid velocity and depth was the same at both bends, therefore resulting in the same k_b. A general k_b for all the slope configurations was used since the head loss in these systems were dominated by the head loss due to the slope as opposed to the bends. The data for the 20 cm slope system was used to determine k_b, resulting in a value of 0.6 (https://figshare.com/s/00ec7e5192c6be962de8, Raceway 2). Even though the k_b will slightly differ for the other slope configurations, these changes had a negligible effect on the total head loss. For the control at different rpms however, the k_b was determined for each case.

Distributed head losses in the straight sections were determined using Equation 3-9 (Chiaramonti et al., 2015):

$$H_d = \lambda \frac{L}{D_h} \frac{v^2}{2g} \qquad \text{Equation 3-9}$$

with L as the length of the straight channel (m), D_h the hydraulic diameter (m) and λ the friction coefficient, calculated iteratively using the Colebrook-White formula (Green and Perry, 2008):

$$\frac{1}{\sqrt{\lambda}} = -2\,log\left(\frac{2.51}{Re\sqrt{\lambda}} + \frac{\varepsilon/D_h}{3.7}\right)$$ Equation 3-10

where ε is the roughness coefficient (m) and Re the dimensionless Reynolds number. The roughness coefficient used for PVC was 0.003 mm (Wallingford, n.d.). The hydraulic diameter was determined with the following equation:

$$D_h = \frac{4A}{2y+w}$$ Equation 3-11

with A being the cross-sectional area of the channel (m^2), y is the fluid depth (m) and w the width of the channel (m).

The energy loss as a result of the slope (ΔH_s) was estimated using the principle of mechanical energy conservation. An energy balance (Equation 3-12) was applied between a point on the slope crest (1) and a point just after the hydraulic jump (2), illustrated in Figure 3-9:

$$(h_s + h_1) + \frac{v_1}{2g} = h_2 + \frac{v_2}{2g} + \Delta H_s$$ Equation 3-12

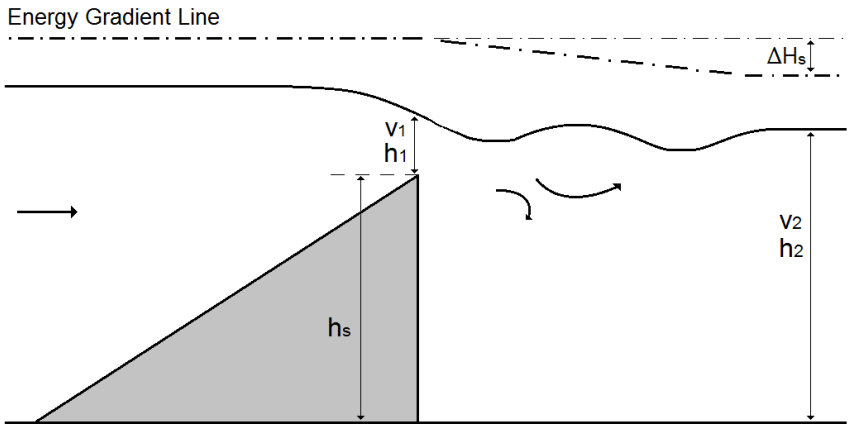

Figure 3-9: Flow over the slope, depicting the head loss from point 1 at the slope crest and point 2 after the hydraulic jump.

Rapidly varied flow such as the flow over a weir or slope often results in a non-uniform velocity distribution which requires the use of a correction factor alongside each velocity term in Equation 3-12. Any deviation from uniformity was assumed to be negligible.

To estimate the fluid velocity at each point the volumetric flow rate was used along with the appropriate cross sectional area. The volumetric flow rate was obtained by dividing the volume of fluid in the raceway by the circulation time. The volume occupied by each slope was accounted for. The depth of the fluid at each section was measured using photographic imagery processed in ImageJ. An LG V20 smartphone was used with the lens positioned 35 cm from the edge of the raceway. The average depth was considered, since the surges created by the paddlewheel led to a variable fluid depth as the pulse travelled through the fluid. A burst shot was taken, from which samples of high and low fluid levels were selected. Similar to measuring the wave size, two such burst shots were taken independently (during the time the wave sizes were also measured). Three samples of the high and low fluid depth were taken (from each burst shot), from which the average fluid depth was determined.

The error in the theoretical energy was propagated from the error in the circulation time and the measured fluid depths (https://figshare.com/s/00ec7e5192c6be962de8, Raceway 2). A notable complication in propagating this error is the Colebrook-White formula (Equation 3-10). This equation is implicit, which does not allow the use of the error propagation equation. To obtain the error in the friction coefficient, a different approach was used similar to a Monte Carlo simulation. This is a brute

force method which relied on computational power. The average fluid velocity and the standard deviation thereof was used to create an array of 10 000 velocities that fit a normal distribution around the mean. The Colebrook-White formula was iteratively solved for each of these velocities, which gave an array of friction factors, from which the standard deviation can be determined. Scilab code was written to perform this calculation (https://figshare.com/s/00ec7e5192c6be962de8, Raceway 2). Incorporating this error in the error propagation however showed that it had a negligible effect on the final error in the theoretical energy and was therefore assumed to be zero throughout.

The energy requirements of Slope PW were calculated using a different approach, since this slope did not lead to a hydraulic jump with a clear difference in head that could more easily be measured. As a simplification, this slope was assumed to be a flat plate immersed in parallel laminar flow. The slope resulted in a drag force acting against the flow. For a flat plate this force is equal to the friction drag. The power required to overcome the friction drag was calculated using Equation 3-13 to Equation 3-15 (Pritchard and Leylegian, 2011)

$$P_s = vF_D \qquad \text{Equation 3-13}$$

with

$$F_D = \frac{1}{2}\rho c_D A v^2 \qquad \text{Equation 3-14}$$

and in the case of laminar flow over a flat plat

$$c_D = \frac{1.33}{\sqrt{Re}} \qquad \text{Equation 3-15}$$

A refers to the area of the slope and c_D is the drag coefficient. P_s (the power required to overcome the drag force) was then added to the power calculated using Equation 3-7.

In all cases, the actual energy consumption, which incorporates the overall efficiency of the fluid driving system, was measured using a Topward 1310 digital Watt meter. The 200 mA setting was used, giving an output to two decimal places. The Watt meter measured the true power, which is the electrical energy consumed by the motor. The reading varied over time and the device did not allow for data logging. A sample of the watt reading was therefore recorded by taking a 25 s video of the meter and logging 25 measurements at 1 s intervals. The average of the 25 readings was taken. This process was repeated a further two times on three independent occasions.

The overall efficiency of the drive system was then calculated by dividing the theoretical power required by the actual power consumed, using Equation 2-4.

3.3.4 Algal cultivation to assess productivity

For the cultivation experiments, two identical raceway ponds were operated simultaneously in batch mode. The raceway without a slope served as a control, which was operated at a fluid depth of 12 cm and paddlewheel RPM of 19.8, since this resulted in a typical fluid velocity used in raceway ponds (18.4 ± 0.3 cm s^{-1}). Three independent runs of the control were performed whereas each slope configuration was evaluated in duplicate. Performing the control in triplicates gave an indication of the variability one can expect from the cultivation experiments. The remaining experiments were performed only in duplicate to save time.

Pre-inoculum for the raceways were first cultivated in three 1 L Schott bottles (0.7 L working volume). Filtered air was supplied at a flow rate of roughly 0.5 vvm and continuous light (Osram cool white fluorescent light) with an intensity of roughly 80 – 100 µmol m^{-2} s^{-1} was used. The cultures were cultivated up to an optical density of roughly 2, measured at a wavelength of 750 nm (OD_{750} = 2). These were used to inoculate a 10 L hanging bag to a starting OD_{750} of roughly 0.5. The working volume of the bag was 7.5 L. Unfiltered air was supplied through an 8 mm inner diameter pipe at a

flowrate of roughly 0.7 vvm. The algae in the hanging bag were cultivated for a period of one week (to an OD_{750} of roughly 2) before inoculating the raceway ponds. As mentioned, two raceway ponds were operated simultaneously. The content of the hanging bag was used to inoculate both raceways. Before inoculating the raceways the growth media was prepared in each pond. For this the raceways were filled with tap water (allowing enough volume for the concentrated media components and inoculum) and run for ± 18 hrs to allow the water to degas and reach equilibrium with the conditions in the lab. Just before inoculation, each of the concentrated media components was added in the appropriate amounts to obtain the correct concentrations for the final volume (corresponding to a 12 cm fluid depth). The raceways were then inoculated so that the starting culture had an OD_{750} of 0.1.

The light intensity around the raceway pond varied between 2 – 180 µmol m^{-2} s^{-1} (https://figshare.com/s/00ec7e5192c6be962de8, Raceway 4). Initially, only the lights along the one outer wall of the raceway (on the side of the paddlewheel) as well as the lights at the bottom of the channel were switched on. This was done to avoid photo-inhibition of the low density algae. Once the culture reached an OD_{750} of approximately 0.3 the remaining lights (along the other outside wall and the inner walls) were switched on. The raceways were operated at room temperature which varied between 22 and 25 °C. Fluid losses due to evaporation were corrected for by topping up the raceway with deionised water before sampling took place. This was typically a volume of around 3 L in 24 hrs.

Algal productivity was obtained by means of a growth curve, which describes the change in biomass concentration over time. The productivity corresponds to the linear slope of the curve before the stationary phase is reached. The specific growth rate was also determined, which corresponds to the linear slope of the curve depicting the natural logarithm of the biomass concentration over time. The biomass concentration was determined using cell dry weights. A 20 mL sample was vacuum filtered onto a pre-dried 0.45 µm cellulose nitrile filter paper (CHM brand). The sample volume was reduced to 10 mL once the dry biomass reached roughly 60 mg. The filter papers were oven dried beforehand for 24 hrs at 80 ^{o}C, after which they were placed in a desiccator for a period of 1.5 hrs to cool to room temperature. Once cooled, the papers were weighed on an analytical scale. After filtration, the biomass on the filter was rinsed with 10 mL of deionised water to remove any residual salts. The filter papers containing the wet biomass were then oven dried for 24 hrs at 80 °C. After drying, the filter papers and dried biomass were placed in a desiccator to cool down to room temperature, after which they were weighed once more on the precision scale.

Samples were consistently taken at the centre of the channel 35 cm after the paddlewheel using a P5000 micropipette. The region after the paddlewheel was turbulent, which ensured that the samples were well mixed. Sampling was performed twice daily and three samples were taken at each time point. Additionally, the OD_{750} along with the temperature and pH (Jenway 3510) were also measured in triplicate. The algae were cultivated for a period of 16 days. The stationary phase was not reached within his timeframe. The final biomass concentration was however not the focus of these experiments as only the productivity was required.

Between each run the raceways were sterilized. The cultures were sterilized using Biocide, which gave a concentration of 300 mg L^{-1} of free chlorine in the culture. After draining the algae the raceways were filled with 50 L of tap water and 10 mL of BlackGo (active ingredient: didecyldimetylammonium chloride) was added. The raceways were then run for 24 hrs at 19.8 rpm. During this time a sponge was used to scrub the walls and paddlewheel. The fluid was then drained and the raceway refilled with 50 L of tap water to rinse any remaining BlackGo. The raceway was again run for 24 hrs at 19.8 rpm after which one more similar rinse was performed.

3.3.5 Summary of experimental blocks

The above mentioned experiments were broken downs into experimental blocks that were performed in succession. The blocks are presented in Figure 3-10 below.

1) Mass transfer experiments for the control, best slope designs of Burke (2016, the factorial DOE and actual power measurement

- Performed in a semi-random order, where the 1st run of each treatment was performed, followed by the 2nd and then 3rd
- Each run on a different day, to eliminate any bias from the equipment or local conditions in the lab
- Three runs for the control was therefore spread out over the entire period
- Actual power requirement also measured

2) Hydrodynamic experiments for the control, best slope designs of Burke (2016) and the factorial DOE

- Conductivity tracer experiments
- Phenolphthalein tracer experiments
- Triplicate runs for all tracer experiments were performed in succession
- Measurement of the wave height and fluid depth

3) Assessing slope PW in terms mass transfer and hydrodynamics

- Three independent mass transfer experiments were performed in succession, although on different days
- Followed by the conductivity and phenolphthalein tracer experiments

4) Assessing the propeller system in terms of mass transfer and hydrodynamics

- Three independent mass transfer experiments were performed in succession, on different days
- Followed by conductivity tracer experiments
- Actual power requirement also measured

5) Model testing to evaluate the efficacy of the models obtained in the factorial DOE

- Different slope configurations (not tested in the DOE) were evaluated i.t.o. k_La and energy requirements, or fluid velocity and mixing time
- Results were compared to those predicted by the models
- Details of the slope configurations tested are presented in Section 4.3

6) Algae cultivation experiments to assess the productivity

- Three independent runs for the control and two for each of the three slope configurations
- Experiments were performed in a semi-random order

Figure 3-10: Summary of experimental blocks, performed in succession.

4 Results and Discussion

4.1 Evaluating the two best performing slope designs of Burke (2016)

The 20 cm and 80 cm slope were compared to a control in terms of the hydrodynamics, CO_2 mass transfer rate and energy requirements. Changes in the mass transfer can be argued from the perspective of different hydrodynamics, which are therefore discussed first.

4.1.1 Hydrodynamics of the control, 20 cm slope and 80 cm slope

The fluid velocity is related to the circulation time obtained from the conductivity tracer experiments. Figure 4-1 depicts the circulation time for the control, 20 cm slope and 80 cm slope and gives a comparison to the data obtained by Burke (2016).

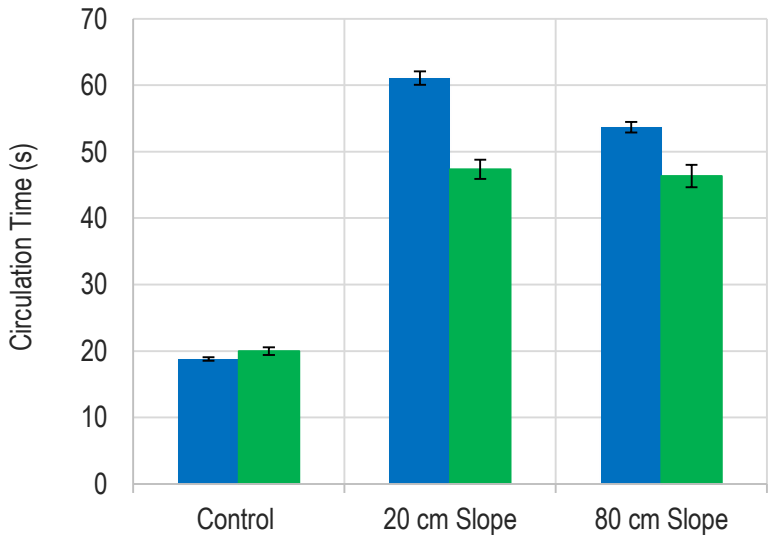

Figure 4-1: Circulation time for the control, 20 cm slope and 80 cm slope (in blue) with a comparison to the data obtained by Burke (2016), depicted in green. Error bars indicate standard error with n = 3.

The circulation time for the control was 18.8 ± 0.3 s. This value was very similar to what was obtained by Burke (2016) and corresponded to an average fluid velocity of 18.4 ± 0.3 cm s^{-1}. The two slopes showed a great increase in the circulation time compared to the control, which correlates to a decrease in the fluid velocity. The circulation time for the 20 cm and 80 cm slope was 61.1 ± 1.0 s and 53.7 ± 0.8 s, respectively, giving an average fluid velocity of 5.7 ± 0.1 cm s^{-1} and 6.4 ± 0.1 cm s^{-1}. The decrease in fluid velocity can be attributed to the resistive force that the slopes exerted on the moving fluid. The moving fluid hits the slope and experienced a reactive force normal to the surface of the slope. To simplify to a two-dimensional perspective with perfectly uniform flow, this force has a horizontal and vertical component. The horizontal component acts against the forward moving fluid, thereby slowing down the overall fluid velocity whereas the vertical component directs the flow over the slope.

The fluid velocity with the 20 cm slope was 12 % lower than that observed with the 80 cm slope. This could be explained by the slope angle. The magnitude of the horizontal component of the force is dependent on the slope angle, meaning a steeper angle leads to a higher force in the horizontal

direction, thereby slowing the fluid down even further. For both the slopes the measured circulation time was higher than what was found by Burke (2016). It is fair to assume that these differences did not arise due to any variation in the fluid properties or the methods and equipment used to obtain the circulation time, since the circulation time for the controls were so similar. These differences are potentially from manufacturing tolerance, the material that the slopes were constructed of and the way the slopes were equipped in the channel. The height of both the slopes was in actuality closer to 10.1 cm and they had a stainless steel surface. This was different from the Perspex slopes used by Burke (2016).

The measured fluid velocity for both slopes was well below the suggested 10 cm s^{-1} to prevent algae from settling (mentioned in Section 2.1.3). This could potentially be problematic for algal cultivation; it was therefore decided to incorporate the paddlewheel rotation rate (rpm) into the factorial DOE used to assess the new slope designs. The control was therefore also evaluated at the high paddlewheel rpm used in the DOE. With only two data points, however, it is not possible to identify any non-linear behaviour. A third rpm was therefore also evaluated for the control. These results are discussed at the end of this section.

Although the slopes contributed to an overall decrease in the fluid velocity, the fluid accelerated over the slope, leading to the formation of a hydraulic jump as the fluid transitioned into subcritical flow after the slope. This was accompanied by the rapid decrease in the fluid velocity. To quantify the surface turbulence, the height of the wave created by each slope was measured. Both these slopes led to the formation of an undular hydraulic jump. The jump however fluctuated in size which was due to a staggered flow pattern created by the paddlewheel. Figure 4-2 illustrates the flow over the 20 cm slope.

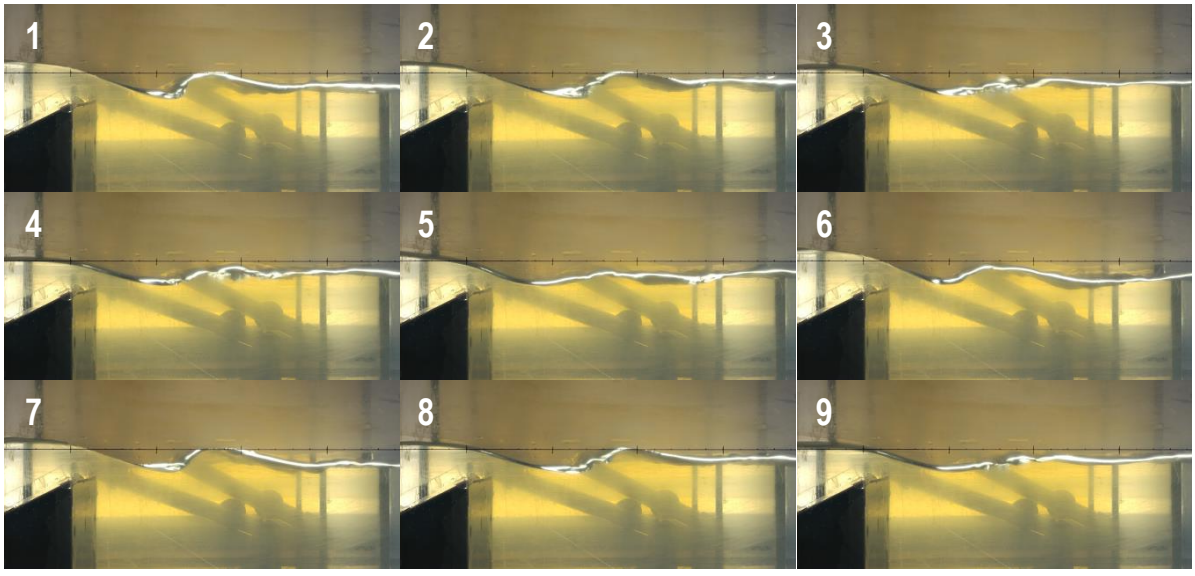

Figure 4-2: Flow pattern over the 20 cm slope showing the undular hydraulic jump. Due to the staggered flow created by the paddlewheel blades the wave was dynamic, reaching a peak height (1 and 7) before collapsing into a flatter surface (5).

The staggered pattern can be explained by the clearance between the paddlewheel blades and the channel bottom. The clearance fluctuated between a point where the blade was vertical (smallest clearance) and a point where the blade had moved half of the distance to the next blade (largest clearance). Variation in the clearance led to a fluctuating flow pattern characterized by a burst of a higher fluid velocity followed by a decrease in the velocity. This is because the size of the clearance affects the amount of backflow due to the difference in head across the paddlewheel. The staggered flow was accentuated by the slope due to an increase in the difference in head across the paddlewheel. The size of the wave after the slope therefore changed between a maximum when the

fluid velocity was at a peak (frame 1 and 7 in Figure 4-2) and a minimum with the decrease in velocity (frame 5 in Figure 4-2). No visual bubble formation was observed for these undular jumps, meaning there was minimal air entrainment.

As mentioned in Section 3.3.1, the amplitude of the wave with the maximum height was considered. The height of the wave created by the 20 cm and 80 cm slope was 13 ± 1 mm and 12 ± 1 mm, respectively. When comparing the two means, the p-value at a 95 % confidence level was 0.42, indicating that one cannot with confidence say that there was a significant difference between the wave size for these two slopes. Even though the 20 cm slope led to a lower fluid velocity, the difference in velocity was only 12 %. Using the volumetric flow rate and average cross sectional area at each crest, the resulting Froude number at each slope crest was 0.847 for the 20 cm slope and 1.021 for the 80 cm slope. These values might suggest that the wave created by the 80 cm slope should have a larger height, although here the effect of the slope angle might be responsible for the similar size. Note that the Froude numbers can be below 1 at the slope crest since critical flow is not achieved exactly at the crest but typically some distance between the crest and the first wave (Chanson and Montes, 1995).

The accelerating fluid over the slope also caused an adverse pressure gradient across the slope as the high velocity fluid (caused by the associated low pressure) rapidly decreased in velocity, accompanied by an increase in pressure. The adverse pressure gradient caused reverse flow, leading to the recirculation zone (discussed in Section 2.4.3). The recirculation zone after the 80 cm slope is depicted in Figure 4-3, visualized using the phenolphthalein tracer. Both the slopes led to the formation of a recirculation zone. This is in contradiction with what was reported by Burke (2016), who stated that the 80 cm slope did not lead to a recirculation zone.

Figure 4-3: Recirculation zone observed after the 80 cm slope. Both the 20cm and 80 cm slopes resulted in a recirculation zone of a similar size, which contradicts what was stated by Burke (2016)

It is possible that there could be no recirculation zone (like what was observed by Burke (2016) for the 80 cm slope). This would however only occur if the adverse pressure gradient is removed which can happen at a sufficiently low fluid velocity. Given that the fluid velocity with the 20 cm and 80 cm slope was very similar and that the slopes had the same height and no downslope, one might expect that both slopes would lead to a recirculation zone. The size of the recirculation zone after the 20 cm slope was estimated to be 2350 ± 200 cm^3 whereas the 80 cm slope created a 2030 ± 160 cm^3 recirculation zone. The error bars of these means overlapped slightly, giving a p-value of 0.09 when comparing the means, meaning there was no significant difference between the two (when considering a 95 % confidence level).

The phenolphthalein experiments also revealed a turbulent mixing layer between the forward moving fluid and the reverse flow below. The recirculating fluid has a lower fluid velocity opposed to the forward moving fluid, which creates a high velocity gradient leading to the mixing layer (Han, 2015). The recirculation zone therefore plays an important role in the mixing brought about by the slopes. As a result, the mixing time was greatly improved with the slopes. Figure 4-4 shows a comparison in the mixing time for the control, 20 cm and 80 cm slope as well as a comparison with the data obtained by Burke (2016).

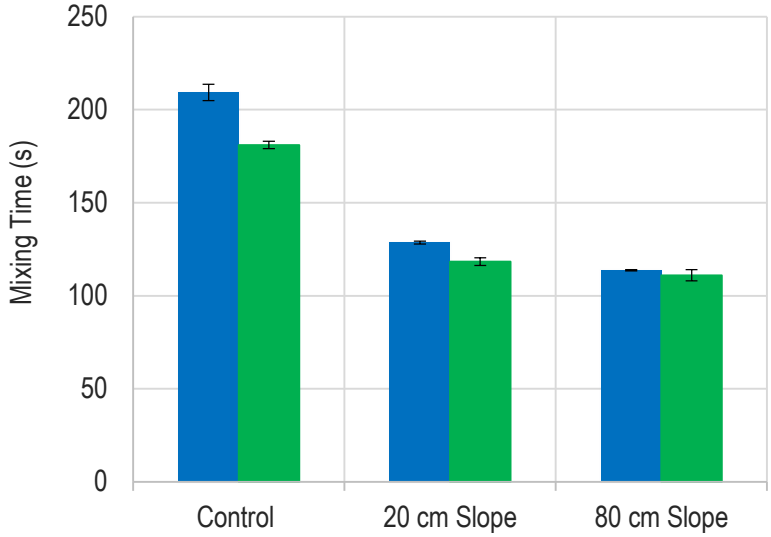

Figure 4-4: Mixing time for the control, 20 cm slope and 80 cm slope (in blue), with a comparison to the results obtained by Burke (2016), depicted in green. For the purpose of comparison the mixing condition was changed from 95% of the final steady state conductivity to 90%. Error bars indicate standard error with n = 3.

To be able to compare the data with the results of Burke (2016), the mixing condition was changed to 90 % of the final steady state value (which Burke used) as opposed to 95 %, used in this study. Similar mixing times were observed for the slope configurations, whereas the control differed with about 7 %.

A 95 % mixing condition was however used throughout this study. The mixing time for the control using the 95 % mixing condition was 255 ± 2 s whereas a mixing time of 158 ± 1 s and 142 ± 1 s was observed for the 20 cm and 80 cm slope, respectively. This is equivalent to a 38 % and 44 % decrease in the mixing time. The mixing time for the 80 cm slope was lower than the 20 cm slope which could be due to the increase in fluid velocity observed for the 80 cm slope and the resulting increase in the Froude number at the slope crest. The slightly higher fluid velocity would result in a more turbulent mixing layer. The measured wave size and the size of the recirculation zone however did not indicate any role in variation of the mixing time.

The slopes also improved the vertical mixing in the raceway, due to the nature of the recirculation zone. The slopes brought the bulk liquid in its entirety close to the liquid interface after which it entered the turbulent mixing layer. Some of the fluid gets projected towards the channel bottom and then recirculated back up once caught in the reverse flow. The Peclet number calculated for the control was 143 ± 2. According to the specifications used by Mendoza et al. (2013a), these flow conditions approached being plug flow since the Peclet number was greater than 100. The Peclet number for the 20 cm and 80 cm slope on the other hand was 27 ± 0 and 29 ± 1, respectively, indicating significant back-mixing as opposed to plug flow behaviour. Enhanced mixing is of great value in raceway ponds and should have a positive effect on the algal productivity. It not only improves vertical mixing, which should enhance the light regime and mass transfer driving force, but should also minimise temperature gradients and concentration gradients in the media. The turbulence accompanied by improved mixing does, however, come at the expense of energy losses. The energy requirements as well as the k_La for each configuration are discussed in the next section.

4.1.2 Mass transfer rate and energy demand for the control, 20 cm slope and 80 cm slope

Figure 4-5 shows the k_La and driving force for the CO_2 mass transfer rate measured for the control and both slope configurations. The mass transfer rate is the product of these two quantities. The axes have been changed to accentuate the differences between the control and slope configurations and therefore do not start at zero. In this case, there is also no direct comparison to the data obtained by Burke (2016) since these experiments were performed in tap water while Burke (2016) performed the experiments in growth media.

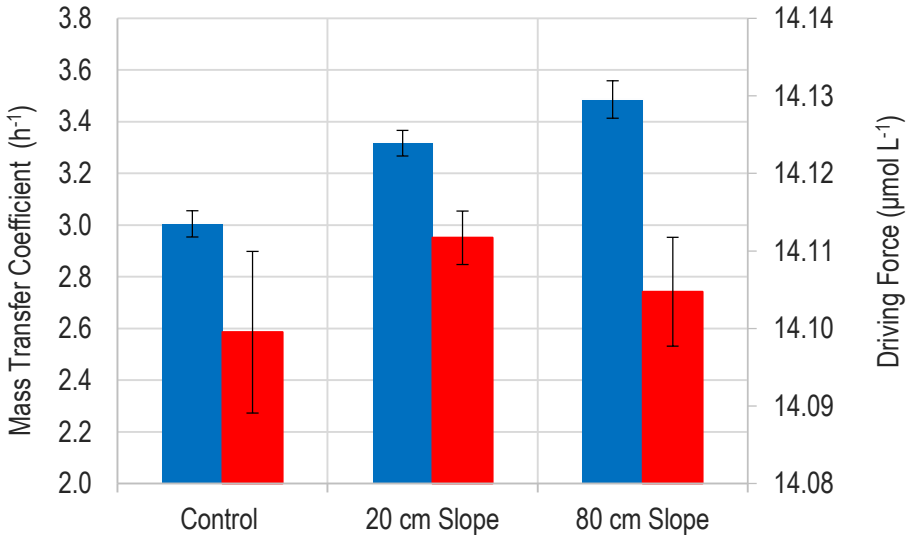

Figure 4-5: Comparison of the mass transfer coefficient (blue) observed for the control, 20 cm and 80 cm slopes, along with the mass transfer driving force (red). Error bars indicate standard error with n = 3.

Compared to the control both slopes led to an increase in k_La. The k_La observed for the 20 cm slope was 3.32 ± 0.05 h^{-1}, which corresponded to a 10 ± 2 % increase over the control whereas the 80 cm slope resulted in a k_La of 3.49 ± 0.07 h^{-1}, an increase of 16 ± 3 %. The driving force on the other hand was constant throughout all configurations. The difference between the average driving force observed with the 20 cm slope and the control was in fact only 0.09 %. This difference was assumed to be negligible and is just accentuated in Figure 4-5 through the chosen axis values. The constant driving force can be explained by the alkaline conditions in which the CO_2 mass transfer rate was measured. The driving force increases with pH (de Godos et al., 2014). At higher pH values the equilibrium in the carbonate system is pushed towards the formation of bicarbonate (HCO_3^-), meaning any dissolved CO_2 in the liquid in converted through the equilibrium reactions, ensuring a high driving force. Changes in the mixing time therefore did not contribute to any improvement in the driving force, as a high driving force was ensured by the alkaline conditions of the liquid. The improvements in the overall mass transfer rate brought about by the slopes can therefore be reflected in the k_La alone, since the driving force was constant throughout all configurations. The constant driving force was observed for all slopes and rpms evaluated. Therefore, from here on out, the focus is only on the k_La,

The observed error in the k_La stems from both random and systematic uncertainty. The random error is associated with the numerous instruments used for measurement of the required parameters to calculate the k_La. Among these are the measurement of the change in pH over time, the salinity and the alkalinity. Slight differences in the properties of the tap water that was used during the experiments (highlighted in Section 3.3.2) could also contribute to the error, along with variation in the fluid temperature (kept at 25 ± 0.5 °C). The method of measuring the alkalinity also introduces two potential sources of systematic errors: the molarity of the acid used in the titration, as well as the approach of using a Gran titration to measure the alkalinity. A different method to measure the

alkalinity could potentially yield different results. However, a standard alkalinity solution was used to verify the method and ensure that the molarity of the acid that was used was accurate (as mentioned in Section 3.3.2).

The k_La is affected by the fluid properties as well as the interfacial surface area and surface turbulence (which decreases the stagnant liquid film thickness). Since the fluid properties were kept constant across each configuration tested, the increase in k_La was brought about by the enhanced surface turbulence and to a far lesser extent the increase in surface area (caused by the hydraulic jump). When comparing the two means, one cannot confidently say that there was a significant difference between the two k_La's for the slopes ($p = 0.13$). This becomes clearer when considering the standard deviation for each observed k_La: 3.32 ± 0.09 h^{-1} for the 20 cm slope and 3.49 ± 0.12 h^{-1} for the 80 cm slope, indicating an overlap in the error bars. Considering the similarity in the wave properties as well as the fluid velocity observed for both slopes, it might be expected that both led to a similar k_La. Even though the differences in the means were insignificant, the average k_La for the 80 cm slope was 5 % higher compared to the 20 cm slope. This could potentially be explained by the slightly higher fluid velocity observed with the 80 cm slope.

The results of Burke (2016) also indicated that there was no significant difference between the k_La's observed for these two slopes. The percentage increase in k_La compared to the control in this study was, however, far lower than that observed by Burke (2016) (58 ± 18 % for the 20 cm slope and 80 ± 25 % for the 80 cm slope). This is potentially due to either the difference in the fluid used during experimentation (tap water as opposed to media) or the higher fluid velocity measured for the slopes by Burke (2016). The 80 cm slope of Burke (2016) led to an average fluid velocity of 7.5 cm s^{-1} as opposed to the 6.4 cm s^{-1} velocity for the 80 cm slope in this study, a 15 % difference. It is however not expected that this change in velocity led to an 80 ± 25 % increase in k_La compared to the control as opposed to a 16 ± 3 % increase. This is shown in Section 4.3, where some of the new slope designs improved the fluid velocity, without a significant improvement in the k_La.

Literature k_La values also vary significantly since it depends on the raceway geometry, operating conditions (including whether sparging is used) and method of measurement (including the placement of instrumentation). Many sources also only report on the O_2 mass transfer coefficient, obtained using a dynamic gassing out method. Mendoza (2013b) found an overall k_La_{O2} of 1.8 h^{-1} in a 100 m^2 raceway using water and no gas sparging in the carbonation sump. In a 2.1 m^2 raceway pond, Cheng et al. (2018) obtained a k_La_{O2} in the range of 1.9 - 7.1 h^{-1} at various operating conditions. In this case gas sparging was used and the experiments were performed in growth media. In each of these instances one can expect the k_La_{CO2} to be slightly lower than k_La_{O2} due to the relative diffusivity of the species in water (Aitchison et al., 2007). This does show that the k_La's obtained for the control and slopes in this study are reasonable, as they are close to what one can expect in a raceway pond.

Even though the slopes showed an increase in k_La compared to control, it is inadequate to judge the slopes solely on the k_La. The energy demand also needs to be considered. The theoretical energy requirement is dependent on the total head loss throughout the raceway and the volumetric flowrate (through Equation 3-7). A breakdown of the total head loss as well as the volumetric flow rate for each configuration is presented in Table 4-1 below.

Table 4-1: Breakdown of head loss and volumetric flowrate for the control, 20 cm slope and 80 cm slope. These two components determine the theoretical energy required. For each value the standard error is also shown, propagated from the error in fluid velocity and the measured fluid depth.

Configuration	Total Head Loss (mm)	Concentrated Head Loss (mm)	Distributed Head Loss (mm)	Head Loss due to Slope (mm)	Volumetric Flowrate (L s^{-1})
Control	2 ± 0	1 ± 0	1 ± 0	-	3.3 ± 0.0
20 cm Slope	12 ± 1	0 ± 0	0 ± 0	12 ± 1	1.0 ± 0.0
80 cm Slope	12 ± 2	0 ± 0	0 ± 0	12 ± 2	1.1 ± 0.0

The total head loss consisted of the concentrated head losses around the bends, the distributed head losses through the straight channels and the head loss due to the slope (if applicable). The concentrated and distributed losses for the control were greater than what was observed for the slope configurations. This is due to the dependency of these head losses on the fluid velocity. The head loss increases exponentially with velocity. The slopes however decreased the fluid velocity, which meant that the head losses around the bends and in the straight channels were much less. These were in fact non-zero, but could not be reported with integer values on a millimetre scale.

Typically in raceway ponds the concentrated head losses dominate the contribution to the total head loss (Chiaramonti et al., 2013). This was however not the case for this raceway, where a more equal split between the concentrated and distributed losses were observed (for the control). This can be explained by the bend loss coefficient, k_b, which was 0.27 for this raceway control as opposed to 1.5 - 4 for typical raceway dimensions. The k_b is dependent on the dimensions of the bend, which was different to typical large scale raceway dimensions. The bend dimensions of larger raceways therefore lead to higher losses in the bends relative to the friction in the straight channel, which are reflected in the higher bend loss coefficient. For the slope configurations however the head loss due to the slope accounted for roughly 97 % of the total head losses (in both cases). These losses occurred due to the hydraulic jump and recirculation zone.

The volumetric flow rate also affects the theoretical energy demand. The control had a volumetric flow rate of roughly three times that of the slope configurations (3.3 ± 0.0 L s^- compared to 1.0 ± 0.0 L s^-). This was however overshadowed by the more than fivefold increase in the total head loss for the slope configurations. This meant that the theoretical energy required for the slope configurations was much greater than that of the control. The theoretical energy requirement is presented in Table 4-2, along with the actual energy input (measured with the power meter), overall efficiency and a comparison in the k_La per unit of energy.

Table 4-2: kLa and energy demand for the control, 20 cm slope and 80 cm slope. Error indicates the standard error.

Configuration	Theoretical Energy Required (W)	Actual Energy Input (W)	Overall Efficiency (%)	k_La per Theoretical Energy Required (W^{-1} h^{-1})	k_La per Actual Energy Input (W^{-1} h^{-1})
Control	0.06 ± 0.00	11.24 ± 0.26	0.55 ± 0.01	48 ± 1	0.27 ± 0.01
20 cm Slope	0.12 ± 0.01	11.16 ± 0.29	0.97 ± 0.06	28 ± 2	0.28 ± 0.01
80 cm Slope	0.13 ± 0.02	11.22 ± 0.22	1.12 ± 0.16	28 ± 4	0.31 ± 0.01

When comparing the slope configurations to the control, the theoretical energy required roughly doubled. This was primarily caused by the head loss due to the slopes, which greatly increased the total head loss. The actual energy input measured using the power meter was however very similar throughout all three configurations (Table 4-2). This meant that the overall efficiency for the slope configurations was greater than the efficiency for the control. The increase in overall efficiency can however be explained when the size of the motor driving the paddlewheel is considered. A 370 W motor was used to produce work of around 11 W. This meant that the motor was oversized and operated at a low efficiency, although in a region where a small increase in the power output coincides with a large increase in the motor efficiency. It would make sense for the slopes to increase the actual power requirements. The greater difference in head across the wheel meant that the water in front of the paddlewheel pushed back against each blade with a higher force. In this case however, the increased power requirement was compensated for by an increase in the motor efficiency, which could explain the similarity in the actual energy input. The low overall efficiencies observed throughout were not too far off from overall efficiencies for paddlewheel driven raceway ponds found in literature. Huang et al. (2015) reported overall efficiencies that varied between 1 and 5 % whereas Chiaramonti et al. (2013) reported an overall efficiency of 5 %.

When considering the k_La per unit of theoretical energy required, the control then outperformed the slope configurations. For these slopes, the increase in the theoretical power required was greater

than the increase in k_La. For this specific raceway setup however, the k_La per unit of actual energy input was better for the slope configurations. It would therefore be better to operate this specific raceway at a higher rpm, along with the addition of a slope. Increasing the rpm would be more energy efficient up to a point where the motor efficiency reaches an ideal value, where it is more stable with changes in the power output of the motor. In practice however it is fair to assume that the motor would operate close to its ideal efficiency. Evaluating the actual energy requirements in this case is therefore not very fruitful, as the outcome is specific to this raceway setup and would change if this raceway had a smaller size motor. In this case the k_La per theoretical energy required is therefore a better metric to evaluate the slopes on and will be used from here on out. It is however not without its limitations.

One limitation is that the theoretical energy demand on its own would only give an accurate indication of the actual power requirements if the overall efficiency remains fairly constant across the different configurations that were evaluated. In such a case, the actual energy demand in all cases could then be obtained by dividing the theoretical energy with the constant efficiency. But a constant overall efficiency is not a given. As literature indicated, the difference in head across the paddlewheel affects the paddlewheel efficiency. With the available information however, it was not possible to determine the paddlewheel efficiency. It was therefore also not possible to determine whether the observed difference in head had a significant effect on the paddlewheel efficiency. In such a case the overall efficiencies would differ. Regardless, if the motor was indeed operated at an ideal efficiency, it is more likely that the control would have a better overall efficiency, since the lower difference in head across the wheel would increase the paddlewheel efficiency.

Since the k_La per unit of theoretical energy required is used to compare the configurations, the control outperformed the slope configurations. This brings up the questions of whether a slope is required as opposed to just increasing the paddlewheel rpm. The control was also evaluated at different rpms (discussed below), but this question is only answered more thoroughly once the improved design have been discussed. As mentioned, the control was evaluated at three different rpms. The higher rpm used in the factorial DOE was assessed as well as a lower rpm to identify any non-linearity in the measured variables with changes in rpm.

4.1.3 Control at different paddlewheel rpms

Figure 4-6 illustrates the change in fluid velocity and mixing time with the paddlewheel rpm. An increase in paddlewheel rpm led to a fairly linear increase in the fluid velocity (R^2 = 0.990) and a linear decrease in the mixing time (R^2 = 0.999).

Mixing in the pond is brought about by the turbulence throughout the pond (related to the fluid velocity) and the turbulence created by the paddlewheel. The linear decrease in mixing time therefore is sensible, considering the fairly linear increase in the fluid velocity. Even though the linear trend in the velocity had a high R^2 value, the increase in velocity appeared to diminish as the rpm increased. This is indeed in accord with literature. Hreiz et al. (2014) found that the fluid velocity increased linearly at low paddlewheel rpms, in which case the paddlewheel behaves like a positive displacement pump. At higher rpms however, Mendoza et al. (2013a) reported that the increase in velocity does not stay linear, but diminishes. This could be explained by the increase in head loss throughout the raceway with an increase in rpm. At a low rpm the difference in head across the paddlewheel might not affect the backflow (through the clearance between the blades and walls) significantly. However, higher rpms accompanied by the greater difference in head across the paddlewheel result in more backflow, which negatively impacts the fluid velocity. A similar non-linear effect might be expected with the mixing time at higher rpms, since the turbulence created by the fluid velocity will diminish at higher rpms.

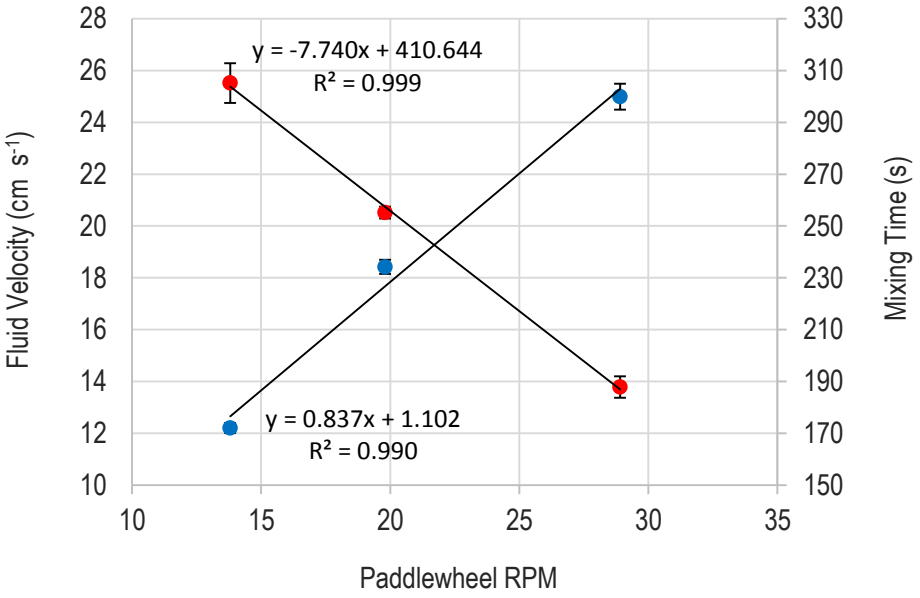

Figure 4-6: Fluid velocity (blue) and mixing time (red) as a function of paddlewheel RPM for the control. With an increase in paddlewheel RPM the fluid velocity increased fairly linearly whereas the mixing time decreased linearly. Error bars indicate standard error with n = 3

Figure 4-7 shows the effect of paddlewheel rpm on the k_La and k_La per unit of theoretical energy required. The k_La increased linearly with rpm (R^2 = 0.997) whereas the k_La per unit of theoretical energy required decreased non-linearly. It is unclear whether this trend will be followed at higher rpms, but based on the linear increase in fluid velocity and mixing time in the range of rpms tested, a linear increase in the k_La could be expected.

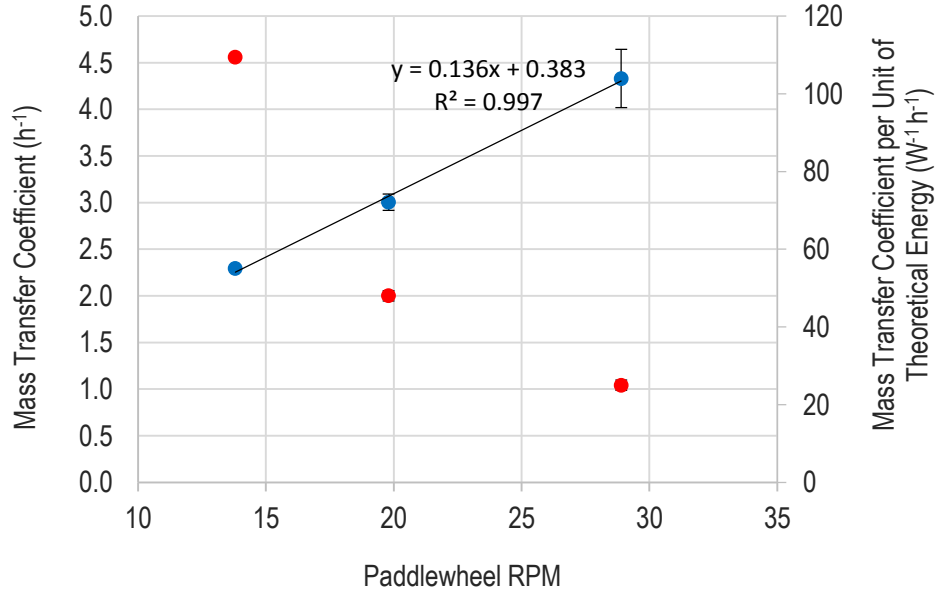

Figure 4-7: The mass transfer coefficient and mass transfer coefficient per unit of theoretical energy as a function of the rpm for the control. The mass transfer coefficient increased linearly with rpm while the mass transfer per unit of theoretical energy decreased non-linearly. Error bars indicate standard error with n = 3, the k_La at 13.8 rpm however was not performed in triplicate and therefore does not have an error bar.

The non-linear decrease in k_La per unit of theoretical energy requirement stems from the relation between the paddlewheel rpm and fluid velocity. Frictional losses increase exponentially with fluid velocity (which can be seen in Equation 3-8 and Equation 3-9). This means that the theoretical energy increases exponentially with the fluid velocity (a non-linear increase in the energy requirements with paddlewheel rpm was also found by Mendoza et al. (2013a)).

As mentioned, the k_La per unit of actual energy input would better reflect raceway ponds in practice as opposed to evaluating the k_La per unit of theoretical energy required. For the control, the k_La per unit of actual energy input increased from 0.22 W^{-1} h^{-1} at 13.8 rpm to 0.34 W^{-1} h^{-1} at 28.9 rpm (as opposed to decreasing like the k_La per unit of theoretical energy requirement). Here it is shown again that the overall efficiency of the system increases with rpm due to the oversized motors. These results indicate that for this specific raceway setup, when the actual energy requirements are considered, it is best to operate at a higher rpm. The maximum rpm at which to operate would likely be determined by the shear stress the algae cells can withstand. When considering the k_La per theoretical energy requirement however, it is best to operate a raceway at a lower rpm. The choice of rpm should then be guided by considering the fluid velocity and its effect on settling and mixing in the pond. It is therefore important to also evaluate the productivity per unit of energy requirement, as the hydrodynamic and CO_2 mass transfer experiments alone cannot be used to obtain ideal operating conditions.

The effect of paddlewheel rpm in conjunction with the slopes are discussed in Section 4.3, which presents the results of the factorial DOE. The DOE was performed to attempt to improve on the weir-like slope designs that create a hydraulic jump. The two designs of Burke (2016) evaluated here were overall very similar in terms of the hydrodynamics, mass transfer and energy requirements. The mixing time was greatly improved compared to the control, although the control showed a better k_La per unit of theoretical energy required. These designs however created a hydraulic jump. A large focus of the work of Burke (2016) was to create breaking waves similar to shoaling ocean waves, but these breakers were never observed. Slope PW was designed with the aim of creating ocean breakers, which is discussed in the next section.

4.2 Creating ocean breakers in the raceway

The second approach to create surface disturbances was to mimic shoaling waves in the ocean. As discussed in the literature review, the motion of the paddlewheel creates a pulse that travels through the raceway. Slope PW was design to utilize this pulse in an attempt to create breaking waves on the slope.

4.2.1 Design considerations for slope PW

A large focus of the slope designs of Burke (2016) was to create breaking waves that mimic shoaling wave in the ocean - but this effect was never observed. A likely cause was the properties of the pulse created by the paddlewheel in relation to the dimensions of the slopes. The properties of the pulse were measured at an RPM of 19.8 with no slope in the channel. It was found that the wave height and length were 8 mm and 413 mm, respectively, giving a wave steepness of 0.019. The wave length was obtained by calculating the wave speed and period using slow motion video (https://figshare.com/s/00ec7e5192c6be962de8, Raceway 1). Such a small wave requires the surface of the slope to be very close to the surface of the water and for a sufficiently long distance to allow the wave to fully develop and break. The depth at which this wave will break is roughly 10 mm, based on calculations using Equation 2-22 and Equation 2-23 (https://figshare.com/s/00ec7e5192c6be962de8, Raceway 1). Equation 2-23 was however determined empirically, and the validity of this equation was in question. Although the wave steepness (0.019) was within the range of the empirical data used to obtain Equation 2-23, the observed wave height was very small. The wave height of 8 mm was much smaller than the waves found in literature on the study of breaking ocean waves. Although this equation predicted that a breaking wave would form at this specific depth, it was unclear whether the

surface tension might be too strong to lead to a proper breaking wave. Regardless, this depth was used as a ballpark to give an idea of how close the slope had to be to the surface of the water.

Slope PW is illustrated in Table 3-3, along with its dimensions. In this design a gentler slope was brought much closer to the water surface to allow the pulse to experience the frictional forces of the slope surface. Since this approach only utilized the pulse created by the paddlewheel, there was no need for it to start from the bottom of the channel. Fluid could therefore travel below the slope which also meant that the fluid velocity and overall head loss would not be drastically impacted.

Applying Equation 2-30 (which relates the slope angle and wave properties to the Iribarren number), a slope angle was chosen to give an Iribarren number roughly in the centre of the range to create spilling breakers. A slope angle of 2 ° was used, which corresponds to and Iribarren number of 0.25 (https://figshare.com/s/00ec7e5192c6be962de8, Raceway 1). Although plunging breakers lead to more turbulence and air entrainment, these waves were even less likely to develop due to the increased surface tension experienced by the waves at this small scale. Plunging breakers also require a steeper slope angle, meaning that for the majority of the slope length the slope surface would be too deep to affect this small wave through friction. The depth of the slope crest was chosen to be slightly below the estimated depth required to form breaking waves (10 mm). The slope length was not calculated in any way.

4.2.2 Hydrodynamics of slope PW

Slope PW had a clear effect on the pulse created by the paddlewheel. Figure 4-8 illustrates the waves observed on the slope. Friction from the slope slowed the fluid down and caused the wave to steepen. The height of the wave depicted in Figure 4-8 a) was roughly 11 mm. It is however clear that this was not enough to form a breaking wave. Instead of the typical patch of turbulence seen on the front face of spilling breakers in the ocean, the front of the wave had a number of ripples on it. A clear front view of the ripples could not be obtained, although they can be seen in the side view from the broken meniscus (Figure 4-8 b). It is likely that surface tension played a significant role in preventing the formation of a proper breaking wave. The ripples on the front of the wave were also not always present. Some of the waves did not develop these ripples, likely due to variation in the approaching pulse created by the paddlewheel.

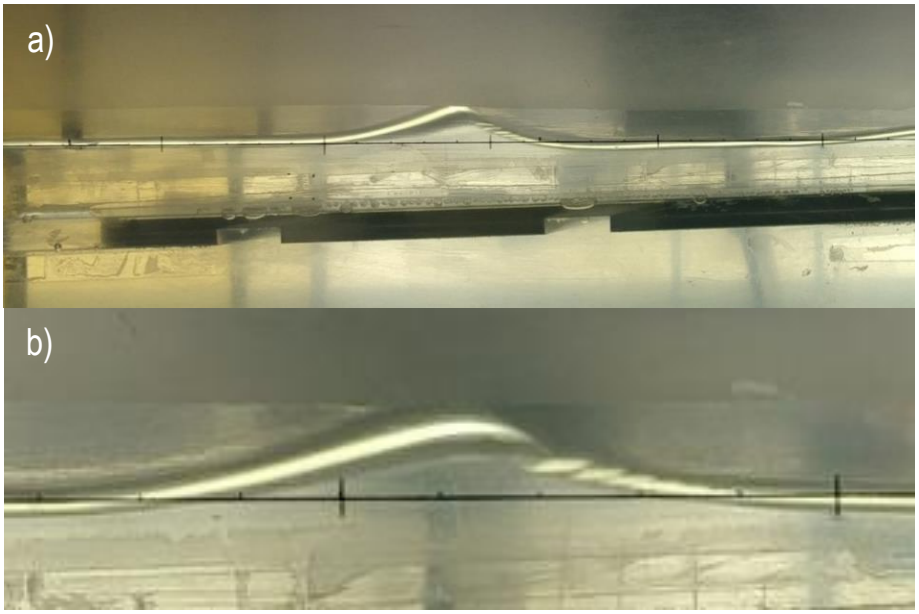

Figure 4-8: a) Progressive wave created by slope PW. The friction from the slope causes the pulse from the paddlewheel to steepen. It was clear however that a breaking wave did not form. There were however a number of ripples that formed on the front of the wave, as seen by the broken meniscus in b).

The waves typically peaked in height just before halfway along the slope. After this the height gradually decreased before collapsing once the wave crossed the end of the slope. The phenolphthalein indicator was used to view the flow pattern created by the slope, illustrated in Figure 4-9. In Figure 4-9 a), it is shown that the fluid velocity on the slope decreased: the bulk fluid in pink has already crossed the end of the slope compared to the fluid on the slope. Figure 4-9 b) occurred a few seconds after a), where the bulk fluid has passed the slope and the pink fluid on top has reached the end of the slope. This image also shows a mixing layer after the slope, brought about by the conversion of two streams with different fluid velocities. The mixing layer was not considered during the design of slope PW. A future consideration in the design of these slopes could be to improve on the mixing layer, for example by increasing the velocity gradient between the two streams. This could potentially be done by exploring a different slope roughness or to further extend the length of the slope to increase friction.

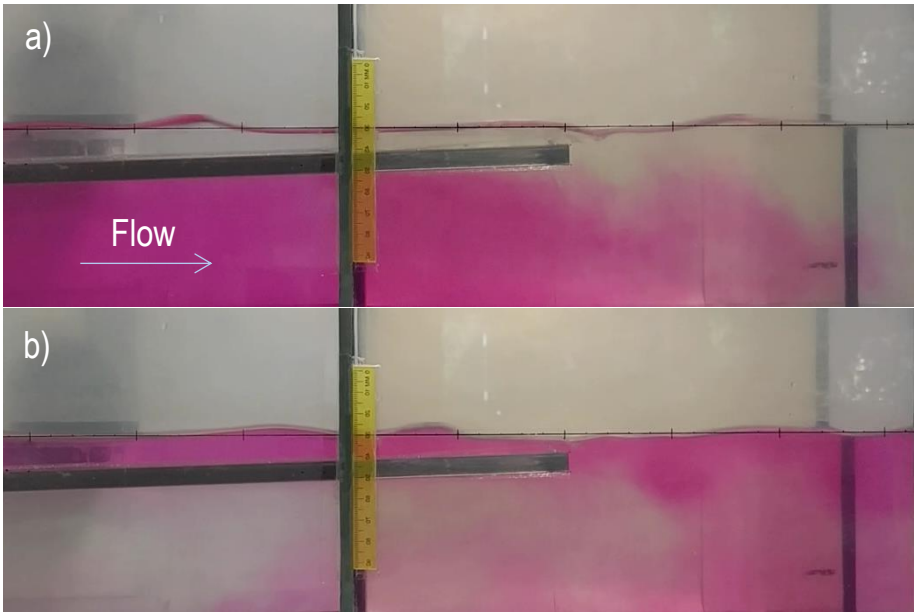

Figure 4-9: Flow pattern over slope PW visualized using phenolphthalein. The fluid on the slope slows down due to friction, as seen in a), where the tracer has not reached the end of the slope compared to the bulk fluid. b) The mixing layer after the slope due to the convergence of two streams with different velocities.

Compared to the control without the slope, the average fluid velocity was not significantly impacted. Table 4-3 shows a comparison in the measured hydrodynamics between slope PW and the control operated at the same rpm. On average the fluid velocity was slightly lower than the control, although the standard errors overlapped. There was no significant difference between the means, at a 95 % confidence interval ($p = 0.25$). This shows that the slope added little resistance to the flow, which is also what one might expect given the gentle angle of the slope.

Table 4-3: Comparison between the control and slope PW in terms of fluid velocity, mixing time and the Peclet number. For each case the standard error is also shown with n = 3.

Configuration	Fluid Velocity (cm s^{-1})	Mixing Time (s)	Peclet Number (-)
Control	18.4 ± 0.3	255 ± 2	143 ± 2
Slope PW	17.9 ± 0.3	210 ± 1	119 ± 2

The mixing time on the other hand decreased by 18 % from 255 ± 2 s to 210 ± 1 s. It is fair to assume that the wave on the slope did not contribute to any turbulence that decreased the mixing time. This decrease can be attributed to the mixing layer after the slope. The back-mixing brought about by the mixing layer is reflected in the decrease in the Peclet number, from 143 ± 2 to 119 ± 2. The mixing time and Peclet number do however not compare to the low values observed for the 20 cm and 80 cm slope. The Peclet number above 100 indicated that there was still primarily plug flow throughout the raceway. The advantage of this slope however is the little effect on the fluid velocity and the lower increase in the energy requirements, discussed next.

4.2.3 k_La and energy demand

A comparison between the k_La and energy demand for Slope PW and the control is presented in Table 4-4.

Table 4-4: Comparison between the control and slope PW in terms of the mass transfer coefficient, theoretical energy and the mass transfer coefficient per unit of theoretical energy. For each case the standard error is also shown with n = 3.

Configuration	k_La (h^{-1})	Theoretical Energy Required (W)	k_La per Theoretical Energy Required (W^{-1} h^{-1})
Control	3.00 ± 0.09	0.06 ± 0.00	48 ± 1
Slope PW	3.07 ± 0.19	0.09 ± 0.02	36 ± 8

At a 95 % confidence level, there was no significant difference in the mean k_La observed for the control and slope PW ($p = 0.65$). This makes sense considering that the waves on slope PW did not break properly. The argument that the waves did not contribute to any turbulence that decreased the mixing time is then also further supported. If the waves did contribute to the lower mixing time through surface turbulence, these effects would likely be reflected in the k_La. There was however a 37 ± 29 % increase in the theoretical energy required. The large error in this percentage increase stems from the error in the calculated theoretical energy requirement for slope PW. The large error was due to the proportionality of the power expended by slope PW to the fluid velocity cubed (v^3), through Equation 3-13. The error in the fluid velocity was greatly amplified when propagated to the error in the theoretical energy required. The k_La per unit of theoretical energy required therefore also had a large error, although the average value was significantly lower than what was observed for the control. This lower value naturally stems from the lack of an increase in k_La in combination with the increase in the theoretical energy requirements.

Again we can ask the question of whether the slope is required in this raceway. Since the control was evaluated at three different rpms, it's possible to obtain the rpm at which the theoretical energy for the control and slope PW are matched. Operating the control at an rpm of 22.4 corresponds to a theoretically required energy of 0.09 W (similar to average of slope PW). At this rpm, the mixing time would be 237 s whereas the k_La would be 3.43 h^{-1} (https://figshare.com/s/00ec7e5192c6be962de8, Raceway 2). The control would therefore have a higher k_La (by 12 %) but also a higher mixing time (by 13 %). The control therefore favours the k_La while the slope favours the mixing time. Both these properties could have an effect on the algal productivity. These relations are explored in more detail in the discussion on the algae cultivation experiments.

Even though breaking waves were not formed on this scale, this slope has interesting implications on a larger scale. In a larger raceway, where the pulse created by the paddlewheel would have a larger amplitude, it might still be possible to form breaking waves on the slope. In such an event, the mixing layer after the slope would have an additional advantage. Fluid on the slope would presumably be enriched with CO_2 due to enhanced gas mass transfer. The mixing layer then promotes distribution of this fluid into the bulk liquid, relieving the CO_2 concentration gradient. Further considerations for scale-

up are discussed in Section 4.6, once the improvements to the weir-like slope designs have also been discussed (which is presented in the next section).

4.3 Improving the weir-like slope designs

The weir-like slope designs led to the formation of a hydraulic jump. The factorial DOE was performed to get a better understanding of how the slope parameters in conjunction with the paddlewheel rpm affected the hydrodynamics (including the size of the wave in the hydraulic jump), k_La and energy demand. The thought process behind the selection of the slope parameters is discussed first, followed by the experimental results for the hydrodynamics, k_La and energy demand. The discussion initially focusses on how and why the factors in the DOE affected the responses and then turns to the preferred slope parameters and the selection of the slopes used for the cultivation experiments.

4.3.1 Design considerations for the new weir-like slopes

The designs of Burke (2016) led to the formation of a hydraulic jump, in which case the slope acted like a weir. This was the second approach to surface turbulence. Improvements to these designs were focused on enhancing the turbulence of the waves formed and removing the recirculation zone after the slope. As stated in the literature review (Section 2.4.3), a larger jump is proportional to higher turbulence which would lead to a higher CO_2 mass transfer into the system. The wave amplitude can be affected by the inflow Froude number and upstream slope angle, where in both cases a higher value could increase the wave amplitude. Turbulence can also be enhanced by decreasing the level of submergence, which could be varied slightly by varying the slope height, although submerged conditions would always remain. The slope height also contributes to the resistance to flow, which affects the energy demand and fluid velocity. Reducing the height increases the fluid velocity, which is considered a good aspect, although there would be some minimum height at which the surface of the fluid is no longer disturbed and this affects the k_La. It would be possible to determine the required height of the slope to ensure critical flow given enough information on the upstream flow conditions (velocity and fluid depth). However, in a raceway setting this would be a difficult task, as the slope height affects the downstream velocity which in return affects the upstream conditions.

Another focus to improve the gas mass transfer was on the recirculation zone. It was speculated that the recirculation zone contributed to a decrease in the mass transfer due to a reduction in turbulence and surface renewal. It was also possible that this zone could be an area where algae would settle, which would reduce the algal productivity. The size of the recirculation zone after the slope can be reduced by incorporating a downstream slope. As mentioned, the down slope reduces the adverse pressure gradient after the slope crest, thereby decreasing the backflow and reducing the size of the recirculation zone. Since energy losses also occur in the recirculation zone, it was speculated that adding the downslope could lead to a slope design that reduces the energy requirements. Decreasing the angle of the downstream slope however could negatively impacts the hydraulic jump, since it removes the abrupt expansion of space directly after the slope crest. This sudden expansion and dissipation of energy is required to form the hydraulic jump.

Initially, the DOE consisted of a 2^3 factorial design, with centre points. The three factors under consideration being the upstream slope angle, downstream slope angle and slope height. In this case the paddlewheel RPM would've been kept constant. However, experimentation on the best slope designs of Burke (2016) showed that the average fluid velocity in the raceway was well below 10 cm s^{-1}. This is a recommended minimum fluid velocity required to prevent algal sedimentation (Becker, 1994; Dodd, 1986). This meant that for these slopes the paddlewheel RPM would need to be increased to obtain a more favourable fluid velocity. But performing the factorial design using a constant fluid velocity throughout was not possible. Keeping the fluid velocity constant would require different paddlewheel RPMs for different slope designs. Since the RPM also affected the CO_2 mass transfer (which was used as a response in the DOE) it had to be incorporated as a factor in the DOE. Increasing the paddlewheel RPM additionally increases the inflow Froude number at the slope which would increase the size of the waves. This however comes with an additional consumption of energy,

adding to the trade-offs tested. A reiterated DOE involved adding the motor frequency as a fourth factor, which related to the paddlewheel RPM. The design was changed to a 2^{4-1} fractional factorial design, which tested eight different slope configurations in which two levels of each factor were evaluated. The fractional design was chosen to significantly reduce the number of runs in the design. Details of the different treatments are depicted in Table 3-2.

The upslope angle of 25 ° was similar to the angle of the 20 cm slope and was used as the low level in the DOE. The higher angle was selected to be roughly in between the angle of 25 ° and 90 °. The low level of the downslope angle (10 °) was selected to create a design similar to a Crump weir (discussed in Section 2.4.3) where the length to height ratio was roughly 1:5. The high level of the angle was selected to be roughly in between the angle of 10 ° and 90 °. The high level of the slope height was selected to be the same as the best designs of Burke (2016), at 10 cm. The height used for the low level was not calculated in any way, but was selected to be 1 cm lower than the high level. The low level of the motor frequency was selected to be the same as the control (13.8 Hz, giving a paddlewheel RPM of 19.8) while the high level (20 Hz, to give 28.9 RPM) corresponded to the RPM required to obtain an average fluid velocity of roughly 10 cm s^{-1} for the 20 cm slope. Since the motor frequency was used as the input, it was possible that the different slopes could lead to a discrepancy between the motor frequency and paddlewheel RPM. For example, a higher slope could result in a greater reactive force exerted on the paddlewheel blades by the water, which could lead to slippage of the drive belt. To ensure that the relation between motor frequency and paddlewheel RPM was consistent throughout all slope configurations, the actual paddlewheel RPM was measured for each configuration using a stopwatch (https://figshare.com/s/00ec7e5192c6be962de8, Raceway 1). No discrepancies were found between the motor frequency and paddlewheel RPM. Since two different paddlewheel RPMs were evaluated in the DOE, the control without a slope was also assessed at the higher RPM.

4.3.2 Factorial DOE to assess hydrodynamics

Surface waves and flow patterns

The initial plan was to use the wave height as a response in the DOE to relate the slope parameters to the size of the wave, which in turn would relate to the surface turbulence and k_La. This however relied on a fixed relation between the wave height and surface turbulence, which was a preliminary assumption. Figure 4-10 illustrates examples of the observed flow patterns.

The eight slope configurations evaluated in the DOE led to different flow patterns after the slope crest. Three distinct patterns were observed: the undular jump, the impinging jet and a flow pattern that more closely resembled the surface jump (as described in the literature review, Section 2.4.3). This third pattern was likely a transition between the undular jump and surface jump, and was characterised by a flatter and longer wave without prominent surface undulations. Due to variation in the flow patterns, the assumption that the surface turbulence was related to the wave height fell away. The DOE was therefore not used to determine the effects of the slope parameters on the wave height. It was however possible to distinguish which factors led to which flow patterns.

The downslope angle primarily governed which flow pattern arose. In general, the 39 ° angle led to the undular jump, which can be seen in Figure 4-10 (a-c), whereas the 10 ° angle led to the transitional flow pattern, shown in Figure 4-10 (d-f). The impinging jet flow pattern on the other hand formed only with slope configuration HHHH and was due to a three-factor interaction. With a slope height of 10 cm in combination with the 39 ° downslope, the impinging jet formed when the paddlewheel rpm was above a certain value. This value was found to be roughly 25 rpm. Figure 4-11 a) shows slope configuration HHHH, operated at the 28.9 rpm used in the DOE, as well as the same slope operated at 25 rpm, which led to an undular jump. With the impinging jet flow pattern a jet of fluid followed along the surface of the downslope, bringing the recirculation zone to the fluid surface as opposed to the bottom. This is visually shown in the next section, when the size of the recirculation zone is discussed. The occurrence of the impinging is likely due to the effect of the rpm on the submergence of the slope, as different rpms affected the upstream and downstream fluid depth.

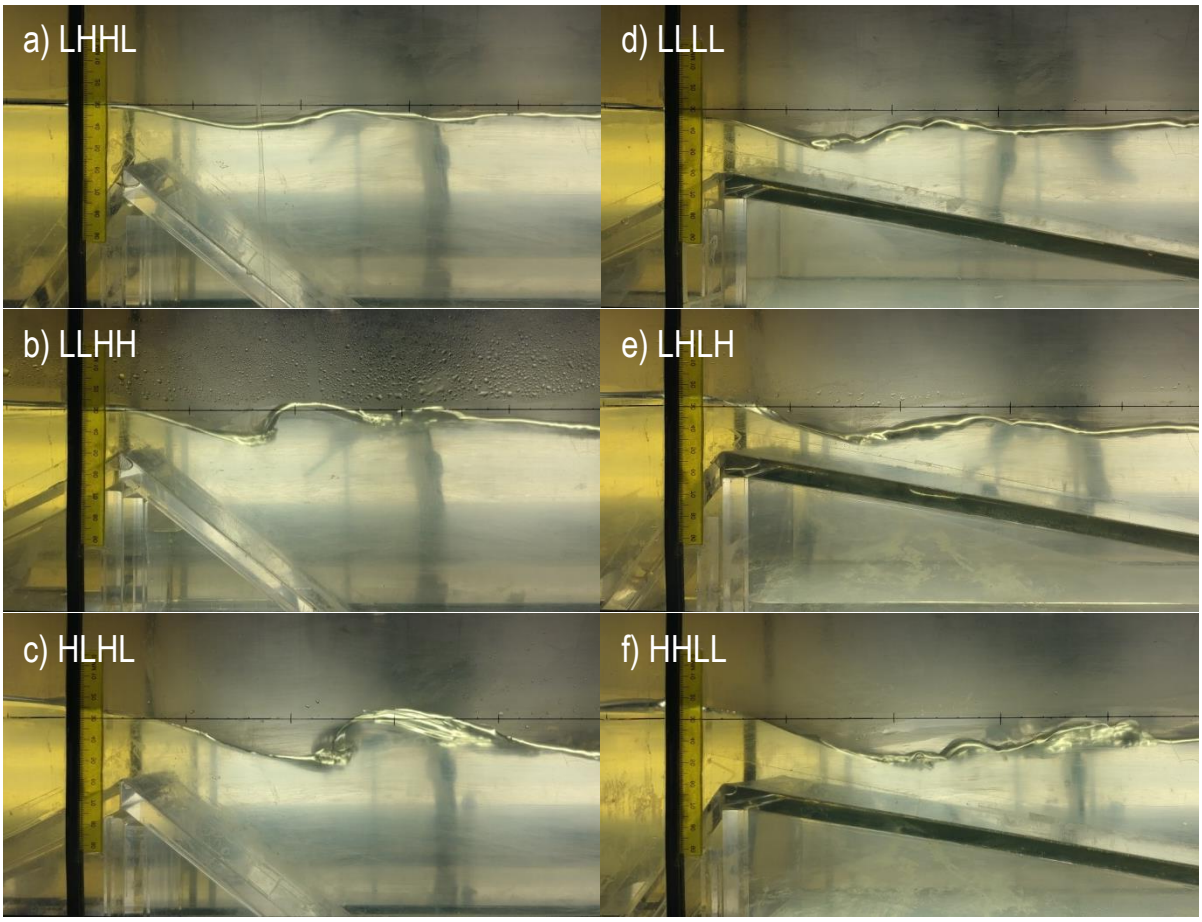

Figure 4-10: Examples of two different wave flow patterns observed for different slope configurations. a-c) depict the undular jump, for slope configuration LHHL, LLHH and HLHL respectively. d-f) depict a pattern closer to a surface jump, for slope configuration LLLL, LHLH and HHLL respectively.

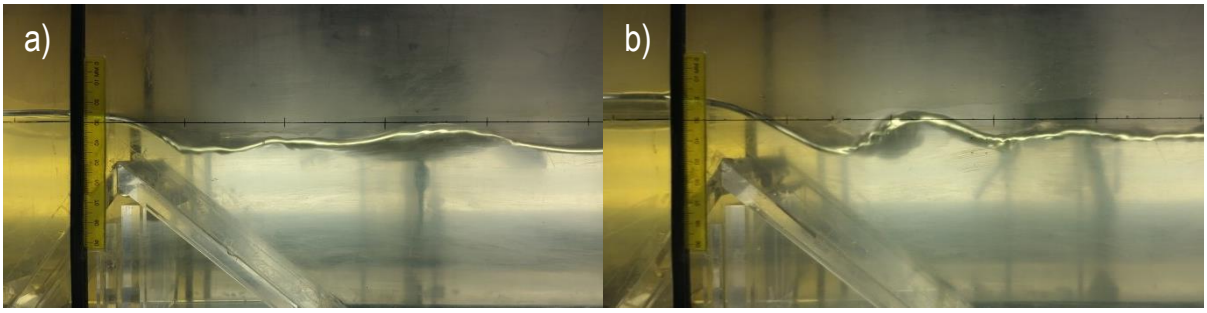

Figure 4-11: a) Impinging jet flow pattern observed for slope configuration HHHH, at 28.9 rpm. This flow pattern emerged from an interaction between the downslope angle, slope height and paddlewheel rpm. b) Slope HHH operated at 25 rpm, which led to an undular jump.

Although the DOE could not be fully utilized, it is possible to hone in on the individual flow patterns to further determine how the factors affected the flow pattern. Figure 4-12 shows the relation between the wave height and the Froude number measured at the slope crest. The undular jump flow patterns are indicated in red while the transitional patterns are indicated in blue. Note that for some of the configurations the Froude number is below 1 since critical flow conditions is not always achieved exactly at the slope crest but typically some distance between the crest and the first wave (Chanson and Montes, 1995).

For the undular jumps, there appeared to be a relation between the Froude number and wave height, which is what was originally expected. As the Froude number increased, the wave height also increased. Configuration LHHL and LLHH had the same paddlewheel rpm, but a decrease in the slope height for LHHL led to a lower Froude number and as a result a smaller wave. HLHL on the other hand had the same height as LHHL but the increase in rpm from 19.8 to 28.9 greatly improved the Froude number and resulting wave height. For the transitional flow pattern however there was no clear relation between the Froude number and the wave height. The Froude numbers were also typically higher than what was observed for the undular jumps but resulted in lower wave heights. This shows why the initial wave height was not a good indicator for surface turbulence as the Froude number is generally also proportional to turbulence. The different flow patterns are again referred to in the discussion on the k_La (Section 4.3.3). In this section it was shown that the downslope angle played a major role in the type of surface flow pattern and the downslope also had a significant effect on the size of the recirculation zone, which is discussed next.

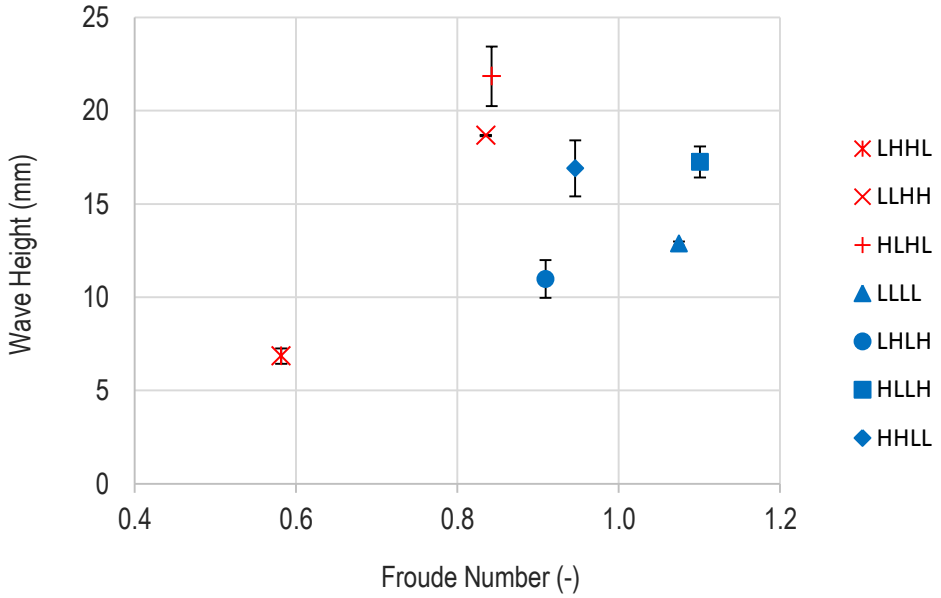

Figure 4-12: Wave size as a function of the Froude number at the slope crest for the slopes that created an undular jump (red) and the transitional flow pattern (blue). For the undular jump, the wave size increased with the Froude number. Error bars indicate standard error.

The recirculation zone after the slope

The addition of a downslope was explored to reduce the size of the recirculation zone as it was suspected that this zone contributed to a decrease in the CO_2 mass transfer rate. Figure 4-13 shows the volume of the recirculation zone measured for the eight different slope configurations tested in the DOE.

The 10 ° downslope did in fact completely remove the recirculation zone. An example of the flow pattern for a 10 ° downslope is illustrated in Figure 4-14, for slope configuration LLLL. This occurred regardless of the paddlewheel rpm, upslope angle or the slope height (within the specific range of values tested in the DOE). It is however possible that an rpm above 28.9 could create an impinging jet flow pattern for the slopes with a 10 ° downslope, similar to the effect observed for slope HHH at different rpms (Figure 4-11).

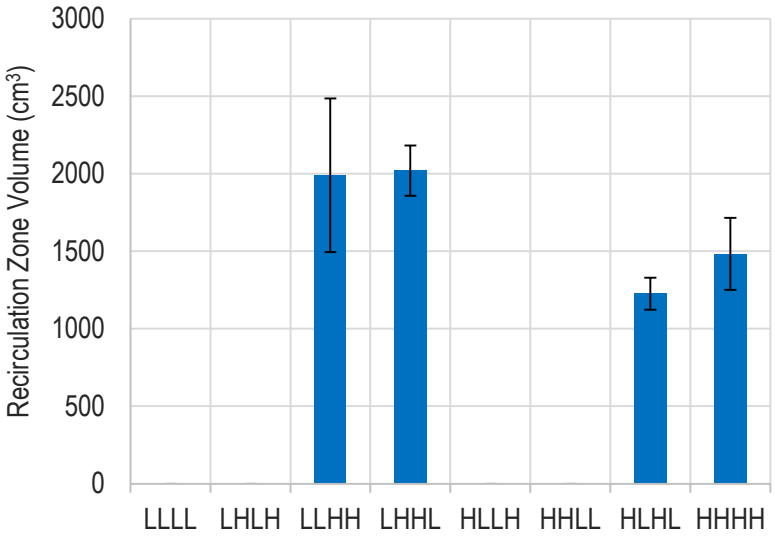

Figure 4-13: Volume of the recirculation zone after each slope tested in the DOE. Slope configurations with the 10 ° downslope completely removed the recirculation zone. Error bars indicate standard error with n=3.

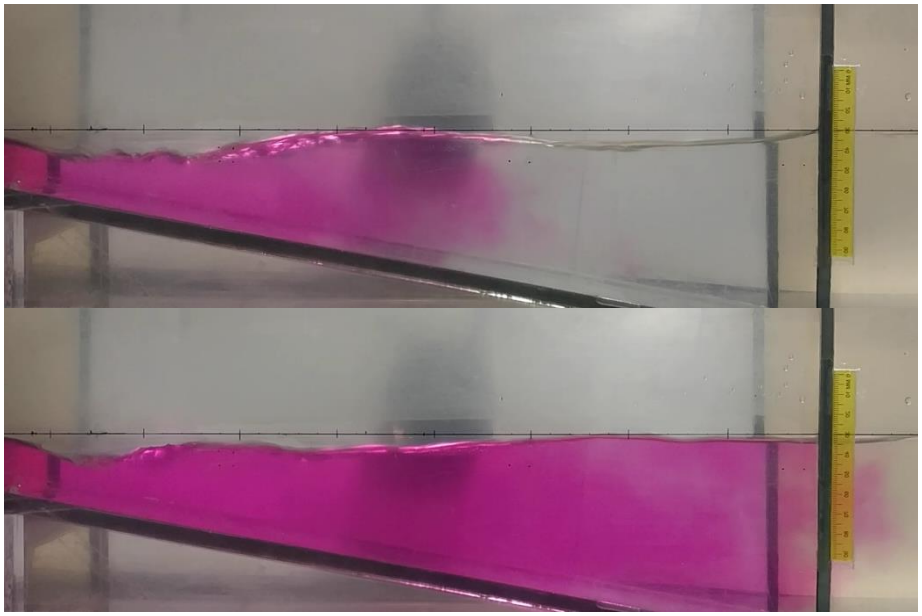

Figure 4-14: Phenolphthalein tracer with slope configuration LLLL. The 10 ° downslope angle removed the recirculation zone, regardless of the slope height, upslope angle or rpm (in the range of values tested).

The phenolphthalein also visually showed the impinging jet flow regime for slope configuration HHHH, which is illustrated in Figure 4-15. Here it is clearly shown how the incoming stream over the slope formed a jet that plunged towards the channel bottom, following the surface of the downslope. The recirculation zone was then brought to the surface of the fluid.

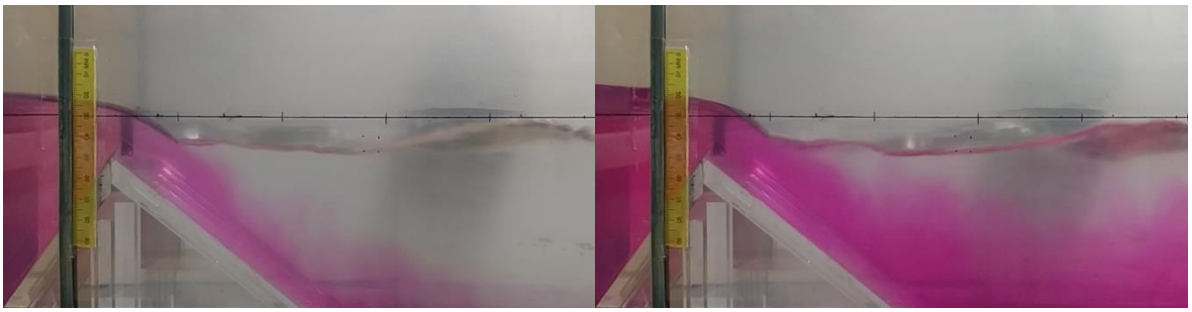

Figure 4-15: Visualizing the impinging jet flow regime (for slope HHHH) with the phenolphthalein tracer. The recirculation zone occurred at the surface as opposed to the floor of the channel.

Figure 4-16 shows the Pareto charts with the recirculation zone size as the response. The results indicate that the size of the recirculation zone was only dependent on the downslope angle and to a far lesser degree, the rpm and a two-factor interaction.

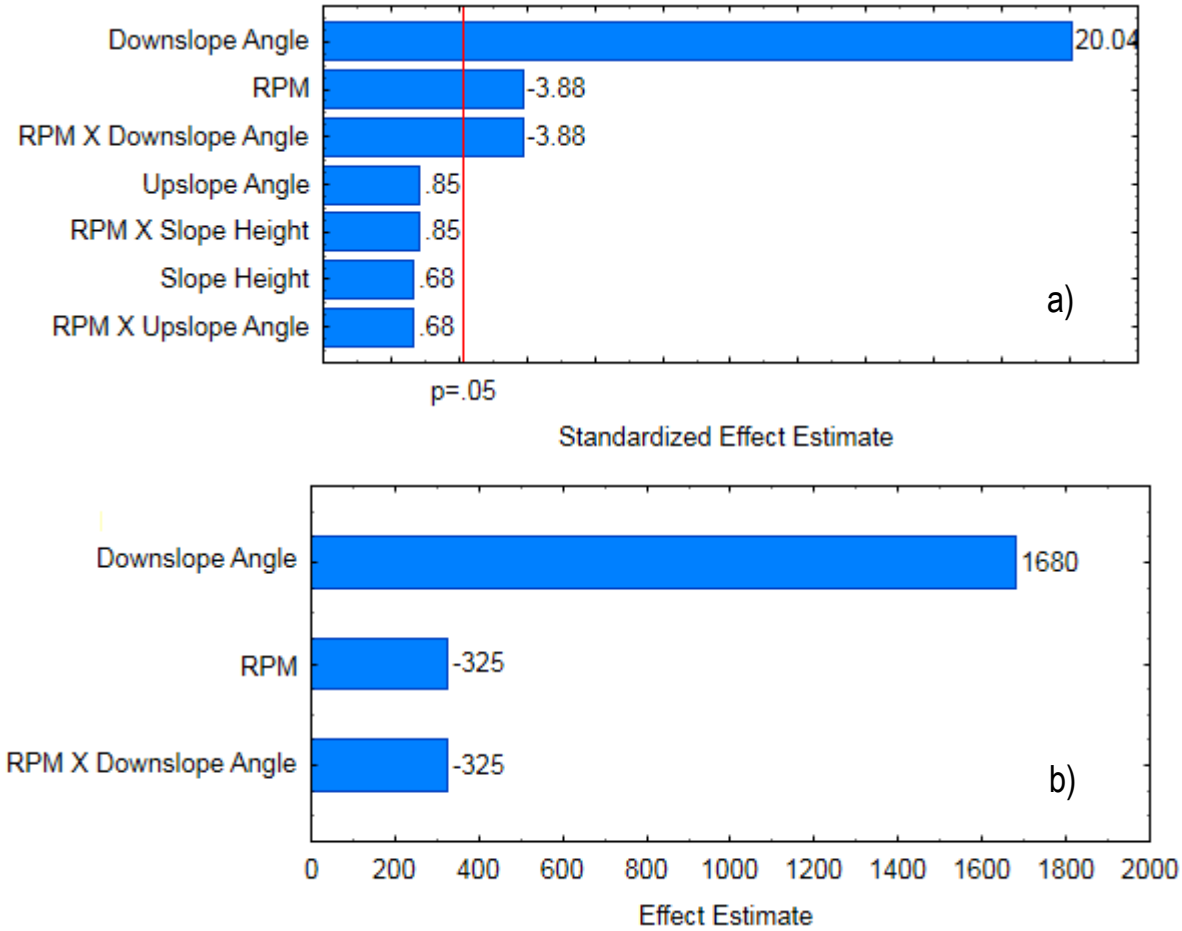

Figure 4-16: Pareto charts showing the standardized effect estimate (a) and effect estimate (b) of each factor on the recirculation zone volume. The effects are presented in a descending order based on its relative magnitude. Effects where the bar graph extends beyond the p = 0.05 line (a) can be considered significant.

The positive effect estimate of the downslope angle shows that increasing the angle from 10 ° to 39 ° increased the size of the recirculation zone. As mentioned in Section 4.1.1, the recirculation zone formed due to the sudden expansion after the slope, allowing the fluid to slow down, which created an

adverse pressure gradient. The 10 ° angle created a more gradual expansion of space after the slope which relieved the adverse pressure gradient to the extent that reverse flow did not occur. Here however the limitation of this DOE is shown as it was not possible to obtain the exact angle where reverse flow would stop to occur, since only two levels of the downslope angle were evaluated.

The rpm had a small effect on the size of the recirculation zone compared to the downslope angle. Increasing the rpm decreased the size. This could be due to two possible reasons. Firstly, an increase in the rpm leads to more turbulent flow and a turbulent boundary layer. For more turbulent flow, stronger adverse pressure gradients are required to lead to flow separation and in such a case the boundary layer can more easily remain attached to the boundary (Cengel and Cimbala, 2014), which would lead to a smaller recirculation zone. On the other hand, it could just be that the turbulent mixing layer was more difficult to accurately size using the method followed. In other words, the specific colour threshold used in ImageJ was too sensitive and picked up on a smaller boundary that did not accurately represent the actual boundary.

There was also one significant two-factor interaction. The interaction between the rpm and downslope angle is confounded with the interaction between the upslope angle and slope height. With the available information, two different models could therefore be constructed that adequately describe the response in this design: one which incorporated the interaction between the rpm and downslope angle and another which incorporated the interaction between the upslope angle and slope height. In reality, this effect estimate might be from a combination of the two interactions. These two effects cannot be distinguished with this DOE. In this case however, it was fair to assume that this effect estimate is purely from the interaction between the rpm and downslope angle, based on effect heredity (discussed in Section 2.4.5). For this interaction, both the main effects (the downslope angle and RPM) had a significant effect on the response, meaning the interaction had strong heredity. With the interaction between the upslope angle and slope height on the other hand, neither of these factors had a significant effect on the response, meaning the interaction likely also does not have a significant effect on the response. The model that therefore best describes the response would include the interaction between the rpm and downslope angle. Additional effects that could be removed from the model are all the insignificant main effects and interactions. The resulting model that describes the volume of the recirculation zone (V_r) looks as follows:

$$V_r = 22.66 \cdot RPM + 117.96 \cdot \beta - 2.47 \cdot RPM \cdot \beta - 1180 \qquad \text{Equation 4-1}$$

Where RPM is the paddlewheel RPM and β is the downslope angle. Removing some of the effects from the model allowed for enough degrees of freedom to determine the lack of fit. The p-value from the Lack of Fit test for this model is 0.672. This indicates that one cannot at a 95 % confidence level say that there isn't any lack of fit in this model, which means this model can adequately describe the response. It should be noted however that this model is only suitable for this specific raceway and cannot be applied in a general sense. It is also likely that this model will become less accurate the further the value of each factor moves away from the values tested in this DOE.

Overall these results indicated that the size of the recirculation zone was mostly affected by the downslope angle and that the angle of 10 ° was sufficient to completely remove the recirculation zone in the range of values tested in the DOE. Since a recirculation zone is typically an area associated with the loss of energy, removing this zone also had implications on the fluid velocity.

Fluid velocity

The average fluid velocity measured for each slope configuration is presented in Figure 4-17. As discussed earlier, the 20 cm and 80 cm slope led to a velocity of 5.7 ± 0.1 cm s^{-1} and 6.4 ± 0.1 cm s^{-1}, respectively. The new slopes operated at the same paddlewheel rpm (LLLL, LHLH, LLHH and LHHL) generally showed an improvement in the fluid velocity. Although for the majority of the configurations the average velocity was still below 10 cm s^{-1}.

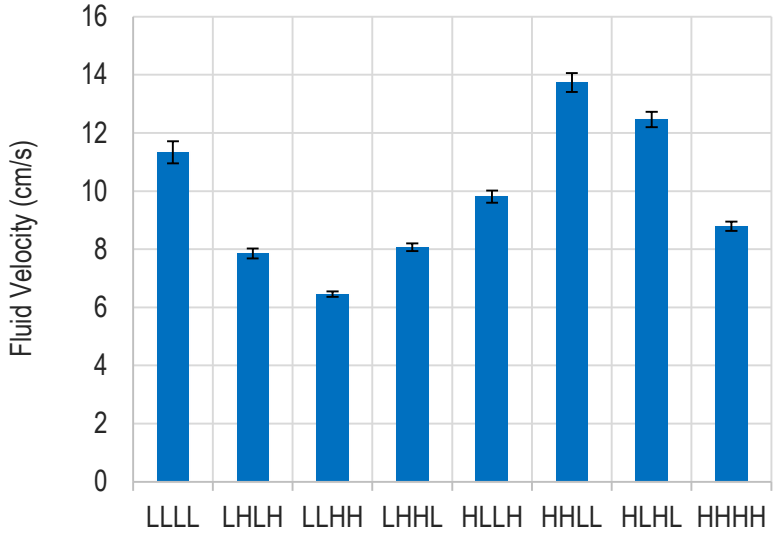

Figure 4-17: Fluid velocity observed with each slope configuration evaluated in the DOE. Error bars indicate standard error propagated from the error in circulation time (n = 3)

It is however possible to operate any of the eight slopes at a velocity of 10 cm s^{-1}, by increasing the paddlewheel rpm. Each slope would require a different rpm to reach this velocity. This rpm can be determined using the model that describes the fluid velocity as a function of the slope parameters and the paddlewheel rpm. These models were in fact used to compare the slopes when operated at the same fluid velocity (Section 4.3.4). Once again a Pareto chart was used to identify the factors which had a significant effect on the velocity and how each factor influenced the velocity. Figure 4-18 shows the Pareto charts.

The results indicate that, in the range of values tested, all four factors and the two-factor interactions had a significant effect on the fluid velocity. The height had the greatest effect on the velocity, followed by the rpm, downslope angle and then the numerous interactions. The upslope angle had the lowest effect (Figure 4-18). In terms of the main effects, increasing the slope height decreased the fluid velocity, which makes sense. The slope was an obstruction to the flow and increasing its height translated to a stronger reactive force that the slope exerted on the forward moving fluid, thereby slowing the fluid down. Increasing the rpm on the other hand increased the velocity, which again is easy enough to explain. The paddlewheel rpm related to the energy input into the fluid, where a higher rpm translated to an increase in the energy supplied to the fluid, resulting in a higher fluid velocity. The velocity was however decreased with an increase in the downslope angle. The gentle downslope angle therefore increased the velocity, which can be explained by its effects on the recirculation zone. A recirculation zone is an area typically associated with turbulence and accompanied energy losses. Removing the recirculation zone therefore promoted uniform flow in the horizontal direction, which resulted in an increase in the fluid velocity. The upslope angle had the least effect on the velocity and showed that increasing the angle decreased the velocity. This is a similar result to what was observed with the 20 cm and 80 cm slopes.

Since all the factors and interactions had a significant effect on the response, there were not enough degrees of freedom to perform a Lack of Fit test. Removing one of the effects from the model was also not adequate. For example, by removing the main effect of the upslope angle (which had the lowest effect on the velocity), the Lack of Fit test could be performed. This however resulted in a p-value of 0.003, meaning such a model showed significant lack of fit. Also, with these results, it was not possible to apply the principle of effect heredity. There were therefore eight possible models that could describe the velocity, each incorporating different confounded interactions between factors. The 8 models are given below, where RPM is the paddlewheel rpm, α is the upslope angle, β the downslope angle and H the slope height. The terms describing the different interactions between the

factors are highlighted in different colours to better indicate which interactions are incorporated in which models.

Model 1

$$v = 9.28 + 1.34 \cdot RPM - 0.11 \cdot \alpha - 017 \cdot \beta - 0.18 \cdot H + 0.004 \cdot \alpha \cdot RPM + 0.004 \cdot \beta \cdot RPM - 0.14 \cdot H \cdot RPM \quad \text{Equation 4-2}$$

Model 2

$$v = 21.94 + 1.45 \cdot RPM - 0.50 \cdot \alpha - 0.06 \cdot \beta - 1.44 \cdot H + 0.004 \cdot \alpha \cdot RPM + 0.04 \cdot \alpha \cdot H - 0.14 \cdot H \cdot RPM \quad \text{Equation 4-3}$$

Model 3

$$v = 39.67 + 0.04 \cdot RPM - 0.08 \cdot \alpha - 0.11 \cdot \beta - 3.18 \cdot H + 0.004 \cdot \alpha \cdot RPM + 0.004 \cdot \beta \cdot RPM - 0.001 \cdot \alpha \cdot \beta \quad \text{Equation 4-4}$$

Model 4

$$v = 52.34 + 0.15 \cdot RPM - 0.46 \cdot \alpha - 0.001 \cdot \beta - 4.79 \cdot H + 0.004 \cdot \alpha \cdot RPM + 0.04 \cdot \alpha \cdot H - 0.001 \cdot \alpha \cdot \beta \quad \text{Equation 4-5}$$

Model 5

$$v = 13.92 + 1.50 \cdot RPM - 0.014 \cdot \alpha - 0.52 \cdot \beta - 0.72 \cdot H + 0.04 \cdot \beta \cdot H + 0.004 \cdot \beta \cdot RPM - 0.14 \cdot H \cdot RPM \quad \text{Equation 4-6}$$

Model 6

$$v = 26.57 + 1.61 \cdot RPM - 0.40 \cdot \alpha - 0.41 \cdot \beta - 2.33 \cdot H + 0.04 \cdot \beta \cdot H + 0.04 \cdot \alpha \cdot H - 0.14 \cdot H \cdot RPM \quad \text{Equation 4-7}$$

Model 7

$$v = 44.31 + 0.19 \cdot RPM + 0.02 \cdot \alpha - 0.46 \cdot \beta - 4.07 \cdot H + 0.04 \cdot \beta \cdot H + 0.004 \cdot \beta \cdot RPM - 0.001 \cdot \alpha \cdot \beta \quad \text{Equation 4-8}$$

Model 8

$$v = 56.97 + 0.30 \cdot RPM - 0.37 \cdot \alpha - 0.35 \cdot \beta - 5.68 \cdot H + 0.04 \cdot \beta \cdot H + 0.04 \cdot \alpha \cdot H - 0.001 \cdot \alpha \cdot \beta \quad \text{Equation 4-9}$$

To determine which of the models had better predictive abilities, the models were tested using experimentation. A few selected slopes were operated at a fluid velocity close to 10 cm s^{-1} (which occurred at a certain paddlewheel rpm). For each of the models, this rpm was substituted into the model, along with the applicable slope parameters, to obtain the velocity the model predicted. Table 4-5 shows the slopes evaluated, along with the actual velocity at the specific rpm and the velocity predicted by each model. For each model, the three two-factor interactions incorporated in the model are shown. The residual sum of squares (RSS) is also depicted and incorporates the standard error in the measured (actual) velocity, which was propagated to the error in the RSS.

Model 1 and Model 5 had the lowest RSS and were therefore the most adequate at predicting the fluid velocity. The difference between these two models was the confounded interaction that was incorporated: either the interaction between the rpm and upslope angle or the interaction between the downslope angle and slope height. Model 5 was however selected. Since the main effect of the upslope angle had the least impact on the velocity it was likely that the interaction between the rpm and upslope angle had a lower contribution to the effect estimate of the confounding pair.

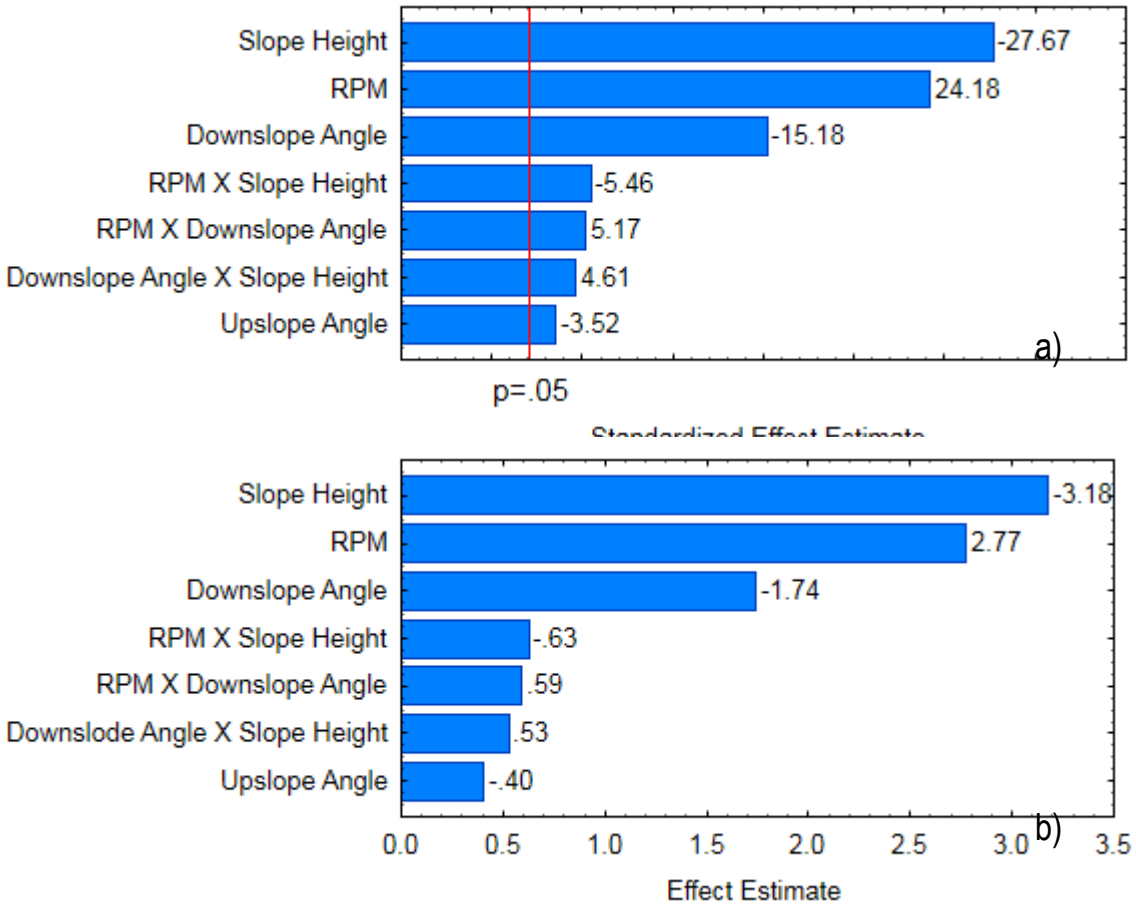

Figure 4-18: Pareto charts showing the standardized effect estimate (a) and effect estimate (b) of each factor on the fluid velocity. The effects are presented in a descending order based on its relative magnitude. Effects where the bar graph extends beyond the p = 0.05 line are considered significant.

Table 4-5: Assessing the predictive abilities of each model describing the fluid velocity. Five different slopes were operated to obtain a fluid velocity close to 10 cm s^{-1}. The actual required rpm was used as an input in each model to obtain the predicted fluid velocity. The residual sum of squares (RSS) is shown for each case.

		Predicted Velocity (cm s^{-1})							
Slope	**Actual Velocity (cm s^{-1})**	**Model 1**	**Model 2**	**Model 3**	**Model 4**	**Model 5**	**Model 6**	**Model 7**	**Model 8**
HHL	10.0 ± 0.3	10.1	9.8	9.8	9.5	9.8	9.6	9.6	9.3
LHL	10.2 ± 0.3	10.3	10.7	10.7	11.1	10.0	10.4	10.4	10.8
HLL	10.1 ± 0.1	9.7	9.0	10.4	9.7	10.3	9.6	11.1	10.4
LHH	9.6 ± 0.1	9.3	8.6	10.1	9.4	10.0	9.2	10.8	10.1
HLH	10.5 ± 0.3	10.7	11.5	11.6	12.4	10.0	10.8	10.9	11.7
	RSS	0.32±0.23	3.76±0.82	1.97±0.74	5.17±1.26	0.49±0.33	0.89±0.36	3.10±0.57	3.43±0.87

As mentioned, a Lack of Fit test could not be performed for this model. Comparing the velocity predicted by Model 5 to the actual measured fluid velocity, the results were typically within 5 %. Also, knowing that three factor interaction could very well arise in this system (as seen by the impinging jet flow pattern), a far better model would separate any confounded pairs. This was not possible with the resolution IV design, although there are strategies, such as 'fold over', which could be applied to build

on this design by adding experimental runs which could separate the confounded pairs (Montgomery, 2013).

Mixing time and Peclet number

As was shown with the 20 cm and 80 cm slopes, the weir-like designs greatly improved the mixing time and reduced the Peclet number in the raceway. These two variables are shown in Figure 4-19 for each slope configuration tested in the DOE.

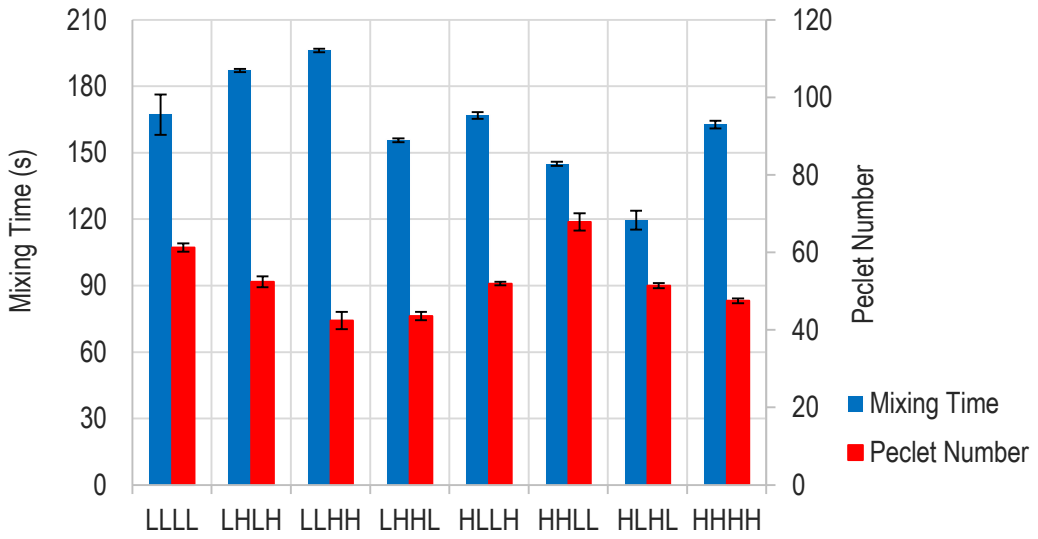

Figure 4-19: Mixing time and Peclet number for each slope configuration tested in the DOE. Error bars depict standard error with n = 3.

From Figure 4-19, there appeared to be an inverse relation between the mixing time and the Peclet number, as a higher mixing time typically coincided with a lower Peclet number. This can be explained in more detail by considering what the Peclet number shows: the relation between convective transportation and dispersion transportation. But first, to better explain this result, the effect of each factor on the mixing time and Peclet number needs to be addressed. The Pareto chart showing the relative effect of each factor on the mixing time is shown in Figure 4-20.

Figure 4-20 shows that the slope height had the greatest effect on the mixing time, closely followed by the paddlewheel rpm. The main effect of the downslope angle was relatively small compared to the slope height and paddlewheel rpm, while the upslope angle did not have a significant effect. Increasing the slope height increased the mixing time. This could be due to the relation between the fluid velocity and mixing, as a higher velocity leads to more turbulence and better mixing. Since the slopes with the 10 cm height decreased the average fluid velocity, the mixing time increased. Here however the limitation of the 2 level factorial DOE is again prominent. Decreasing the slope height should decrease the mixing time up to a certain point, since when the slope height is equal to zero (which is basically the control without a slope) the mixing time is high again. This factorial design cannot indicate where the ideal height is. With the designs tested, it is however clear that the height of 9 cm was preferred when considering only the mixing time. The paddlewheel rpm had a similar correlation to the fluid velocity. This is also shown by the Pareto chart, where an increase in the paddlewheel rpm resulted in a decrease in the mixing time. On top of this, the local mixing at the paddlewheel was also enhanced at a higher rpm due to turbulence created by the increase in the blade tip speed.

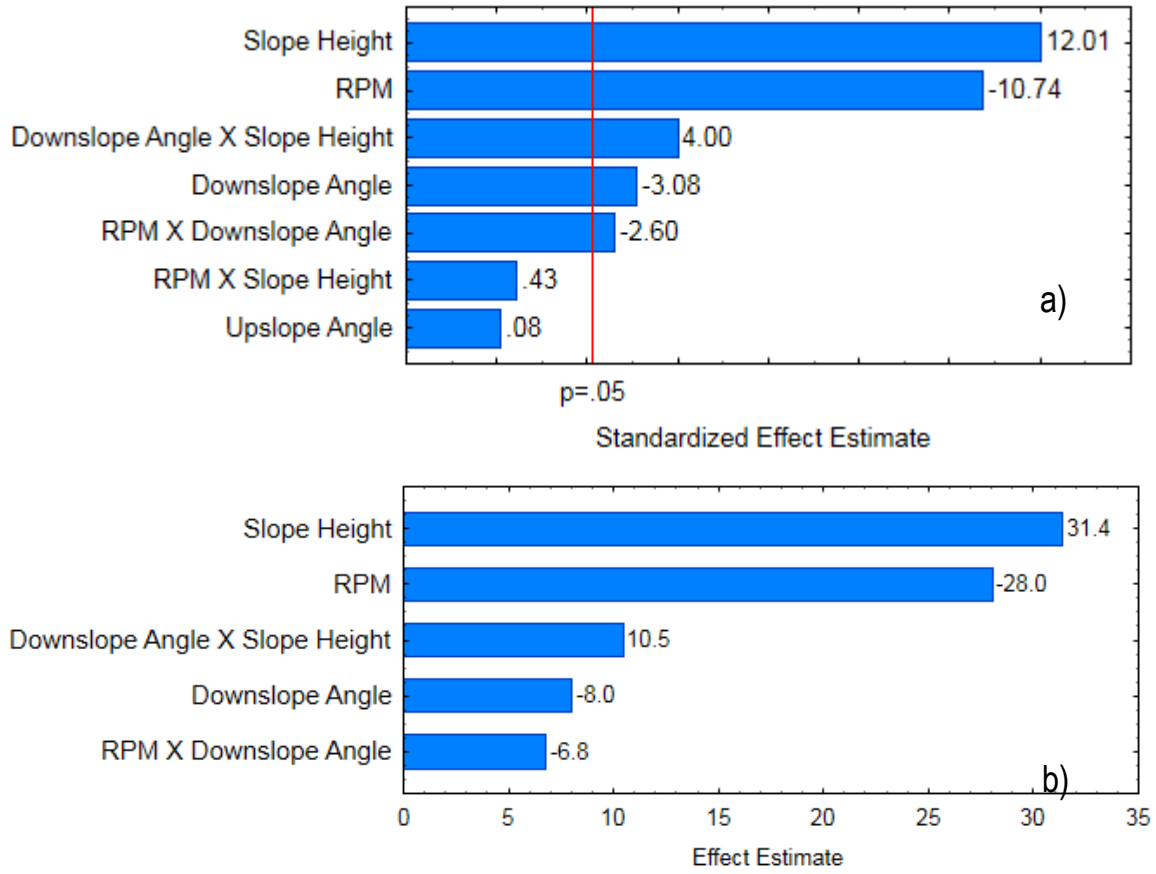

Figure 4-20: Pareto charts showing the standardized effect estimates (a) and effect estimates (b) of each factor with the mixing time as the response. The effects are presented in a descending order based on its relative magnitude. Effects where the bar graph extends beyond the p = 0.05 line are considered significant.

The downslope also affected the fluid velocity, but the results however indicated that an increase in the downslope angle decreased the mixing time even though increasing the angle decreased the velocity. Here two opposing forces were at play. The lower angle increased the fluid velocity which intuitively should lead to a decrease in the mixing time. But it also removed the recirculation zone and the resulting mixing layer, which should increase the mixing time. Since it is shown that increasing the downslope angle decreased the mixing time, the effects of the mixing due to the recirculation zone were therefore more dominant than the effects of a greater fluid velocity supplied by the low downslope angle. These two opposing forces could be why the effect of the downslope angle was so small relative to the slope height and paddlewheel rpm.

There were only two interaction effects that were significant, meaning four models that describe the mixing time could be constructed. Based on effect heredity, the interaction between the downslope angle and slope height as well as the rpm and downslope angle would likely be optimal to include in the model, as opposed to interactions with the upslope angle. This is because the upslope angle did not have a significant effect on the mixing time. The predictive abilities of all four of the models were however tested through experimentation. Table 4-6 compares the predicted mixing time by each model with the actual measured mixing time for a few slopes operated at a fluid velocity close to 10 cm s^{-1}. The four models are described below.

Model 1

$$t_{mix} = -84.42 - 1.94 \cdot RPM + 098 \cdot \beta + 31.37 \cdot H + 0.09 \cdot \alpha \cdot RPM - 0.05 \cdot \beta \cdot RPM$$ Equation 4-10

Model 2

$$t_{mix} = 83.45 - 1.82 \cdot RPM - 5.88 \cdot \beta + 13.70 \cdot H + 0.72 \cdot \beta \cdot H - 0.05 \cdot \beta \cdot RPM$$ Equation 4-11

Model 3

$$t_{mix} = -53.71 - 6.51 \cdot RPM - 0.28 \cdot \beta - 40.17 \cdot H + 0.09 \cdot \alpha \cdot RPM - 0.22 \cdot \alpha \cdot H$$ Equation 4-12

Model 4

$$t_{mix} = 114.16 - 3.08 \cdot RPM - 7.13 \cdot \beta - 13.72 \cdot H + 0.72 \cdot \beta \cdot H - 0.22 \cdot \alpha \cdot H$$ Equation 4-13

Table 4-6: Testing the mixing time models by assessing the predictive abilities of each model. Five different slopes were operated to obtain a fluid velocity close to 10 cm s^{-1}. The actual required rpm was used as an input in each model to obtain the predicted mixing time. The residual sum of squares (RSS) is also shown.

		Predicted Mixing Time (s)			
Slope	**Actual Mixing Time (s)**	**Model 1**	**Model 2**	**Model 3**	**Model 4**
HHL	141 ± 6	146	140	145	139
LHL	139 ± 1	146	142	146	141
HLL	178 ± 0	167	171	164	176
LHH	156 ± 6	145	152	144	157
HLH	163 ± 5	165	158	166	152
	RSS	318±151	93±76	397±160	123±118

Based on the RSS, Model 2 and 4 were the best at predicting the mixing time. The difference between these two models was whether the interaction between the rpm and downslope angle or the interaction between the upslope angle and slope height was incorporated. Model 2 was however chosen, since the main effect of the upslope angle had an insignificant effect on the mixing time. Again using the principle of effect heredity, the interaction between the upslope angle and slope height therefore had weaker heredity. Since some effects could be removed from the model, there were enough degrees of freedom to perform the Lack of Fit test. The p-value was 0.92, indicating that one can't confidently say that there is any lack of fit. For this model, the predicted values typically fell within 5 % of the measured mixing time.

It was shown that the fluid velocity played an important role in the mixing time as the factors that affected the velocity affected the mixing. The Peclet number had a similar dependency (which can be related to the velocity term describing the convective transportation, as seen in Equation 3-1). The Peclet number was however also dependent on the dispersion coefficient, D, which was determined using Equation 3-1. It was then found that the dispersion coefficient was inversely proportional to the mixing time (https://figshare.com/s/00ec7e5192c6be962de8, Raceway 1). This is key in understanding the observed relation between the Peclet number and mixing time.

The Pareto chart showing the relative effect of each factor on the Peclet number is depicted in Figure 4-21. It shows that the downslope angle had the biggest impact on the Peclet number, followed by the slope height and paddlewheel rpm. The upslope angle had an insignificant effect (in the range of values tested).

Increasing the downslope angle reduced the Peclet number. Since the Peclet number is affected by the fluid velocity and the dispersion coefficient, this result can be explained by the effect of the downslope on these two elements. For the main effect of the downslope angle, it was shown that increasing the angle decreased the fluid velocity and decreased the mixing time. A decrease in the mixing time corresponds to an increase in the dispersion coefficient. So when considering Equation 3-1 which describes the Peclet number, the numerator is decreased and the denominator is increased, which has the overall effect of decreasing the Peclet number. Increasing the downslope angle therefore decreases the Peclet number. With the slope height and paddlewheel rpm however, the effects of the fluid velocity and dispersion coefficient on the Peclet number were in opposite

directions. For example, the Pareto chart shows that increasing the slope height reduced the Peclet number. The increase in height however coincided with a decrease in the fluid velocity (which should indeed decrease the Peclet number) but also an increase in the mixing time, which corresponds to a reduction in the dispersion coefficient and therefore an increase in the Peclet number. This showed that there was a difference in the extent that the velocity and dispersion coefficient affected the Peclet number and could also be used to explain the inverse relation between the Peclet number and the mixing time.

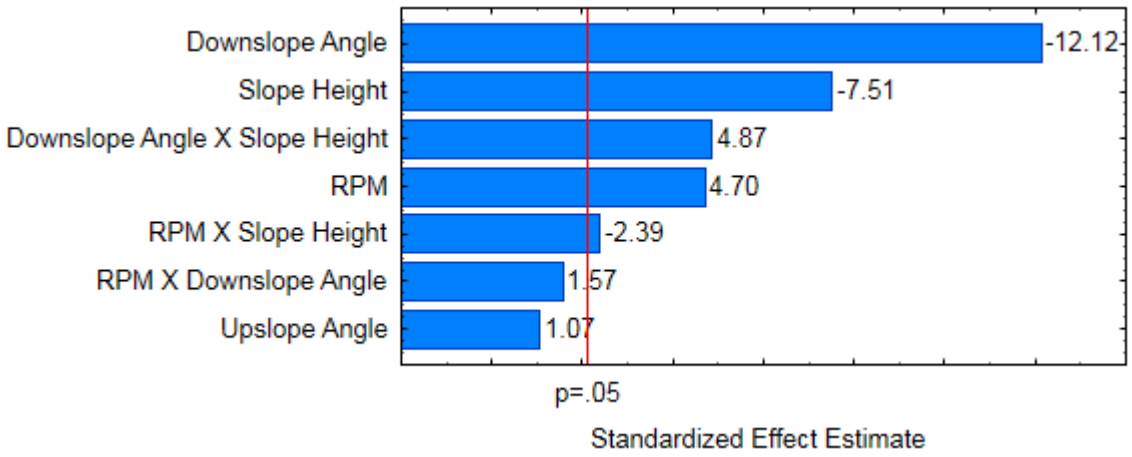

Figure 4-21: Pareto chart showing the standardized effect of each factor with the Peclet number as the response. The effects are presented in a descending order based on its relative magnitude. Effects where the bar graph extends beyond the p = 0.05 line are considered significant.

The inverse relation between the mixing time and the Peclet number gives some indication as to the extent that the factors affected the fluid velocity and mixing time. With a change in the level of a certain factor, the change in the fluid velocity was greater than the change in the dispersion coefficient (or mixing time). To illustrate this, the results of slope configuration LLLL and LHLH can be compared. Due to the negligible effect of the upslope angle on the mixing and Peclet number, the difference between these two configurations was primarily the slope height. The dispersion coefficient for configuration LLLL and LHLH was 0.64 m^2 s^{-1} and 0.52 m^2 s^{-1}, respectively, which is a 21 % difference. The fluid velocity on the other hand was 11.3 cm s^{-1} and 7.9 cm s^{-1}, respectively, which is a 36 % difference. The Peclet number for configuration LHLH was therefore lower, even if it had a greater mixing time, due to the greater decrease in the fluid velocity compared to the reduction in the dispersion coefficient. This however begs the question of whether the Peclet number is a good metric to use when comparing the slopes, since the lower Peclet number was due more to the fact that the fluid velocity was lower. In selecting the best slope design, a lower mixing time should be favoured as opposed to a lower Peclet number due to the importance of the fluid velocity on algae cultivation. The Peclet number therefore served a better purpose of illustrating the difference between the control and the slopes, by showing plug flow for the control and more back-mixing for the slopes. It can also add more value if the individual areas in the raceway were considered. When performing the conductivity tracer experiment with multiple conductivity probes in the raceway, it would allow one to determine the Peclet number associated with a specific area in the raceway. In such a case, the Peclet number in the straight channel section, for example, could be compared to the Peclet number in the area after the slope.

Overview

Overall, with the weir-like slope designs, it is desired to have surface turbulence to improve k_La, a good mixing time (with vertical mixing to enhance the light regime) and a sufficient fluid velocity to prevent significant settling. These results showed that the slope parameters led to different types of

surface flow patterns, although as a result it was not possible to draw a direct correlation between the wave height and surface turbulence. It was however possible to say which slope parameters led to which flow patterns, and the downslope angle played a major role. The surface flow patterns in relation to the k_La are discussed in Section 4.3.3, to shed more light on whether there is a desired flow pattern. But considering the effects of the downslope angle on the mixing time, it might be advantageous to have a steeper downslope, which typically led to the undular hydraulic jump.

The mixing time and fluid velocity were significantly improved through a decrease in the slope height. It was also shown that the slope height was the factor with the greatest impact on both these variables. The slopes with a height of 10 cm require a higher rpm to reach a favourable velocity. An increase in rpm however does greatly improved the mixing time although since the slope height had a greater effect, it might be more desirable to reduce the slope height as a means of improving the fluid velocity and mixing time. The fluid velocity was also improved with a gentler downslope and it was shown that the 10 ° angle was enough to completely remove the recirculation zone. This however reduced the mixing time and vertical mixing due to the removal of this zone. The abrupt expansion of space after the slope is exactly what is needed to create the better mixing layer and improve vertical mixing. Of all the factors evaluated, the upslope angle had the least effect on all the measured responses. This could on the one hand be due to not using a wide enough range in the levels of the upslope angle tested in this DOE. But nonetheless, it showed that upslope angles between 25 ° and 54 ° did not lead to significant differences in the responses. With only the results on the hydrodynamics however, it is not possible to draw any final conclusions on the preferred slope parameters. The next section discusses the effects of each factor on the k_La and energy demand.

4.3.3 Factorial DOE to assess k_La and energy demand

Similarly to the hydrodynamic variables, the k_La and energy demand were also used as responses in the factorial DOE, from which the most relevant factors in the design were identified. As discussed in Section 4.1.2, the mass transfer driving force was constant throughout all configurations evaluated and the k_La alone was used to compare the slopes. Table 4-7 depicts the k_La measured for each slope configuration in the factorial DOE, along with the percentage increase in k_La compared to the control at the paddlewheel rpm of 19.8 and 28.9. The first four configurations presented were those operated at the paddlewheel rpm of 19.8 (LLLL, LHLH, LLHH, LHHL) and the last four were those operated at 28.9 rpm (HLLH, HHLL, HLHL, HHHH).

An interesting pattern immerged. Based on these results, the slopes led an increase in k_La compared to the control, although the different slope parameters had no effect on variation in the k_La; it was only the paddlewheel rpm that affected the k_La. This can be seen by the similar k_La for each of the slopes operated at the same paddlewheel rpm. Compared to the control at 19.8 rpm the average increase in k_La for the slopes operated at 19.8 rpm was 12 ± 2 %. This was increased to an average of 68 ± 5 % for the slopes operated at 28.9 RM. When comparing the slopes at 28.9 rpm to the control at the same rpm, the average increase in k_La was 16 ± 5 %. The case that the slope parameters did not lead to variation in k_La is naturally not true for all the values of the slope parameters, but just the values tested in this DOE. For example, decreasing the slope height further should at some point lead to no surface disturbances, where the k_La would then likely not have the same increase compared to the control at the same paddlewheel rpm.

Table 4-7: k_La for each slope configuration tested in the DOE along with the control at 19.8 rpm and 28.9 rpm. The percentage increase in k_La compared to the controls are also presented. For each case the standard error is also shown with n = 3.

Configuration	k_La (h^{-1})	Percentage increase in k_La compared to control at 19.8 rpm (%)	Percentage increase in k_La compared to control at 28.9 rpm (%)
Control (19.8 rpm)	3.00 ± 0.09	-	- 30.6 ± 3.1
Control (28.9 rpm)	4.33 ± 0.31	44.1 ± 6.5	-
LLLL	3.38 ± 0.20	12.4 ± 4.3	-22.7 ± 3.8
LHLH	3.34 ± 0.04	11.2 ± 2.0	-23.5 ± 2.8
LLHH	3.37 ± 0.15	12.4 ± 3.5	-22.7 ± 3.4
LHHL	3.36 ± 0.11	12.1 ± 2.9	-22.9 ± 3.2
HLLH	5.16 ± 0.22	71.9 ± 5.0	18.2 ± 5.1
HHLL	5.06 ± 0.34	68.6 ± 7.1	15.9 ± 6.1
HLHL	5.06 ± 0.22	68.4 ± 5.1	15.8 ± 5.1
HHHH	4.87 ± 0.34	62.1 ± 7.0	11.4 ± 6.0

These results also indicate that, to effectively increase the k_La for this raceway setup, one can very easily just increase the paddlewheel rpm without the use of a slope. This is shown with the first four slope configuration (LLLL, LHLH, LLHH and LHHL), where there was not an increase in the k_La compared to the control operated at 28.9 rpm. The dominating effect of the paddlewheel rpm is further supported by assessing the Pareto chart with the k_La as the response, depicted in Figure 4-22.

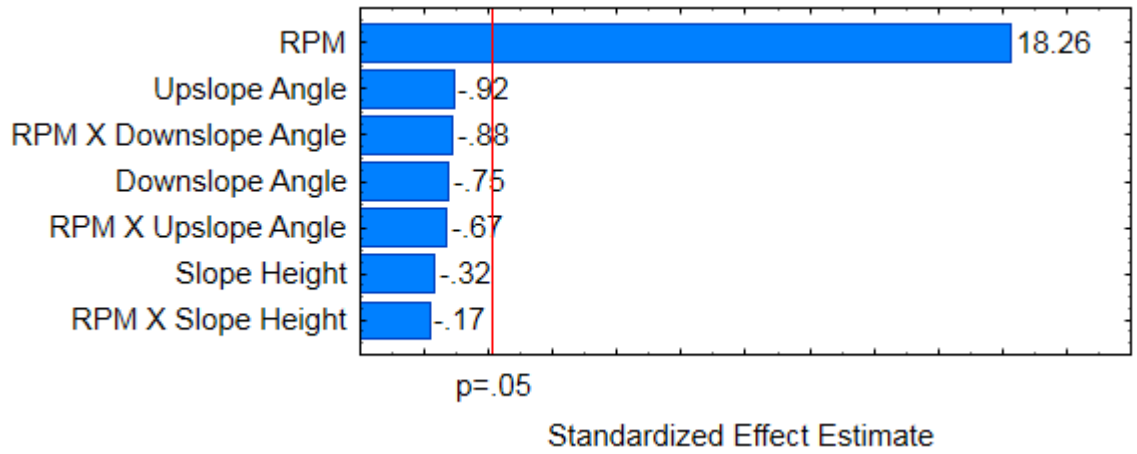

Figure 4-22: Pareto chart showing the standardized effect of each factor on the mass transfer coefficient. The effects are presented in a descending order based on its relative magnitude. Effects where the bar graph extends beyond the p = 0.05 line are considered significant.

Figure 4-22 confirms that the slope parameters or any two-factor interaction did not have a significant effect on the measure k_La. Since the slope parameters led to different wave patterns, one might say that there was not a measurable difference in terms of surface turbulence between the different flow patterns. The preferred surface flow pattern could therefore not be argued from the perspective of the k_La. With this in mind however, an extreme example that needs to be explained is the difference

between slope configuration LHHL and LLHH (Figure 4-10 a and b), operated at the same paddlewheel rpm. There was a big difference in the initial wave created by these two slopes, primarily due to the slope height which led to different Froude numbers at the slope crests. The initial wave was in fact a small part of the overall turbulence created by the slopes. The surface disturbances typically extended to just before the raceway bend after the slope. It is possible that the difference in wave height was negligible when taking this entire region into account. Figure 4-23 gives a top view of the surface disturbances created by configuration LHHL and LLHH. The affected area stretched to more or less the same length and this visually suggests that the two slopes led to a similar degree of surface turbulence. The proper tools were however not available to quantify the surface turbulence in its entirety. A potential option to better quantify the surface turbulence is Particle Image Velocimetry, which can be used to create a velocity field at the fluid surface, stretching the entire length of the straight channel section.

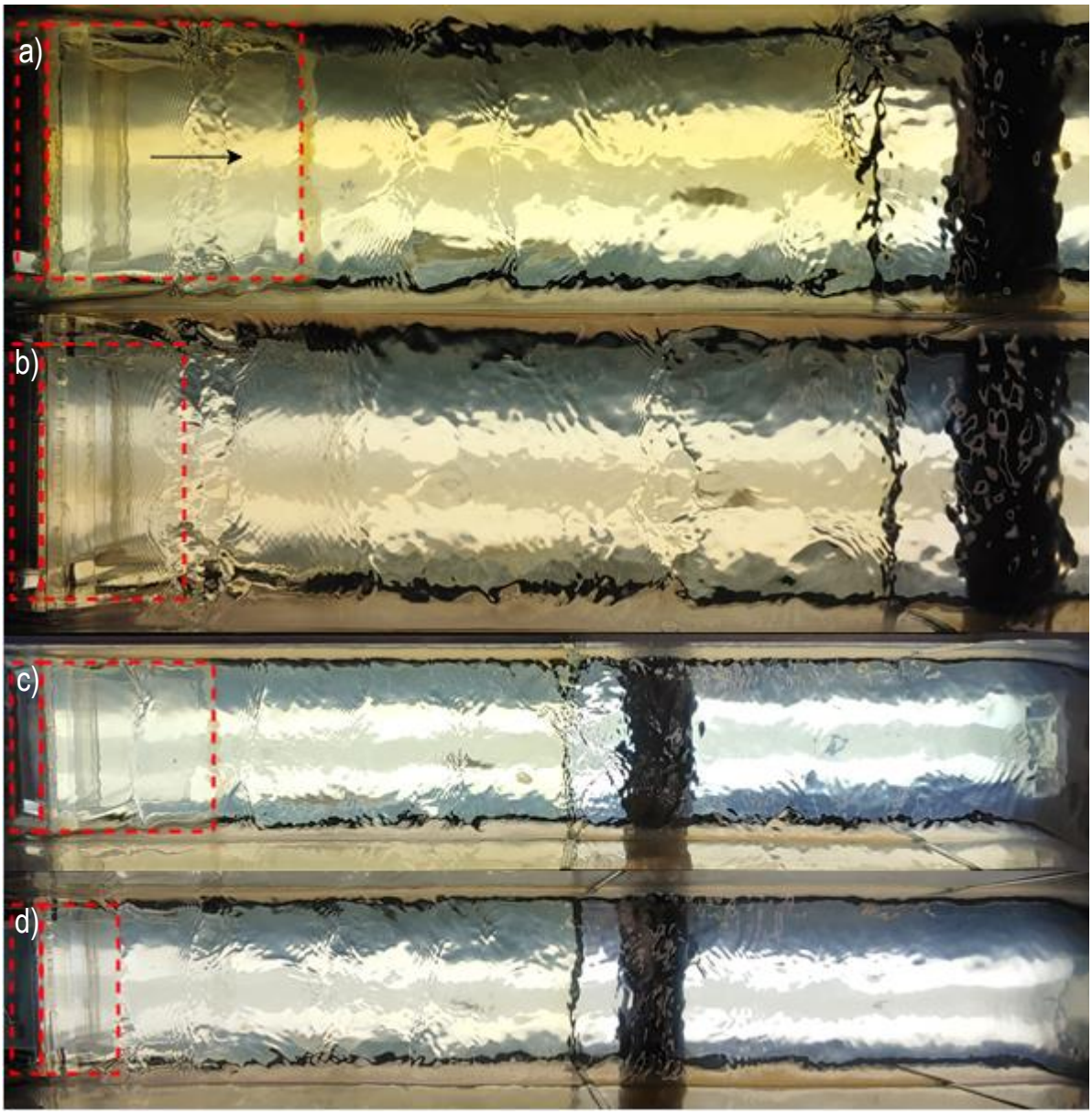

Figure 4-23: Top view of the flow pattern for slope configuration LHHL and LLHH at an RPM of 19.8. The slopes are indicated in red, and the direction of flow is left to right. a) Close-up of the surface disturbance created by LHHL, b) Close-up of the surface disturbance created by LLHH, c) Full view of the surface disturbance created by LHHL, d) Full view of the surface disturbance created by LLHH.

Even though the slope parameters had a negligible effect on the k_La, these did in fact affect the energy requirements. The k_La per unit of theoretical energy required was therefore different for each slope configuration. As discussed in Section 4.1.2, the theoretical energy is dependent on the total head loss and the volumetric flow rate. These variables are depicted in Table 4-8 for each slope configuration evaluated in the factorial DOE.

Table 4-8: Theoretical energy required for each slope configuration tested in the DOE, along with the head loss and volumetric flow rate. For each value the standard error is also shown which was propagated from the error in the circulation times and measured fluid depths.

Configuration	Theoretical Energy Required (W)	Total Head Loss (mm)	Head Loss due to Slope (mm)	Volumetric Flowrate (L s^{-1})
LLLL	0.19 ± 0.02	10 ± 1	9 ± 1	1.9 ± 0.1
LHLH	0.16 ± 0.01	13 ± 1	12 ± 1	1.3 ± 0.0
LLHH	0.11 ± 0.01	10 ± 1	10 ± 1	1.1 ± 0.0
LHHL	0.10 ± 0.01	7 ± 0	7 ± 0	1.4 ± 0.0
HLLH	0.34 ± 0.03	21 ± 1	20 ± 1	1.7 ± 0.0
HHLL	0.41 ± 0.03	18 ± 1	18 ± 1	2.3 ± 0.1
HLHL	0.35 ± 0.02	17 ± 1	16 ± 1	2.2 ± 0.0
HHHH	0.29 ± 0.02	19 ± 1	19 ± 1	1.5 ± 0.0

The results presented in Table 4-8 are used to explain the effects that each factor had on the theoretical energy. Figure 4-24 depicts the Pareto chart showing the effect estimate of each factor on the theoretical energy. In this case however, it was not possible to determine whether these effects were significant. This is because of the way in which the experiments were performed. The theoretical energy was determined from the fluid velocity and the measured fluid depth (used to obtain the head loss over the slope). These measurements were however done independently and were not directly related. Therefore, it was not possible to obtain three true replicates of the theoretical energy. So instead of using three true replicates of the theoretical energy as input into Statistica in a design where each configuration was repeated three times, the design was changed to contain a single run for each configuration. The average theoretical energy obtained from the average fluid velocity and average fluid depths was used as the input.

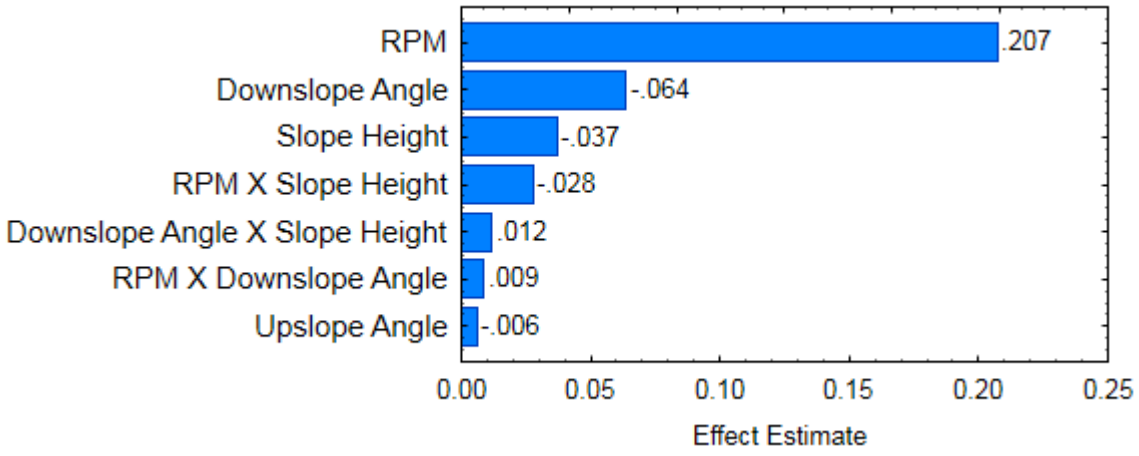

Figure 4-24: Pareto chart showing the effect estimate of each factor with the theoretical energy requirement as the response. The effects are presented in a descending order based on its magnitude.

Figure 4-24 shows that the paddlewheel rpm had by far the greatest effect on the theoretical energy requirement, followed by the downslope angle, slope height, two-factor interactions and then the upslope angle. Since the effect of the upslope angle on the theoretical energy was so small, it is very likely that this effect was insignificant. With respect to the paddlewheel rpm, increasing the rpm greatly increased the theoretical energy which can be explained by its effects on the head loss and volumetric flow rate. Increasing the downslope angle on the other hand decreased the theoretical energy requirement, which is not what was originally expected. Since a gentle downslope can remove the recirculation zone, it would be fair to think that a slope with a lower downslope angle would lead to a reduction in the energy losses, as energy is usually lost in the turbulence of the recirculation zone. However, since the raceway is a circular system in a closed loop, the lower downslope angle increased the fluid velocity. As a result the volumetric flow rate was increased, but also the head loss over the slope. This can be seen in Table 4-8 by comparing the slope configurations with the same rpm and height. For example, the head loss due to the slope for configuration LHLH was 12 ± 1 mm, slightly higher than the 10 ± 1 mm for LLHH. This difference was likely due to the downslope angle, since although the upslope angle also varied between these two configurations, the effect of the upslope angle on the theoretical energy was extremely low. The head loss due to friction on the downslope surface was included in the calculation of the head loss due to the slope. The increase in head loss due to the slope could also be as a result of higher friction, since the 10 ° downslope was much longer than the 39 ° downslope. The much higher fluid velocity over the slope along with the lack of a recirculation zone meant that the friction experienced by the fluid increased.

Increasing the slope height also decreased the theoretical energy demand. Here two opposing forces are present, one being more dominant than the other. Increasing the height decreased the volumetric flow rate and as a result the theoretical energy requirement. The increase in height however also led to an increase in the head loss due to the slope, thereby increasing the theoretical energy demand. This can be seen in Table 4-8 by comparing the configurations with the same rpm and downslope angle. With LLLL, for example, the head loss due to the slope was 9 ± 1 mm, compared to LHLH where the head loss due to the slope was 12 ± 1 mm. Since the overall effect of the slope height was to decrease the theoretical energy required, the effect of the height on the volumetric flow rate was dominant. But as mentioned in the literature review (Section 2.4.2), even though the greater height decreases the theoretical energy requirement, the increase in head loss likely means that the actual energy requirement will increase, due to the effect on the paddlewheel efficiency.

The effects of the slope parameters on the k_La per unit of theoretical energy required can be explained by their effects on the theoretical energy. This is because the slope parameters did not have an effect on the k_La. With the k_La per unit of theoretical energy as the response, it could again not be determined whether the effects were significant, since the theoretical energy was measured independently of the three mass transfer runs for each configuration. The average k_La per unit of theoretical energy was therefore used in a factorial DOE with a single run for each configuration. Figure 4-25 shows the Pareto chart with the k_La per unit of theoretical energy as the response.

The main effect of the paddlewheel rpm was the greatest, followed by the downslope angle and a two-factor interaction. The remaining interactions as well as the slope height and upslope angle had a small effect. Increasing the paddlewheel rpm decreased the k_La per unit of theoretical energy required. Even though the k_La was increased with an increase in rpm, the increase in the theoretical energy requirement was greater. This was also observed for the control operated at different paddlewheel rpms. This again indicates that lower rpms are favoured when the energy requirement is considered. Increasing the downslope angle on the other hand increased the k_La per unit of theoretical energy required. It was shown that increasing the downslope angle decreased the theoretical energy demand, meaning the k_La per unit of theoretical energy increased. What is interesting is that the height had a similar magnitude effect as the upslope angle, whereas the height had a greater effect than the upslope angle on the theoretical energy demand. Both these effects were however small relative to the downslope angle and rpm for both responses.

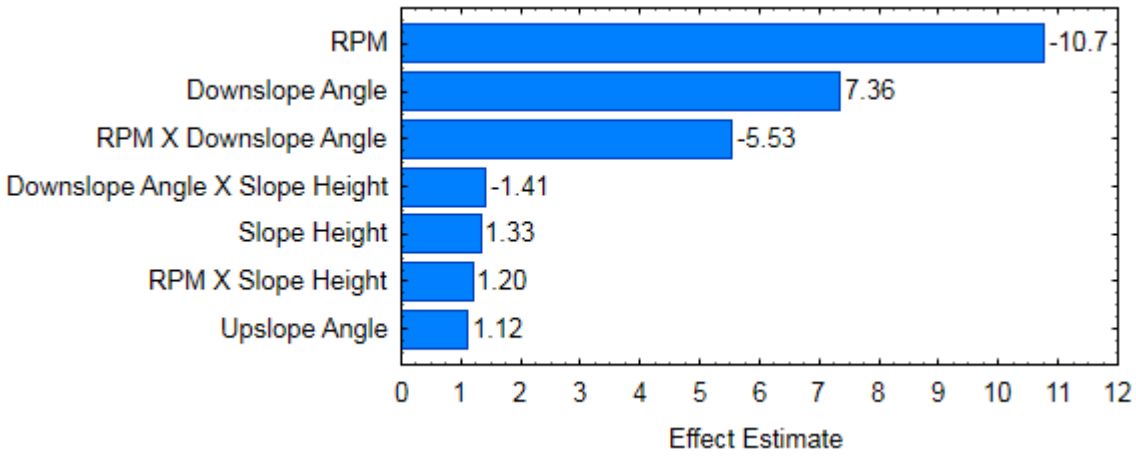

Figure 4-25: Pareto chart showing the effect estimate of each factor with the mass transfer coefficient per unit of theoretical energy required as the response. The effects are presented in a descending order based on its magnitude.

Since it was not possible to determine which effects were insignificant, there were eight possible models that could describe the k_La per unit of theoretical energy required. Three different slope configurations were operated at a fluid velocity close to 10 cm s^{-1} to evaluate the predictive abilities of the models. Table 4-9 compares the predicted k_La per unit of theoretical energy required to the actual measured value. The average fluid velocity for each case is also depicted. Only one run for each configuration was performed, meaning the actual k_La per unit of theoretical energy required does not include error bars.

Model 1

$$k_La/P_{Theo} = 53.89 - 2.23 \cdot RPM + 0.30 \cdot \alpha + 1.27 \cdot \beta - 5.07 \cdot H - 0.01 \cdot \alpha \cdot RPM - 0.04 \cdot \beta \cdot RPM + 0.26 \cdot H \cdot RPM \quad \text{Equation 4-14}$$

Model 2

$$k_La/P_{Theo} = -64.29 - 3.26 \cdot RPM + 3.92 \cdot \alpha + 0.25 \cdot \beta + 10.00 \cdot H - 0.01 \cdot \alpha \cdot RPM - 0.38 \cdot \alpha \cdot H + 0.26 \cdot H \cdot RPM \quad \text{Equation 4-15}$$

Model 3

$$k_La/P_{Theo} = -4.20 + 0.27 \cdot RPM + 0.23 \cdot \alpha + 1.16 \cdot \beta + 1.33 \cdot H - 0.01 \cdot \alpha \cdot RPM - 0.04 \cdot \beta \cdot RPM + 0.003 \cdot \alpha \cdot \beta \quad \text{Equation 4-16}$$

Model 4

$$k_La/P_{Theo} = -122.38 - 0.76 \cdot RPM + 3.85 \cdot \alpha + 0.14 \cdot \beta + 16.41 \cdot H - 0.01 \cdot \alpha \cdot RPM - 0.38 \cdot \alpha \cdot H + 0.003 \cdot \alpha \cdot \beta \quad \text{Equation 4-17}$$

Model 5

$$k_La/P_{Theo} = 41.52 - 2.65 \cdot RPM + 0.04 \cdot \alpha + 2.20 \cdot \beta - 2.69 \cdot H - 0.10 \cdot \beta \cdot H - 0.04 \cdot \beta \cdot RPM + 0.26 \cdot H \cdot RPM \quad \text{Equation 4-18}$$

Model 6

$$k_La/P_{Theo} = -76.66 - 3.68 \cdot RPM + 3.66 \cdot \alpha + 1.18 \cdot \beta + 12.39 \cdot H - 0.10 \cdot \beta \cdot H - 0.38 \cdot \alpha \cdot H + 0.26 \cdot H \cdot RPM \quad \text{Equation 4-19}$$

Model 7

$$k_La/P_{Theo} = -16.58 - 0.15 \cdot RPM - 0.03 \cdot \alpha + 2.09 \cdot \beta + 3.72 \cdot H - 0.10 \cdot \beta \cdot H - 0.04 \cdot \beta \cdot RPM + 0.003 \cdot \alpha \cdot \beta \quad \text{Equation 4-20}$$

Model 8

$$k_La/P_{Theo} = -134.75 - 1.18 \cdot RPM + 3.59 \cdot \alpha + 1.07 \cdot \beta + 18.79 \cdot H - 0.10 \cdot \beta \cdot H - 0.38 \cdot \alpha \cdot H + 0.003 \cdot \alpha \cdot \beta \quad \text{Equation 4-21}$$

Table 4-9: Assessing the predictive abilities of the models that describe the k_La per unit of theoretical energy required. Three different slopes were operated at a fluid velocity close to 10 cm s^{-}. The actual required rpm was used as an input in each model to obtain the predicted response. The residual sum of squares (RSS) is also depicted.

			Predicted k_La/P_{Theo} (W^{-1} h^{-1})							
Slope	**Fluid Velocity (cm s^{-})**	**Actual k_La/P_{theo} (W^{-1} h^{-1})**	**Model 1**	**Model 2**	**Model 3**	**Model 4**	**Model 5**	**Model 6**	**Model 7**	**Model 8**
LHH	9.6±0.1	15	13	20	11	19	11	18	10	17
HLH	10.5±0.5	14	13	5	11	3	15	7	13	5
HLL	10.0±0.1	23	23	30	21	29	21	28	19	27
		RSS	6.2	162.1	26.7	162.1	18.9	91.2	44.6	96.4

Model 1 led to the lowest RSS and was the most adequate at predicting the response. A Lack of Fit test could again not be performed since the number of degrees of freedom did not allow it. For this model, the predicted k_La/P_{theo} fell within 12 % of the experimentally determined values.

Overview

The k_La was only dependent on the paddlewheel rpm and not on the slope parameters (in the range of values tested for each parameter). Since the slope parameters affected the flow pattern over the slope, this also meant that the different type of surface flow patterns (discussed in Section 4.3.2) did not lead to variation in the k_La. Therefore, with the gas mass transfer in mind, there was no preferred type of flow pattern over the slope. These results also meant that the second hypothesis was incorrect since the slope parameters did not impact the gas mass transfer. The presence of the recirculation zone did not impact the mass transfer driving force, since a high driving force was ensured by the highly alkaline environment. The relation between wave height and surface turbulence was also not as simple as was assumed and a better way to quantify surface turbulence is required. A potential improvement to evaluate the surface turbulence after the slope could be to place an additional pH probe close to the surface in this zone, to measure a more local mass transfer. This was not done since more equipment would've been required. With only one pH probe, it would be biased against the control to place the probe in this zone. Alternatively, one could potentially use techniques such as surface Particle Image Velocimetry to better quantify the surface turbulence.

The k_La per unit of theoretical energy required however varied depending on the slope parameters. It was again shown that operating at higher paddlewheel rpms greatly reduced the k_La per unit of theoretical energy required. So although a higher paddlewheel rpm also improved the fluid velocity and mixing time, the increase in energy requirements were unfavourable. This trade-off is better quantified in Section 4.3.4, where the slope selection for the algae cultivation experiments is discussed. The 10 ° downslope also negatively impacted the theoretical energy demand by increasing the fluid velocity and head loss due to the slope. Using a downslope with a lower angle therefore does not lead to a more energy efficient slope design, as originally thought. The theoretical energy demand was in fact increased. Although the increased fluid velocity might be favourable to prevent settling, it was also shown in the previous section that the lower downslope angle reduced the mixing time. Finally, the slope height and upslope angle had a small effect on the k_La per unit of theoretical energy demand compared to the rpm and downslope angle. The final considerations for each factor evaluated in the DOE are discussed in the next section, where the slopes are compared to each other when operated at the same fluid velocity. The models obtained from the DOE were used to predict the value of the major responses for a fluid velocity of 10 cm s^{-1}. Based on these results the slopes that were used in the cultivation experiments were selected.

4.3.4 Slope selection for cultivation experiments

To select the ideal slope configuration, the trade-offs between the effects of the factors on the responses were better quantified and the slopes were also compared when operated at a fluid velocity of 10 cm s^{-1} (using the models obtained from the factorial DOE). Three slope configurations were selected to compare to the control in terms of algal productivity. Although three different paddlewheel rpms were evaluated for the control, the rpm used in the cultivation experiments was 19.8. This rpm was chosen since it was shown that lower rpms favour the k_La per unit of theoretical energy required and a suitable fluid velocity was also maintained (18.4 ± 0.3 cm s^{-1}).

To quantify the trade-offs of the factors, the factorial DOE was used to illustrate how changing each factor from the low to high value impacted the fluid velocity, mixing time, theoretical energy requirement and k_La per unit of theoretical energy required. Table 4-10 depicts the value of the four responses under consideration for slope configuration LLLL, which are the values when all four factors are on the low level. Under each of the four factors it is shown how changing the level of the factor to the high value affected the response, by showing with what amount the value of the response would increase or decrease. For example, changing the rpm to the high value of 28.9 (i.e. slope configuration HLLL) would increase the fluid velocity with 2.8 cm s^{-1} (a 24 % increase). To simplify this comparison, only the main effects were considered, without any interactions.

From Table 4-10 it is shown that higher paddlewheel rpms are not favourable, as increasing the rpm to 28.9 would increase the fluid velocity by 24 % and decrease the mixing time by 17 % but at the expense of a 108 % increase in the theoretical energy demand. Although the higher rpm would increase the k_La, the resulting k_La per unit of theoretical energy required would decrease with 61 %. The higher downslope angle would reduce the fluid velocity with 15 % but also decrease the mixing time with 5 % and theoretical energy demand with 33 %. Increasing the height would increase the k_La per unit of theoretical energy required with 8 %, although it would also decrease the fluid velocity with 28 % and increased the mixing time with 19 %. Overall the upslope angle had very little impact on the responses (< 6 % changes). Combined, these results suggest operating at a low paddlewheel rpm, high downslope angle and low slope height.

Table 4-10: Quantifying the trade-offs between the effects of the factors on the responses. Slope LLLL is used as a base case, depicting the resulting fluid velocity, mixing time, theoretical energy and k_La per unit of theoretical energy required. Under each of the factors it is shown how increasing the level from low to high would affect these four variables.

	Fluid velocity (cm s^{-1})	Increase (%)	Mixing time (s)	Increase (%)	P_{Theo} (W)	Increase (%)	k_La/P_{Theo} (W^{-1} h^{-1})	Increase (%)
LLLL	11.3	-	167	-	0.19	-	18	-
rpm	+2.8	24	-28	-17	+0.21	108	-11	-61
Upslope	-0.4	-4	0	0	-0.01	-3	+1	6
Downslope	-1.7	-15	-8	-5	-0.06	-33	+7	42
Height	-3.2	-28	+31	19	-0.04	-19	+1	8

An additional comparison was made between the effects of each factor by comparing the slopes when operated at the same fluid velocity. Table 4-11 depicts the major responses predicted by the models for each slope when operated at a fluid velocity of 10 cm s^{-1}. The predicted paddlewheel rpm to obtain this fluid velocity is also shown. In Table 4-11, the last four slopes (LLH, HLH, LHH and HHH) had a height of 10 cm. It is shown that a much higher paddlewheel rpm would be required to obtain a fluid velocity of 10 cm s^{-1} for these four slopes. Even though the higher paddlewheel rpm contributed to a reduction in the mixing time an increase in the k_La, it was shown in Table 4-10 that the effects on the theoretical energy requirement made the use of higher rpms less feasible. The k_La per unit of theoretical energy required for these four slopes would therefore be the lowest when

operated at a fluid velocity of 10 cm s^{-1}. The height of 9 cm is therefore preferred, as these slopes do not require a high paddlewheel rpm to obtain a favourable fluid velocity and the lower height also decreases the mixing time (to a greater extent than the paddlewheel rpm). Decreasing the height to 9 cm also did not have a negative effect on the k_La for the rpms evaluated.

Regarding the downslope angle, it was shown that the presence of the recirculation zone led to a lower mixing time and an improvement in the vertical mixing. It was therefore also concluded that this zone would not decrease the mass transfer rate through less surface renewal. Although the 10 ° downslope improved the fluid velocity, it removed the recirculation zone and also increased the theoretical energy requirement and the mixing time. A higher downslope angle was therefore preferred, meaning the 39 ° angle was more favourable. It was also shown that the upslope angle had a very little impact on the majority of the evaluated responses. When comparing slope LHL and HHL (Table 4-11), which both had a height of 9 cm and the 39 ° downslope, the difference in the upslope angle showed little effect on the k_La per unit of theoretical energy or mixing time. As mentioned before, it's possible that the range of values selected for the upslope angle was too small.

Table 4-11: Comparison of the eight different slopes evaluated in the factorial DOE when operated at a fluid velocity of 10 cm s^{-1}. The models describing the responses were used to determine the value of each response at this fluid velocity.

Slope	Paddlewheel rpm	Predicted k_La (h^{-1})	Predicted k_La/P_{theo} (W^{-1} h^{-1})	Predicted Mixing Time (s)	Predicted Recirculation Zone Size (cm^3)
LLL	15.5	2.56	20	177	0
HLL	16.8	2.81	23	174	0
LHL	23.3	4.00	24	142	1757
HHL	24.2	4.17	24	138	1691
LLH	30.0	5.23	15	164	0
HLH	32.3	5.67	13	158	0
LHH	31.6	5.53	13	152	1164
HHH	32.9	5.77	9	147	1068

Since the slope components were modular, it was also possible to create a slope that was not tested in the factorial DOE, although within the limits of the specific values used for the slope parameters. For example, since a higher downslope angle resulted in a lower mixing time, no downslope (similar to the 20 cm and 80 cm slope) would in fact lead to the best mixing time. A new slope was formulated, which consisted solely of the 10 ° downslope (with the height of 9 cm) used as the upslope. The 10 ° upslope angle also improved the fluid velocity, as this was much lower than the angles assessed in the DOE. This slope, which will be referred to as slope UL, was evaluated based on the fluid velocity, mixing time and k_La per unit of theoretical energy. Due to the much lower upslope angle, it in fact led to a fluid velocity of 9.7 ± 0.2 cm s^{-1} at the same paddlewheel rpm as the control (19.8). The measured responses for this slope are summarized in Table 4-12, with a comparison to slope HHL, both at a higher rpm (to achieve roughly 10 cm s^{-1}) and at the same rpm of 19.8. The 20 cm and 80 cm slopes are also included to compare the chosen designs to the best designs of Burke (2016).

Table 4-12: Summary of the three slope configurations that were selected for algal cultivation experiments, along with a comparison to the 20 cm and 80 cm slope.

Slope	Paddlewheel rpm	Fluid Velocity (cm s^{-1})	k_La (h^{-1})	k_La/P_{theo} (W^{-1} h^{-1})	Mixing Time (s)
HHL	19.8	8.1 ± 0.1	3.36 ± 0.11	33 ± 2	156 ± 1
HHL	24.2	10.0 ± 0.3	3.84	19	141 ± 6
UL	19.8	9.7 ± 0.2	3.47	29	112 ± 0
20 cm	19.8	5.7 ± 0.1	3.32 ± 0.09	27 ± 1	158 ± 1
80 cm	19.8	6.4 ± 0.1	3.49 ± 0.12	28 ± 4	142 ± 1

The responses for HHL at 24.2 rpm and UL were first predicted with the models but then confirmed with actual experimentation. The mass transfer experiments were however only performed once, which is why the k_La and k_La per unit of theoretical energy required do not show error bars. These three slope configurations had interesting pairings. Since HHL at 19.8 rpm and UL led to the same k_La, any differences in productivity are not related to the CO_2 mass transfer. HHL at 24.2 rpm compared to UL had a higher k_La but a lower mixing time, which could shed light on the importance of k_La compared to the mixing time. Operating the same slope (HHL) at two different rpm also directly shows the impact of paddlewheel rpm on the algal productivity with a slope equipped in the channel.

Slope UL and HHL at 19.8 rpm could also more directly be compared to the 20 cm and 80 cm slope, as these were operated at the same paddlewheel rpm. The major change to the designs was a decrease in the slope height, which ultimately led to improvements in the fluid velocity and mixing time while maintaining a similar k_La per unit of theoretical energy required (shown in Table 4-12). But even with these designs, the k_La per unit of theoretical energy required was lower than the control when operated at the same paddlewheel rpm (which was 48 ± 1 W^{-1} h^{-1}).

Once again the slope and control could be compared on a more level basis in terms of theoretical energy requirement, by determining the rpm required for the control to match the energy requirement of a slope. The theoretical energy requirement for slope UL was used as an example, with corresponded to 0.12 W. This would require a paddlewheel rpm of 25.4 for the control. At this rpm the mixing time would be 214 s (91 % higher than for slope UL) and the k_La would be 3.82 h^{-1} (10 % higher than what was observed for UL). This highlights the fact that at this scale, the slopes are good mixing devices but are less efficient at aeration compared to using just the paddlewheel. It has however been shown that operating at lower rpms result in a better k_La per unit of theoretical energy requirement. With the control, it would be possible to operate at even lower rpms since the fluid velocity would remain adequate. The slopes however don't have this luxury, as the fluid velocity quickly falls below 10 cm s^{-1} with a reduction in the paddlewheel rpm.

With the slopes tested in this DOE, the k_La per unit of theoretical energy required could therefore not significantly be improved in relation to the slopes depicted in Table 4-12. For this raceway pond, the control therefore favoured the k_La per unit of theoretical energy requirement but the slopes favoured the mixing time. As mentioned previously, both these variables can influence the productivity. The cultivation experiments therefore shed some light on which effect had the greatest impact on the productivity.

4.4 Algal productivity with a slope equipped in the raceway

Three slope configurations were selected to compare to a control without a slope in terms of algal productivity. The chosen parameters for each slope configuration were selected based on favourable effects on the hydrodynamics and the k_La per unit of theoretical energy required. The thought process behind the selection was discussed in Section 4.3.4.

All the hydrodynamics and mass transfer experiments were performed in only the one raceway. To ensure that the second raceway would lead to comparable results, a few hydrodynamics experiments were performed in that raceway and compared to the results obtained in the first (https://figshare.com/s/00ec7e5192c6be962de8, Raceway 1), which led to similar results. Additionally, marine silicon was used to seal the spacing between the slope and the channel walls during algae cultivation experiments, as opposed to the tape used in the hydrodynamic experiments. To confirm that there was no difference between using the clear tape and the marine silicon, the mixing and circulation time of slope configuration LHHL was also determined for the case where silicon was used. At a 95 % confidence level, there was no significant difference in the circulation time ($p = 0.65$) and the mixing time ($p = 0.06$) (https://figshare.com/s/00ec7e5192c6be962de8, Raceway 1). To further eliminate any bias between the two raceways, one of the duplicate runs for each slope was performed in the one raceway while the other run was performed in the second. Since only one of each slope was available, a control was typically run alongside each slope.

The initial two cultivation experiments performed were of the control alongside slope HHL at a paddlewheel rpm of 19.8. The use of slope HHL at 19.8 rpm, which led to an average fluid velocity of 8.1 ± 0.1 cm s^{-1}, showed significant settling of algal biomass. These two runs were stopped prematurely and a different cultivation routine was established. Instead of leaving the settling throughout the course of the run, any settling was mixed into the bulk fluid before each sample was taken. The mixer resembled a window cleaner and was constructed of PVC bars in a t-shape with a piece of silicon along the edge. This was used to scrape the walls and floor of the channel. Regardless of whether there was settling or not, the entire channel surface would be scraped, after which a period corresponding to the mixing time was waited before the samples were taken. Section 4.4.1 discusses the settling that occurred for the initial two runs, which shows a comparison between the settling observed for the control with that of a system containing a slope. Section 4.4.2 presents the productivity data obtained with the new regime where any settling was mixed into the bulk liquid throughout the course of the run.

4.4.1 Settling due to the slopes

The settling due to the slope was a direct result of the lower fluid velocity throughout the raceway. The settling however occurred in an unpredictable manner, where there were periods where a lot of settling would occur in a very short period of time. Figure 4-26 shows the optical density (OD_{750}) of the bulk fluid over time for the control and slope HHL at 19.8 rpm. The OD_{750} related to the growth of algae over time. A sudden drop in the OD_{750} indicated that there was algal settling, as the algae no longer resided in the bulk liquid.

Two significant drops in the OD_{750} were observed for slope HHL. Within the first 24 hours of cultivation, there was a sudden drop in the OD_{750} from the initial value of 0.111 down to 0.053, after which steady growth was maintained. This drop was not observed for the control. It was also likely that settling did occur during the period of steady growth, but at a more constant rate that was lower than the growth of the algae. This growth however was only maintained up to a period between day 5 and 6. Another sudden and significant drop in the OD_{750} was observed between day 5 and 6, this time also present in the control to a lesser degree. For slope HHL the OD_{750} dropped from 0.323 to 0.131 in a period of 24 hours. The settling occurred in areas where one would expect dead zone to be: after the raceway bends, especially at the bend before the paddlewheel. This coincided with areas where the fluid velocity was at its lowest. Figure 4-27 a) illustrates the settling observed within the first 24 hours for slope HHL after the bend before the paddlewheel. Surprisingly the area after the slope showed no visual settling (Figure 4-27 b), which was originally expected to be an area where settling could occur. This meant that the recirculation zone was turbulent enough to prevent settling and further supported the argument that downslope was not required.

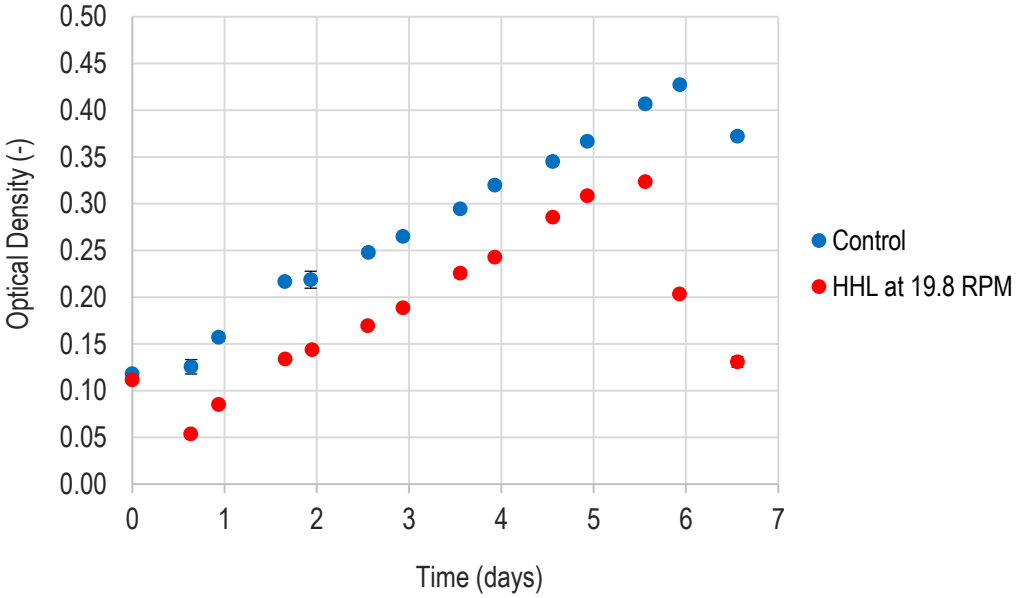

Figure 4-26: A comparison between the control and slope HHL at 198 rpm, showing the growth of algae over time through the optical density. These initial runs illustrated the problem of settling in the raceway pond due to the slope. Error bars indicate standard error with n = 3.

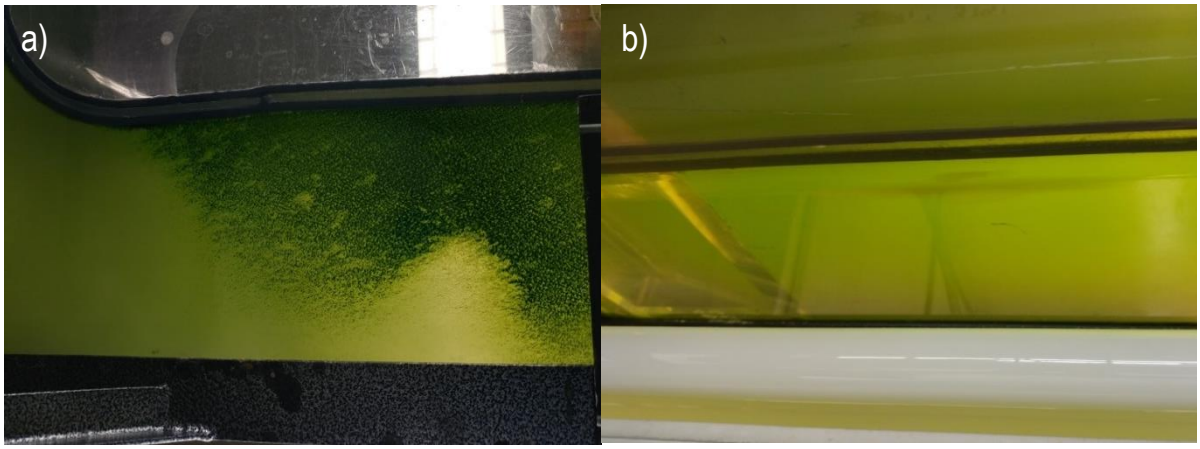

Figure 4-27: Settling observed with slope HHL at 19.8 rpm within the first 24 hours after inoculation, explaining the sharp decrease in the optical density. The settling primarily occurred before the paddlewheel (shown in a) and before the slope (after the first bend). The area after the slope however did not have settling, shown in b), indicating that the recirculation zone was indeed turbulent enough to prevent settling.

The decrease in OD_{750} between day 5 and 6 however was brought about by the sudden onset of wall growth. Before day 5, no wall growth was observed in both cases. Once wall growth started it became easier for more algae to accumulate onto the walls as they now lashed onto the algae that were already anchored, which explains the rapid decrease in the OD_{750}. The wall growth occurred throughout the entire raceway although was concentrated in the areas which would have the lowest fluid velocity. This again coincided with the areas where one would expect a dead zone. Figure 4-28 illustrates the settling on day 6 for slope HHL in comparison to the control. As mentioned, with the new cultivation regime, any settling was mixed into the bulk liquid prior to sampling.

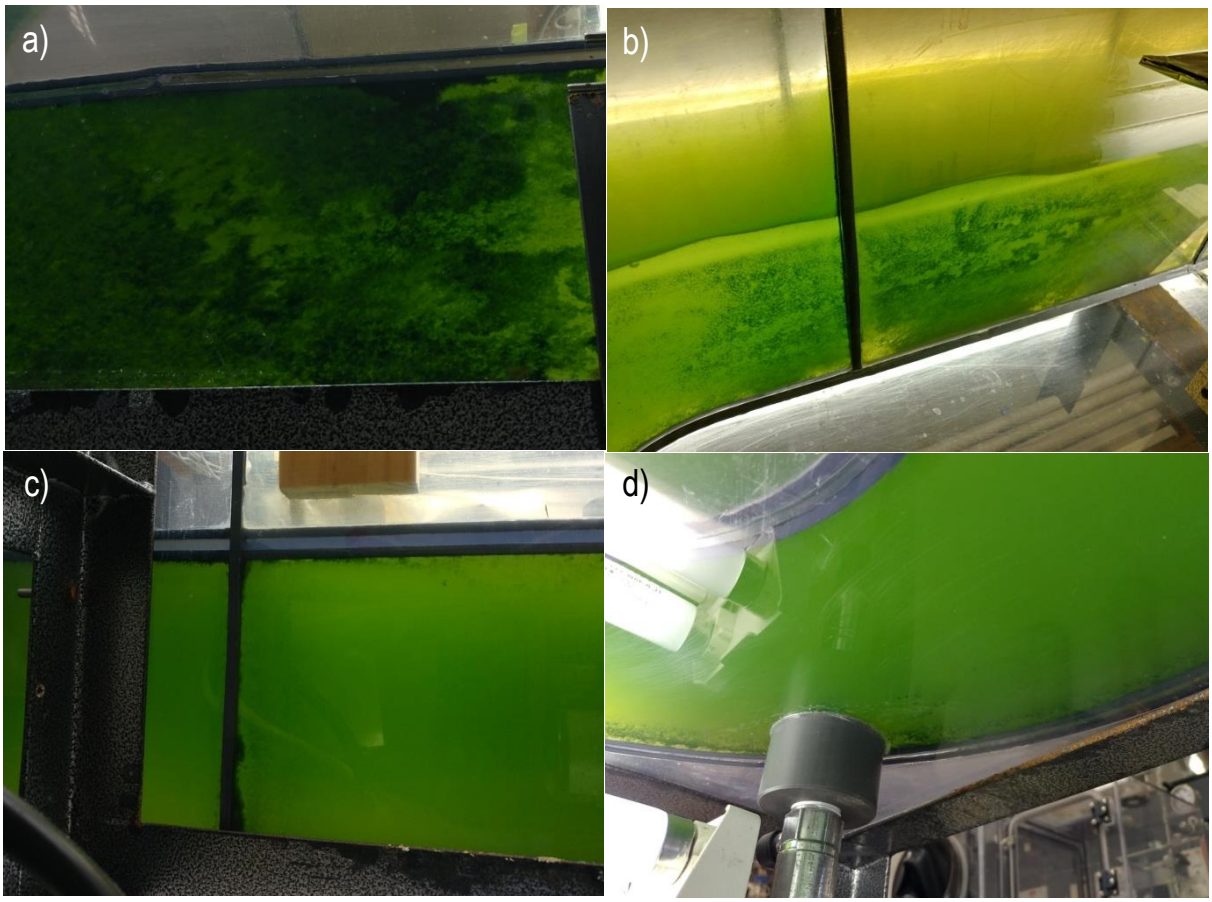

Figure 4-28: Settling observed at day six with a comparison between slope HHL at 19.8 rpm (a and b) and the control (c and d). A sudden increase in the wall growth was observed with slope HHL. The control also showed settling, but far less compared to the slope.

4.4.2 Increase in algal productivity due to the slopes

With the new cultivation regime, where the settling was mixed into the bulk liquid before sampling, three runs of the control were performed along with duplicate runs for each of the three slope configurations. A sample of the growth along with the change in pH over time is shown in Figure 4-29 (for Run 1 of slope UL).

The cultures were CO_2 limited, which can be seen in the graph of pH over time (Figure 4-29 a). The graph depicts three distinct stages (separated with the red lines): a rapid increase in the pH (day 4 – 7), followed by a period of deceleration up until the pH stabilized (day 7 – 13), and then a decrease in the pH (after day 13). This pattern was observed for all the runs. The increase in pH shows that the dissolution of CO_2 into the system could not keep up with the rate of photosynthesis, since the dissolution of CO_2 would decrease the pH while the process of photosynthesis increases the pH. This increase can be explained by a net uptake of H^+ by the algae to regulate internal pH as OH^- is produced during the conversion of HCO_3^- to CO_2 inside the cells (Chi et al., 2011). CO_2 (as opposed to HCO_3^-) is required in the Calvin cycle, where it is utilized in the carboxylation of ribulose bisphosphate, the first step in the production of carbohydrates from inorganic carbon (Masojídek et al., 2021).

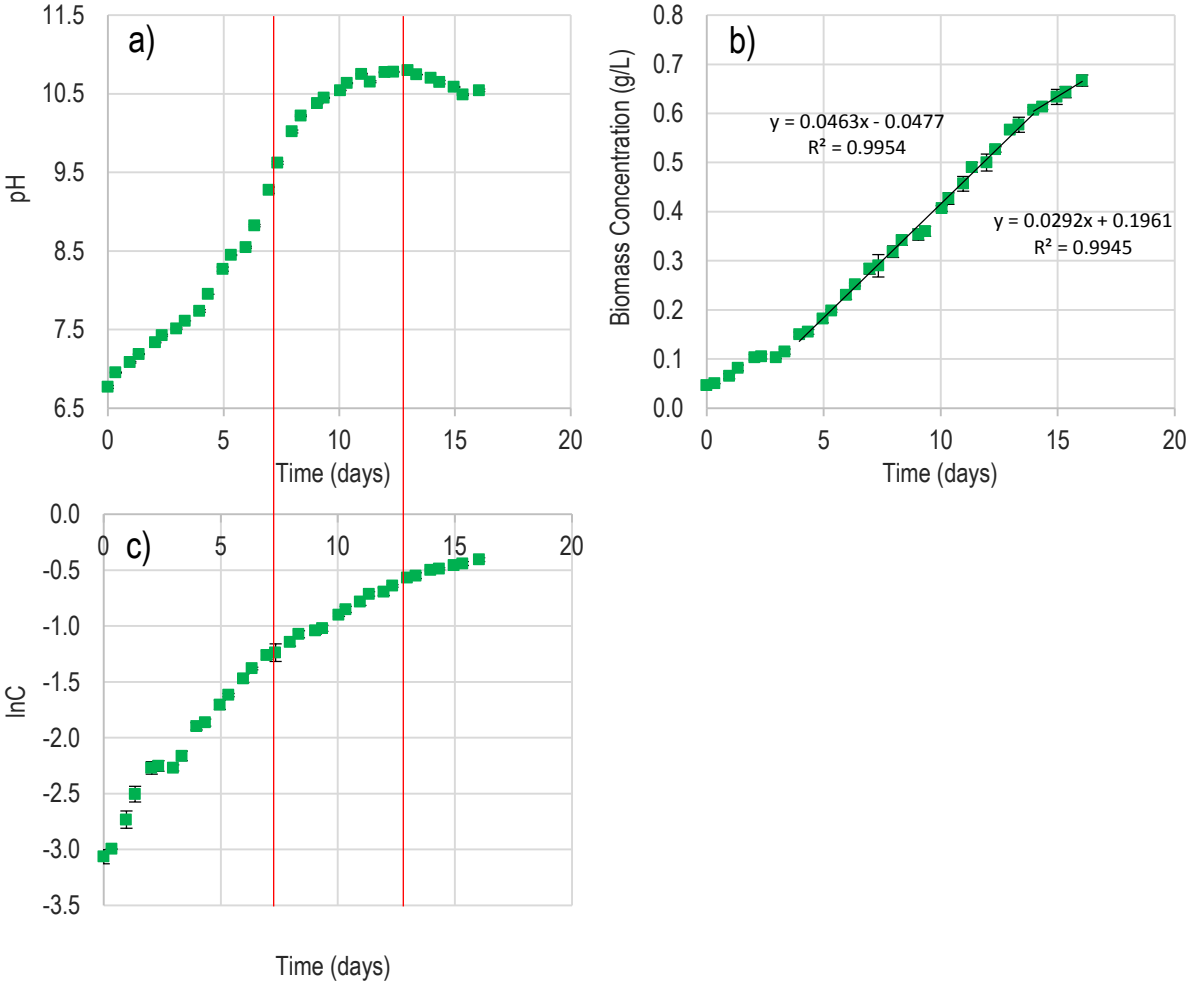

Figure 4-29: Run 1 for slope UL showing the a) pH over time, b) biomass concentration over time, c) natural logarithm of the biomass concentration over time. Error bars depict standard deviation with n = 3.

The change in pH also dictated the speciation of inorganic carbon in the culture. At a pH value around 8.5 the inorganic carbon would no longer be in the form of aqueous CO_2, but primarily in the form of HCO_3^- (the exact pH would differ slightly with temperature and salinity) (Pedersen et al., 2013). As the pH further increased, more of the inorganic carbon converted to CO_3^-, which the algae are not able to utilize (Lohman et al., 2015; Pedersen et al., 2013). This coincided with a gradual decreased in the specific growth rate over time (seen in Figure 4-29 c, where the specific growth rate corresponds to the slope of the curve). The drop in specific growth rate after day 7 was likely a response to the decrease in available inorganic carbon. The decrease in the specific growth rate then caused the pH to stabilize, as the rate of CO_2 assimilation eventually became equal to the amount utilized during photosynthesis.

The decrease in pH from day 13 indicates that there was a reduction in the rate of photosynthesis. This showed that there was something other than carbon that limited the growth. It's possible that this was a switch from carbon limitation to light limitation, as this typically occurred around a biomass concentration of 0.6 g L^{-1} (although this was not always the case). The increase in concentration of algae meant that the mutual shading of cells increased up to a point where the light no longer sufficiently penetrated into the culture. A lower algal productivity (from day 14, shown in Figure 4-29 b) was also observed after 0.6 g L^{-1} was reached. For comparative purposes, the algal productivity was therefore calculated up to the point when the culture first reached a concentration of about 0.6 g L^{-1}. As mentioned however, the drop in pH did not always occur when the culture reached a concentration of 0.6 g L^{-1} - specifically for the two runs for slope HHL at 24 rpm. In these two runs, the

drop in pH occurred before 0.6 g L^{-1} was reached. A comparison was made between measuring the productivity up to the point where the pH first started to drop compared to measuring it up to 0.6 g L^{-1} (https://figshare.com/s/00ec7e5192c6be962de8, Raceway 4). Both methods however led to similar results, and it was decided to measure the productivity up to 0.6 g L^{-1}.

Figure 4-30 shows the biomass concentration over time for the control and three slope configurations. The time axes were corrected to align the data from different runs as the culture typically experienced variation (0 – 1 days) in the lag phase. The starting point from which the productivity was measured was therefore chosen to be the time the culture first reached a pH of 7.5.

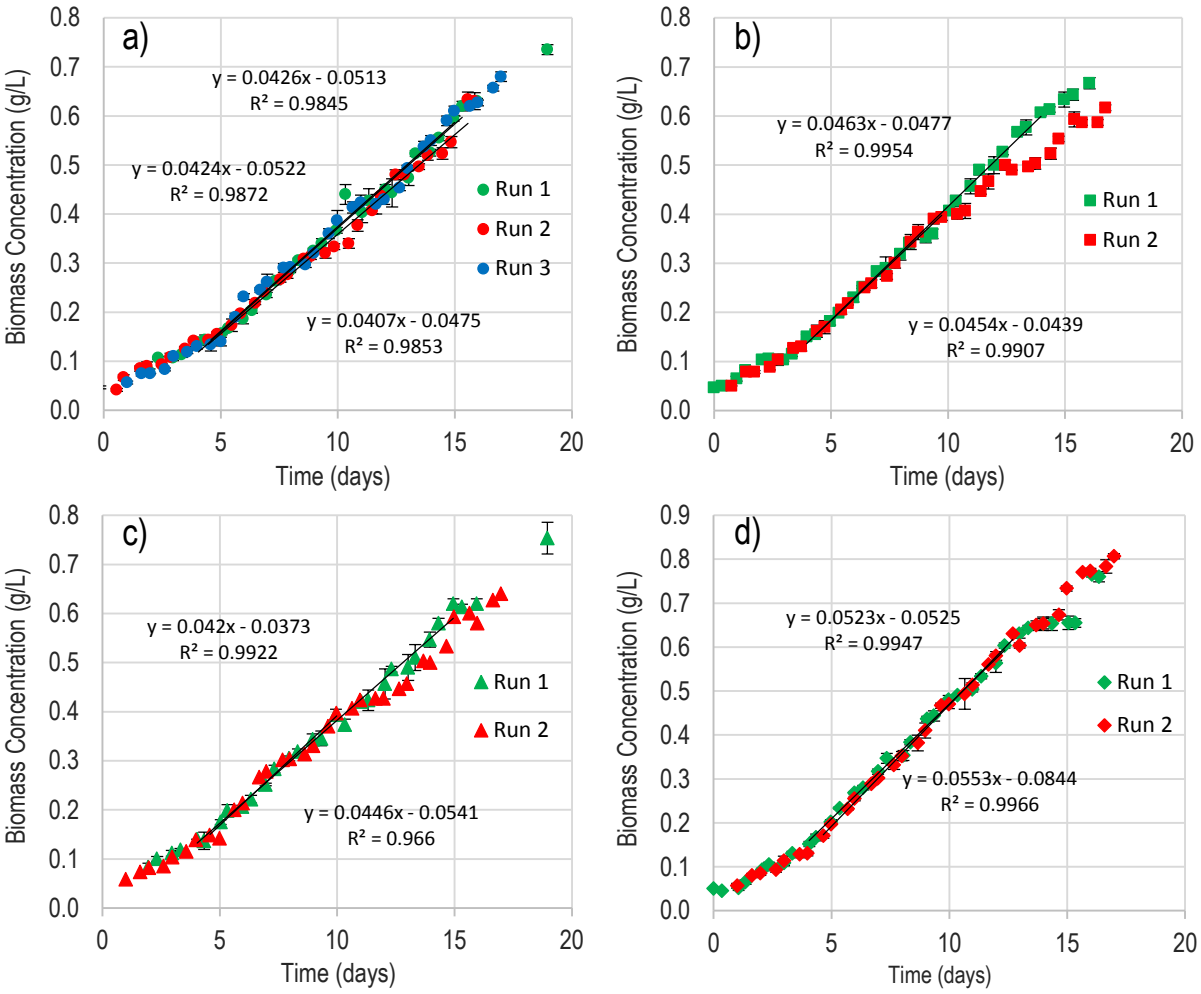

Figure 4-30: Biomass concentration over time for a) control without a slope, b) slope UL at 19.8 rpm, c) slope HHL at 19.8 rpm, d) slope HHL at 24 rpm. The productivity is shown in the slope of the curve. Error bars depict standard deviation with n = 3.

In two of the runs for the slope configurations the productivity was not calculated up to a concentration of 0.6 g L^{-1}. This was because there was a clear decrease in the productivity after a certain point before 0.6 g L^{-1}, meaning there was another factor affecting the growth. With Run 2 of slope HHL at 19.8 rpm (Figure 4-30 c), the room temperature in the lab was 18 – 19 °C, much lower than the average 24 °C for the other runs. For this run (along with Run 3 of the control, operated in parallel to this run), a single aquarium heater was placed in the raceway after the paddlewheel to maintain a temperature of 25 °C in the raceway. The heater was added on day 9. This was however detrimental to the algae in the case of slope HHL, but did not impact the control. The low fluid velocity due to slope HHL (8.1 ± 0.1 cm s^{-1} compared to 18.4 ± 0.3 cm s^{-1} for the control) meant that the algae spent a longer time close to the heater, which had a temperature much higher than 25 °C on its surface. A

thick layer of green foam was observed around the heater. This indicated that the high temperature destroyed some of the algae cells, causing the decrease in the productivity after day 9. The temperature of the heater was gradually decreased once the foam was observed, although this did not alleviate the problem. The productivity for Run 2 of HHL was therefore only considered up to day 9. Measuring the productivity up to a concentration of 0.6 g L^{-1} gave a value of 0.038 g L^{-1} day^{-1}, 15 % lower than the productivity measured up to day 9.

A clear decrease in productivity was also apparent in Run 2 of slope UL (Figure 4-30 b) after day 10. For this run the pH started to drop earlier compared to the first run and this culture had a slightly dull colour with more clumping than usual. A sample of the culture was observed under a microscope, which also revealed that there was a different organism present in the culture, resembling a protozoan flagellate (https://figshare.com/s/00ec7e5192c6be962de8, Raceway 4). Given that the raceway ponds are open systems, it is not surprising that there could be a different micro-organism in the culture. Flagellates can be heterotrophic, feeding on bacteria and smaller algae (Asleigh, 2000). This can potentially cause clumping in an algae culture, as a defence mechanism against predation (Wiltshire et al., 2003). It was however not clear whether this organism was feeding on the algae as it was also the same size as the algae. On top of this the highly alkaline conditions ensured that bacteria and pests were kept at bay as these do not typically thrive in a high pH environment. With the other runs the cultures were not actively monitored under the microscope, meaning it's not possible to say whether a flagellate was present in the other cultures as well. These occurrences showed that it would be advantageous to actively monitor the culture. Due to the drop in productivity after day 10, the growth data only up to this point was used to determine the productivity of Run 2 for slope UL, as it is also clear that the growth up to this period was very similar to Run 1. The productivity measure up to a biomass concentration of 0.6 g L^{-1} (0.036 g^{-1} L^{-1} day^{-1}) was 20 % lower than the productivity up to day 10 (0.045 g/L/day).

Table 4-13 depicts a comparison between the average productivity observed for the control and slope configurations. The productivity per theoretical energy requirement and the increase in k_La compared to the control is also included.

Table 4-13: Comparison between the algal productivity for the control and slope configurations, along with the increase in k_La and productivity per theoretical energy requirement. The standard error is included for the control, with n=3.

Configuration	Productivity (g^{-1} L^{-1} day^{-1})	Increase in Productivity (%)	Increase in k_La (%)	Productivity per theoretical energy requirement (g^{-1} L^{-1} day^{-1} W^{-1})
Control	0.042 ± 0.001	-	-	0.66 ± 0.02
UL	0.046	10	15	0.38
HHL at 19.8 rpm	0.043	3	12 ± 3	0.42
HHL at 24 rpm	0.054	27	28	0.27

The productivity observed for the control was 0.042 ± 0.001 g^{-1} L^{-1} day^{-1}. Variation in the three runs for the control was acceptable, where the relative standard deviation (standard deviation divided by average productivity) was 4.3 %. The resulting standard error was therefore small. The slopes did indeed lead to an increase in the productivity compared to the control. The percentage increase in productivity was very similar to the percentage increase in k_La for both slope UL (10 % and 15 %, respectively) and HHL at 24 rpm (27 % and 28 %, respectively). The relation between the increase in k_La and productivity makes sense considering the fact that the cultures were CO_2 limited. This pattern was however not observed for slope HHL at 19.8 rpm, which showed a much lower increase in productivity compared to the increase in k_La (3 % and 12 ± 3 %, respectively). Given that both slope UL and HHL at 19.8 rpm led to a similar k_La (since they were operated at the same paddlewheel rpm), it was expected that these two slope configurations would lead to the same productivity. A possible reason that slope HHL led to the lower productivity is the lower fluid velocity and higher mixing time, which could be responsible for more settling.

In general, the observed productivities (0.042 – 0.054 g $L^{-1}day^{-1}$) were relatively low compared to the productivity of *Scenedesmus* sp. cultured in raceway ponds, although within range of what one might expect. There are however no studies with the exact same operating conditions for a direct comparison. A volumetric productivity between 0.046 and 0.115 g L^{-1} day^{-1} (3.5 – 8.7 g m^{-2} day^{-1}) was observed by Eustance et al. (2016) for *Scenedesmus* sp. cultivated in an outdoor raceway of 30.4 m^2 (2300 L) with CO_2 sparging. Kannan and Venkat (2019) cultured *Scenedesmus* sp. in an outdoor raceway pond of 3.2 m^2 (1000 L) with CO_2 sparging. The productivity varied between 0.011 and 0.072 g L^{-1} day^{-1} (3.5 – 22 g m^{-2} day^{-1}) where the lower productivity in the range was observed during colder winter months. One might expect the algal productivity to be lower in a raceway where CO_2 sparging was not utilized, as the culture in this study was CO_2 limited. On the other hand, with a smaller indoor raceway it would be reasonable to think that the productivity could be higher due to better mixing.

The productivity per theoretical energy required was the highest for the control, at 0.66 ± 0.02 g L^{-1} day^{-1} W^{-1}. This was due to the significantly lower theoretical energy requirement compared to the slopes. This result suggests that, if the energy requirements are also considered, the slopes might not be required in these specific raceway ponds. On the smaller scale the paddlewheel has a more dominating effect on the overall mixing and gas mass transfer rate (this idea is discussed in more detail in Section 4.5 and 4.6). As a result it would be just as easy to merely increase the paddlewheel rpm as opposed to adding a slope in the raceway. With this specific raceway, although the same productivity would be achievable by simply increasing the rpm without the use of a slope, there could exist a maximum rpm, dictated by the shear the algae can withstand. Then, for any given rpm, it was shown that adding a slope would further increase the productivity. This does mean that adding a slope would be beneficial strictly in terms of space and time utilization, assuming that the shear stress caused by the paddlewheel blade tips is more than the shear in the hydraulic jump and recirculation zone.

Even though the productivity per unit of energy requirement is a parameter that should ideally be maximized, a better comparison might be obtained when incorporating costs. The specific selling price of the biomass relative to the cost of electricity and other inputs, such as growth media, could lead to a different conclusion. With the implementation of a renewable energy source, for example, the slopes are certainly favoured, since they did improved the algal productivity through enhanced gas mass transfer and significantly reduced the mixing time. Decreasing the energy requirements of the pond was further explored by comparing a propeller system to the paddlewheel, discussed in the next section. The growth experiments on this scale have also shown the need to scale up the slopes to larger raceway ponds. Some considerations for scale-up are discussed in Section 4.6.

4.5 Substituting the paddlewheel with a propeller

It was shown that the slopes led to a much higher head loss that greatly increased the energy demand of the system. As discussed in the literature review, paddlewheels have relatively low efficiencies and could potentially be replaced by more energy efficient fluid driving devices. The paddlewheel was replaced with a propeller to evaluate its effects on the hydrodynamics, gas mass transfer and energy demand.

Table 4-14 shows a comparison between the mixing time and Peclet number for the paddlewheel system and the propeller system. The propeller was set to produce a fluid velocity that matched the velocity produced by the paddlewheel control operated at an rpm of 19.8. There was no significant difference between the measured fluid velocities at a 95 % confidence level (p = 0.49).

At the same fluid velocity the propeller showed a slight improvement in the mixing time compared to the paddlewheel system, which corresponded to a 6 ± 3 % decrease. The improved mixing in relation to the similar fluid velocity meant that the Peclet number was also decreased, indicating that there was better back-mixing. But since the Peclet number remained above 100 the flow was still closer to plug flow conditions. Although the global hydrodynamics were fairly similar between the two systems, there were great differences in the measured k_La and energy input.

Table 4-14: Fluid velocity, mixing time and Peclet number for the control with a paddlewheel compared to a propeller as the fluid driving device. For each case the standard error is shown with n = 3.

Configuration	Fluid Velocity (cm s^{-1})	Mixing Time (s)	Peclet Number (-)
Paddlewheel	18.4 ± 0.3	255 ± 2	143 ± 2
Propeller	17.7 ± 0.7	240 ± 8	124 ± 17

Table 4-15 shows a comparison between the two systems in terms of the k_La, theoretical energy requirement, actual energy input and the k_La in relation to the energy requirements. The k_La measured for the propeller system was 28 % lower than that of the paddlewheel driven system. This is interesting considering the similarity in the global hydrodynamics (such as the mixing time and fluid velocity), but makes sense when one considers the local hydrodynamics at each device. The paddlewheel led to numerous flow characteristics that favour gas mass transfer. As each blade left the water a waterfall was created when the fluid that was scooped up plunged into the fluid in front of the paddlewheel (Figure 4-31 a). This also created splashing and turbulence which favours gas mass transfer. Furthermore, each blade was covered in a thin layer of fluid when not submerged. This enhanced the surface area for mass transfer compared to the propeller which was fully submerged. The propeller occasionally created bubbles (Figure 4-31 b) which should increase the mass transfer surface area, but this was clearly not enough to compete with the paddlewheel. With these factors in mind the paddlewheel is simply a better gas mass transfer device.

Table 4-15: Comparison in k_La and energy demand for the paddlewheel and propeller system. For each value the standard error is also shown with n = 3.

Configuration	k_La (h^{-1})	Theoretical Energy Required (w)	Actual Energy Input (W)	k_La per Theoretical Energy (W^{-1} h^{-1})	k_La per Actual Energy (W^{-1} h^{-1})
Paddlewheel	3.00 ± 0.09	0.06 ± 0.00	11.24 ± 0.26	48 ± 1	0.27 ± 0.01
Propeller	2.15 ± 0.05	0.06 ± 0.00	5.10 ± 0.05	39 ± 2	0.42 ± 0.01

Since the fluid velocity was matched, the calculated theoretical energy requirement for each system was very similar, as indicated in Table 4-15. As a result however, the k_La per unit of theoretical energy required for the paddlewheel system was better than that of the propeller system due to higher k_La measured with the paddlewheel. But taking the overall efficiency of the devices into account led to major differences in the actual energy input, which was measured using the power meter. Here the efficiency of the propeller driven system is demonstrated, as the actual energy input was 5.10 ± 0.05 W compared to the 11.24 ± 0.26 W for the paddlewheel system, a 56 % decrease. Granted, the paddlewheel system did suffer from the lower motor efficiency due to the oversized motor. The resulting k_La per unit of actual energy input was 0.42 ± 0.01 W^{-1} h^{-1} for the propeller and 0.27 ± 0.01 W^{-1} h^{-1} for the paddlewheel system. This could be attributed to the greater efficiency of the propeller system. Based on these results however, one cannot state with complete certainty that the propeller system was more favourable, since this paddlewheel system was not ideal.

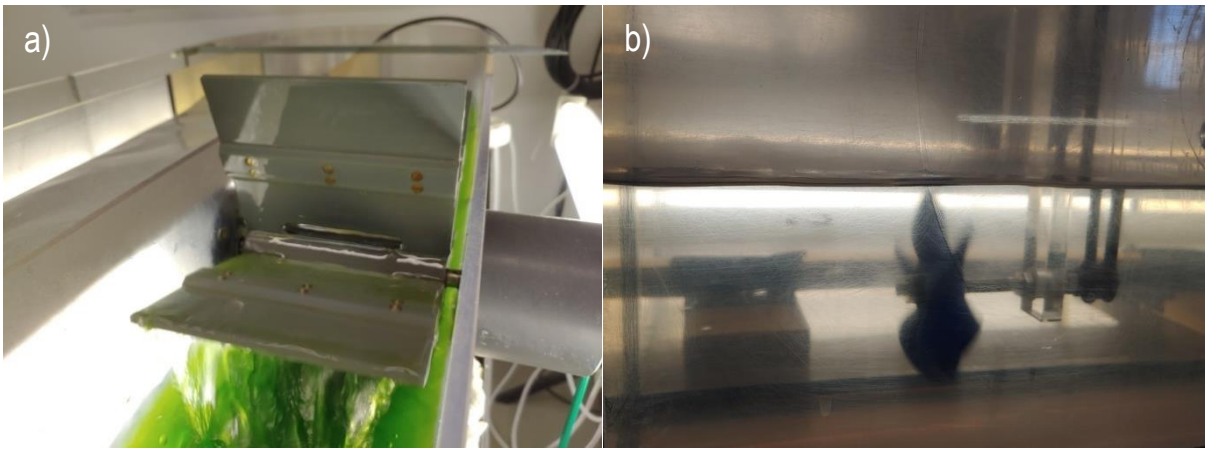

Figure 4-31: Comparison of the local flow pattern at each fluid driving device. a) The paddlewheel created a waterfall that plunged into the fluid in front of it and also created a thin layer of fluid on each blade. b) The propeller would often create a small number of bubbles but did not create the same degree of surface turbulence as the paddlewheel.

An interesting consideration is the dominance of the paddlewheel's contribution to the k_La for this raceway pond. The average fluid velocity was kept the same, so one might expect the k_La around the bends and in the straight channel to be relatively similar between the two systems. The difference in k_La between the systems could therefore be attributed to the fluid driving device and the surrounding area. In general, the k_La measured close to the paddlewheel should be much larger than the k_La measured at the bends or in the straight channel sections. An estimate of the global k_La could then be obtained by accounting for the area where the mass transfer is measured relative to the total surface area of the pond. For a small raceway, such as the one used in this study, the area affected by the paddlewheel is large relative to the total surface area of the raceway. This should lead to a higher contribution of the paddlewheel to the mass transfer. For larger scale raceways however the contribution of the paddlewheel to the global mass transfer decreases due to the way in which raceway ponds scale. Since only the area of the pond is increased, the area affected by the paddlewheel is much smaller relative to the total surface area. The surface area of the straight channel sections then become much larger, meaning the global k_La becomes more dominated by the k_La measured in the straight channel sections. The fact that the fluid driving device is a good gas mass transfer device then becomes less important on a larger scale. The effects of the propeller on the k_La per unit of energy input would therefore only be amplified on a larger scale. This justifies the evaluation of a propeller system on a larger scale raceway pond as it is likely to outperform the paddlewheel system in terms of k_La per unit of energy input.

In summary, it was shown that the propeller improved the mixing time to a small extent when the fluid velocity was kept the same relative to the paddlewheel system. The paddlewheel however proved to be a better gas mass transfer device. The k_La per theoretical energy required was therefore higher for the paddlewheel system, but when the efficiency of the devices were considered the propeller showed a greater k_La per unit of actual energy input. These effects should be amplified on a larger scale, as the contribution of the fluid driving device to the global k_La becomes less dominant. A similar argument about the dominance of the paddlewheel to the contribution of k_La could be made for the slopes. Since the slopes affect the surface turbulence in the straight channel section, it might be possible that the increase in the global k_La compared to the control will be higher on larger scales. Considerations for scale up are discussed in the next section, where it is justified that further studies should be performed on a larger scale.

4.6 Considerations for scale-up

An argument can be made to evaluate both types of slope designs on a larger scale (slope PW used to create ocean breakers as well as the weir-like slope designs that create a hydraulic jump). Slope PW failed to create breaking waves but this was likely due to the strong effects of surface tension on the small waves created by the paddlewheel used in this study. On a larger scale it might be possible to form breaking waves as the pulsating wave created by the paddlewheel would be larger. Whether the breaking waves would have a significant effect on the CO_2 mass transfer is however still in question. With regard to the weir-like designs the increase in k_La was not enough relative to the increase in the energy demand, which meant that the productivity per unit of theoretical energy required was lower than what was observed for the control. But a similar argument for the use of a propeller on a larger scale could be made for the slopes. Since the overall k_La on a large scale becomes more dominated by the k_La throughout the straight channel sections, it might be possible that the effects of the slope on the k_La could be amplified, as the surface turbulence is created in the straight channel.

Furthermore, a larger scale outdoor raceway experiences diurnal changes not observed in the lab scale raceway used in this study. Outdoor raceways undergo large variations in the fluid temperature, as the raceway cools down during night time and needs to heat up during the day. Light limitation also plays a more dominating role when not in peak daylight hours. Proper mixing then becomes more important, as better mixing means that the raceway heats up quicker due to alleviated temperature gradients and vertical mixing relieves the limitation on light penetration. It was shown that the slopes greatly improved the mixing time and also enhanced vertical mixing. The effect the slopes had on the mixing were however not as important in the lab scale raceway since the room temperature was controlled and light was supplied from the sides and bottom of the raceway as well. On the smaller scale, the productivity was more limited by the CO_2 mass transfer alone.

A foreseeable problem with scale-up however would be the use of multiple of the weir-like slopes in one raceway. Since the length of the straight channels increases it is likely that more than one slope would be required, as the surface area affected by the slope also decreases in relation to the total surface area. Using more than one of the weir-like slope designs in a raceway could be problematic due to the drastic decrease in the fluid velocity. Adding more slopes would mean that the fluid velocity decreases even further which would require much higher paddlewheel rpms to ensure critical flow over the slopes. This problem would not occur with slope PW, since the fluid velocity was not significantly impacted. This slope did however not lead to the same amount of mixing as the weir-like designs. A possible solution could then be to use one weir-like slope design with focus on improving the mixing coupled with numerous slopes similar to slope PW, granted that slope PW has a significant effect on the CO_2 mass transfer.

For the weir-like slope designs, one thing that needs to be considered is to what extent the results obtained in this study are applicable to a larger scale. The major dimensional difference between the two scales is a change in the surface area, brought about by an increase in the straight channel lengths and width, meaning the cross-sectional area of the channel is also larger. The fluid depth and velocity however typically remain the same, although might vary slightly. With free-surface flows such as flow in open channels, scaling is typically done based on Froude similitude, to give dynamic similarity, which implies that the Froude number for the small and large scale systems should be similar (Chanson, 2004; Henderson, 1966). Since the velocity and fluid depth are typically kept the same for raceway ponds, this means that the Froude number will also be the same. For a larger raceway pond operated at a depth of 12 cm, it would be reasonable to assume that the fluid will behave in a similar way as in the lab scale. In this case, the relative effect of each slope parameter on the responses will likely not drastically change compared to what was observed in this study, in the sense that the upslope angle would have a very small effect on the responses compared to the slope height, as an example. It is however very unlikely that each slope parameter would affect the responses to the same degree in terms of magnitude. For example, changing the slope height from 10 cm to 9 cm will not lead to the same percentage decrease in the mixing time on a larger scale.

This study therefore showed dead ends that do not need to be re-evaluated on a larger scale. It is unlikely that increasing the paddlewheel rpm would be a good tactic to increase the fluid velocity when a slope is in the channel, because the energy demand also increases non-linearly with paddlewheel rpm on a larger scale. Changes in the upslope angle in the range evaluated in this study would likely not have a significant effect on the responses. The presence of the recirculation zone after the slope would not affect the CO_2 mass transfer and the turbulence in this zone should be sufficient to prevent the algae from settling there. A trade-off that could potentially be different on a larger scale however is the effect of the downslope angle. It was shown in this study that the downslope angle affected the mixing time in two opposing ways: a lower angle removed the recirculation zone but increased the fluid velocity throughout the pond. The mixing brought about by the presence of the recirculation zone was dominant compared to the mixing due to the improved fluid velocity, so a higher downslope angle was preferred. The mixing layer and recirculation zone on the small scale however consisted of a much larger volume with respect to the total volume of the raceway when compared to a larger scale raceway.

On a larger scale the mixing brought about by the slope through the recirculation zone will likely be dampened and it's possible that a higher fluid velocity would have a more dominating effect on the overall mixing time. It's therefore possible that a lower downslope angle might be preferred. The slope height is however the major element that would need to be optimized, as it was shown in this study to be the factor with the highest impact on the fluid velocity and mixing time, although did not have an effect on the k_La in the range of values tested. The slope height could be decreased to a point just above the height where the k_La starts to decrease due to the diminishing surface turbulence. On a larger scale it would therefore be interesting to evaluate the effects of the slope height and downslope angle and also focus more on the length of the surface turbulence created, in other words, the total surface area affected by the slope as opposed to the wave height (as was the focus in this study).

5 Conclusion and Recommendations

This study explored an alternative method to enhance the CO_2 mass transfer rate into raceway ponds to improve the productivity of microalgal growth. The method aimed to create surface turbulence in the form of waves, which was brought about by adding a slope in the raceway channel. Previous work by Burke (2016) showed the potential of this method. The main objectives of this study were to get a better understanding of how the slope parameters affect the hydrodynamics and gas mass transfer and to improve on the previous slope designs. A propeller was also explored as an alternative fluid driving device, to decrease the energy demand of the system. Table 5-1 gives a comparative summary of a few key configurations tested in the raceway pond, to highlight some of the major findings from this work.

Table 5-1: Comparison of important parameters and slope configurations to highlight major findings in this work. Errors indicate Standard Error with n=3. Values with no errors were either obtained from models or evaluated only a single time.

Configuration	RPM	Fluid Velocity (cm s^{-1})	Mixing Time (s)	k_La (h^{-1})	Productivity (g L^{-1} day^{-1})	P_{Theo} (W)
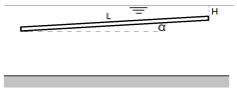 Slope PW	19.8	17.9 ± 0.3	210 ± 1	3.09 ± 0.11	-	0.09 ± 0.02
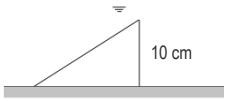 Burke (2016)	19.8	5.7 ± 0.1	158 ± 1	3.32 ± 0.05	-	0.12 ± 0.01
 Slope UL	19.8	9.7 ± 0.2	112 ± 0	3.47	0.046	0.12
 Control	19.8	18.4 ± 0.3	255 ± 2	3.00 ± 0.05	0.042 ± 0.001	0.06 ± 0.00
 Control	25.4	22.7	214	3.82	-	0.12
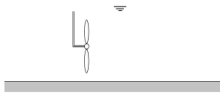 Propeller System	248	17.7 ± 0.7	240 ± 8	2.15 ± 0.03	-	0.06 ± 0.00

Slope PW (designed to emulate ocean waves) did not lead to the formation of breaking waves, which did not result in an increase in k_La compared to the control without a slope (Table 5-1). It was observed that the pulse travelling over the slope steepened, but never got to the point of breaking. It was likely that the surface tension of the water was too great to form a breaking wave on this scale. This slope did however lead to a decrease in the mixing time (by 18 %) due to the formation of a mixing layer after the slope. An advantage of this slope was that the fluid velocity was not changed relative to the control and the increase in energy demand was not as high as the weir-like slope designs. These results have accentuated the trouble of scaling down systems. This slope would be

interesting to evaluate on a larger scale, as it might be possible to form breaking waves since a larger paddlewheel would create a pulse with a higher amplitude.

It was originally hypothesised that, with the weir-like slopes, the increase in CO_2 mass transfer rate could further be improved by creating waves with a larger height and by removing the recirculation zone after the slope. The results showed that, at any given rpm, the different slope parameters led to different flow patterns over the slope, with variation in the size of the waves. There was however not a clear relation between the wave height and k_La, as the increase in k_La was the same regardless of the slope parameters. The initial wave height was therefore not an accurate representation of the total surface turbulence. Additionally, it was shown that the presence of the recirculation zone had no impact on the CO_2 mass transfer rate. Summarized in Table 5-1, the new slope design could not significantly improve on the increase in k_La, although the fluid velocity and mixing time was improved upon. The upslope angle typically had an insignificant effect on the responses. The downslope angle showed counteracting effects, where a smaller angle improved the fluid velocity, but also increased energy losses and reduced the mixing time by removing the recirculation zone after the slope. Reducing the slope height improved the mixing time and fluid velocity, although there would exist a minimum limit of the height where the surface would no longer be disturbed. A limitation of the specific DOE utilized was that the optimal slope height could not be determined. Reducing the height could further improve the fluid velocity and mixing time but should at some point lead to a lower k_La due to less surface turbulence.

Regardless, the slopes led to an increase in k_La (by 12 ± 2 % on average) compared to the control without a slope operated at the same rpm. However, a limitation of the weir-like slopes was the considerable increase in the energy demand. Table 5-1 highlights the comparison between the two slopes (at 19.8 rpm) and the control (at 25.4 rpm) when operated at the same theoretical energy expense. It was shown that in this case the control led to a higher k_La while the slopes led to a better mixing time. This shows that the paddlewheel is a better gas mass transfer device on a small scale. However, as the scale increases, there is a limitation on the increase in gas mass transfer supplied by the paddlewheel, while the overall k_La throughout the pond is lower due to the extended straight channel sections. Improvements in mixing (especially in the vertical direction) also become increasingly important. This suggests that it would be valuable to supplement the straight channel sections with elements that improve the local mixing and gas mass transfer. It is therefore important to understand how the slopes impact these variables, and these results show sufficient potential for it to be important to study at scale.

It was also hypothesised that the weir-like slopes would increase the algal productivity compared to the control due to an increase in the CO_2 mass transfer rate and enhanced mixing. The productivity was increased up to 10 % when the rpm was kept the same as the control (19.8 rpm, Table 5-1). The increase in productivity was closely related to the increase in k_La with two of the three slopes evaluated in the cultivation experiments, indicating that the cultures were CO_2 limited. When incorporating the energy demand, the productivity per unit of theoretical energy required was greater for the control than for the slopes (0.67 ± 0.02 g L^{-1} day^{-1} W^{-1} compared to the highest value of 0.42 g L^{-1} day^{-1} W^{-1} observed for a slope). This again suggests that the use of a slope would be dependent on the size of the raceway, where with a smaller pond the slopes are less effective. However, since the slopes lead to an increase in productivity, the space-time utilization of a raceway can be improved upon with the addition of a slope, which can be an important consideration.

The propeller system was evaluated to explore the possibility of decreasing the energy demand of the system. When operated at the same fluid velocity, the propeller led to a lower k_La compared to the paddlewheel (by 28 %), but the k_La per unit of actual energy input was greater (by 58 %). This showed that the propeller was more energy efficient, although this paddlewheel system utilized an oversized motor, which contributed to the high actual energy input of the paddlewheel. This meant that the increase of 58 % is an overestimation. The k_La for the paddlewheel system was better as it led to numerous flow characteristics that enhanced gas mass transfer (such as an increased surface area and higher turbulence). Although the paddlewheel was better at improving the gas mass transfer, the propeller system could still be viable on a larger scale due to the nature in which

raceways scale. On scale-up, the gas mass transfer capability of the fluid driving device becomes less relevant and the energy considerations become more important.

Overall, these lab scale experiments showed the need to evaluate the slopes and propeller on a larger scale, which is the logical next step. Care should be taken to properly show that the slopes are a simple and low cost alternative to sparging CO_2 gas into the system. The groundwork laid out in these experiments can be used to guide the designs for the large scale slopes. For further investigations, the following recommendations are made:

- A better way to quantify the surface turbulence is required, as opposed to measuring the surface wave height. A possibility would be to measure the local CO_2 mass transfer rate in the affected area using an additional pH probe. Another possibility is the use of Particle Image Velocimetry technology.
- It would also be advantageous to be able to directly measure local fluid velocities and at multiple locations in the pond. This could be done through acoustic Doppler velocimetry.
- Both the weir-like slope design and the progressive wave slope design should be evaluated on a larger scale.
- For the weir-like slope designs, based on the results of the DOE, the slope height is the most important parameter that needs to be optimized, followed by the downslope angle. These parameters had typically had the greatest effect on the responses.
- On a larger scale, the use of more measuring probes would be advantageous to determine the hydrodynamics and CO_2 mass transfer rate in the different regions of the pond.
- In large scale experiments, the slopes should again be compared to a traditional sparging system, while also quantifying costs of energy expenditure and other inputs (media and CO_2) for a clear comparison.
- Further studies on this lab scale raceway pond, regardless of the use of a slope, could be enriched by suitable equipment to properly quantify the efficiency of the motor, such as a torque meter.

References

Abu-Ghosh, S., Fixler, D., Dubinsky, Z., Iluz, D., 2016. Flashing light in microalgae biotechnology. Bioresour. Technol. 203, 357–363. https://doi.org/10.1016/J.BIORTECH.2015.12.057

Aitchison, T.F., Timmons, M.B., Bisogni, J.J., Piedrahita, R.H., Vinci, B.J., 2007. Using Oxygen Gas Transfer Coefficients to Predict Carbon Dioxide Removal. Int. J. Recirc. Aquac. 8. https://doi.org/10.21061/ijra.v8i1.1416

Ali, S., 2013. Flow Over Weir-like Obstacles. PhD Thesis. Delft University of Technology.

Ansari, F.A., Shekh, A.Y., Gupta, S.K., Bux, F., 2017. Microalgae for Biofuels: Applications, Process Constraints and Future Needs, in: Algal Biofuels. Springer International Publishing, Cham, pp. 57–76. https://doi.org/10.1007/978-3-319-51010-1_3

Asleigh, M., 2000. Trophic Strategies, in: The Flagellates, Unity, Diversity and Evolution. Taylor and Francis Limited, pp. 147–165.

Azimi, A.H., Rajaratnam, N., Zhu, D.Z., 2014. Submerged Flows over Rectangular Weirs of Finite Crest Length. J. Irrig. Drain. Eng. 140, 06014001. https://doi.org/10.1061/(ASCE)IR.1943-4774.0000728

Bai, R., Zhu, D., Chen, H., Li, D., 2019. Laboratory study of secondary flow in an open channel bend by using PIV. Water (Switzerland) 11, 16–18. https://doi.org/10.3390/w11040659

Bascom, W., 1980. The Surf, in: Waves and Beaches: The Dynamics of the Ocean Surface. Anchor Press, pp. 216–246.

Battjes, J.A., 1974. Surf Similarity. Coast. Eng. Proc. 1, 26. https://doi.org/10.9753/icce.v14.26

Becker, E.W., 1994. Microalgae : Biotechnology and Microbiology, 1st ed. Cambridge University Press.

Benedetti, M., Vecchi, V., Barera, S., Dall'Osto, L., 2018. Biomass from microalgae: The potential of domestication towards sustainable biofactories. Microb. Cell Fact. 17, 173. https://doi.org/10.1186/s12934-018-1019-3

Bień, A.K., 1984. Mass transfer to the free interface in stirred vessels. Chem. Eng. Commun. 31, 155–183. https://doi.org/10.1080/00986448408911148

Blackburn, S.I., Volkman, J.K., 2012. Microalgae: A Renewable Source of Bioproducts, in: Dunford, N.T. (Ed.), Food and Industrial Bioproducts and Bioprocessing. Wiley and Sons, pp. 221–242.

Borowitzka, M.A., 2013. High-value products from microalgae—their development and commercialisation. J. Appl. Phycol. 25, 743–756. https://doi.org/10.1007/s10811-013-9983-9

Borowitzka, M.A., 2005. Culturing Microalgae in Outdoor Ponds, in: Algal Culturing Techniques. Elsevier, pp. 205–218. https://doi.org/10.1016/b978-012088426-1/50015-9

Borowitzka, M.A., Moheimani, N.R., 2013. Open Pond Culture Systems, in: Borowitzka, M.A., Moheimani, N.R. (Eds.), Algae for Biofuels and Energy. Springer, pp. 133–152.

Burke, M., 2016. Carbon Dioxide Mass Transfer Within Algal Raceway Ponds and the Potential for Improvement Using Slopes to Create Waves. MSc Thesis. University of Cape Town.

Camenen, B., Larson, M., 2007. Predictive Formulas for Breaker Depth Index and Breaker Type. J. Coast. Res. 234, 1028–1041. https://doi.org/10.2112/05-0566.1

Carvalho, A.P., Silva, S.O., Baptista, J.M., Malcata, F.X., 2011. Light requirements in microalgal photobioreactors: an overview of biophotonic aspects. Appl. Microbiol. Biotechnol. 89, 1275–1288. https://doi.org/10.1007/s00253-010-3047-8

Cengel, Y.A., Cimbala, J.M., 2014. Approximate Solutions of the Navier-Stokes Equation, in: Fluid Mechanics: Fundamentals and Applications. McGraw Hill Education, pp. 515–593.

Chanson, H., 2011. Hydraulic jumps: turbulence and air bubble entrainment. La Houille Blanche 5–16. https://doi.org/10.1051/lhb/2011026

Chanson, H., 2004. The Hydraulics of Open Channel Flow: An Introduction, 2nd ed. Elsivier Butterworth-Heinemann.

Chanson, H., Jaw-Fang, L., 1997. Plunging jet characteristics of plunging breakers. Coast. Eng. 31, 125–141. https://doi.org/10.1016/S0378-3839(96)00056-7

Chanson, H., Montes, J.S., 1995. Characteristics of Undular Hydraulic Jumps: Experimental

Apparatus and Flow Patterns. J. Hydraul. Eng. 121, 129–144. https://doi.org/10.1061/(ASCE)0733-9429(1995)121:2(129)

Chaudhry, M.H., 2008. Rapidly Varied Flow, in: Open-Channel Flow. Springer Science+Business Media, pp. 199–241.

Chella, M.A., Bihs, H., Myrhaug, D., Muskulus, M., 2015. Breaking characteristics and geometric properties of spilling breakers over slopes. Coast. Eng. 95, 4–19. https://doi.org/10.1016/j.coastaleng.2014.09.003

Cheng, J., Guo, W., Cai, C., Ye, Q., Zhou, J., 2018. Alternatively permutated conic baffles generate vortex flow field to improve microalgal productivity in a raceway pond. Bioresour. Technol. 249, 212–218. https://doi.org/10.1016/j.biortech.2017.10.031

Cheng, J., Yang, Z., Ye, Q., Zhou, J., Cen, K., 2015. Enhanced flashing light effect with up-down chute baffles to improve microalgal growth in a raceway pond. Bioresour. Technol. 190, 29–35. https://doi.org/10.1016/j.biortech.2015.04.050

Chi, Z., O'Fallon, J. V., Chen, S., 2011. Bicarbonate produced from carbon capture for algae culture. Trends Biotechnol. 29, 537–541. https://doi.org/10.1016/j.tibtech.2011.06.006

Chiaramonti, D., Prussi, M., Casini, D., Tredici, M.R., Rodolfi, L., Bassi, N., Zittelli, G.C., Bondioli, P., 2013. Review of energy balance in raceway ponds for microalgae cultivation: Re-thinking a traditional system is possible. Appl. Energy 102, 101–111. https://doi.org/10.1016/j.apenergy.2012.07.040

Chiaramonti, D., Tredici, M.R., Prussi, M., Biondi, N., 2015. Algae Biofuels, in: Handbook of Clean Energy Systems. John Wiley & Sons, Ltd, pp. 85–100.

Chisti, Y., 2016. Large-Scale Production of Algal Biomass: Raceway Ponds. Springer, Cham, pp. 21–40. https://doi.org/10.1007/978-3-319-12334-9_2

Chisti, Y., 2013. Raceways-based production of algal crude oil. Green 3, 195–216. https://doi.org/10.1515/green-2013-0018

Chisti, Y., 2007. Mass Transfer, in: Kirk-Othmer Encyclopedia of Chemical Technology. John Wiley & Sons, Inc., Hoboken, NJ, USA. https://doi.org/10.1002/0471238961.1301191903080919.a01.pub2

Clarke, K., 2013. The oxygen transfer rate and overall volumetric oxygen transfer coefficient, in: Bioprocess Engineering: An Introductory Engineering and Life Science Approach. Woodhead Publishing Limited, pp. 147–169.

Cokelet, E.D., 1977. Breaking waves. Nature 267, 769–774. https://doi.org/10.1038/267769a0

Crump, E.S., 1952. A New Method of Gauging Stream Flow With Little Afflux By Means of a Submerged Weir of Triangular Profile. Proc. Inst. Civ. Eng. 1, 749–767. https://doi.org/10.1680/iicep.1952.10982

Csanady, G., 2001. The Transfer Laws of the Air-Sea Interface, in: Air-Sea Interaction: Laws and Mechanics. Cambridge University Press, Cambridge, pp. 1–48.

Davis, M.E., Davis, R.J., 2003. Nonideal Flow in Reactors, in: Fundamentals of Chemical Reaction Engineering. McGraw Hill Higher Education, pp. 260–285.

Davis, R., Markham, J., Kinchin, C., Grundl, N., Tan, E., Humbird, D., 2016. Process Design and Economics for the Production of Algal Biomass: Algal Biomass Production in Open Pond Systems and Processing Through Dewatering for Downstream Conversion. Natl. Renew. Energy Lab. 128.

de Godos, I., Mendoza, J.L., Acién, F.G., Molina, E., Banks, C.J., Heaven, S., Rogalla, F., 2014. Evaluation of carbon dioxide mass transfer in raceway reactors for microalgae culture using flue gases. Bioresour. Technol. 153, 307–314. https://doi.org/10.1016/j.biortech.2013.11.087

Deane, G.B., Stokes, M.D., Deane, G.B., Stokes, M.D., 1999. Air Entrainment Processes and Bubble Size Distributions in the Surf Zone. J. Phys. Oceanogr. 29, 1393–1403. https://doi.org/10.1175/1520-0485(1999)029<1393:AEPABS>2.0.CO;2

Demory, D., Combe, C., Hartmann, P., Talec, A., Pruvost, E., Hamouda, R., Souillé, F., Lamare, P.-O., Bristeau, M.-O., Sainte-Marie, J., Rabouille, S., Mairet, F., Sciandra, A., Bernard, O., 2018. How do microalgae perceive light in a high-rate pond? Towards more realistic Lagrangian experiments. R. Soc. open Sci. 5, 180523. https://doi.org/10.1098/rsos.180523

Dodd, J.C., 1986. Elements of Pond Design and Construction, in: Richmond, A. (Ed.), Handbook of Microalgal Mass Culture. pp. 265–284.

Elhajj, J., Al-Hindi, M., Azizi, F., 2014. A review of the absorption and desorption processes of carbon dioxide in water systems. Ind. Eng. Chem. Res. 53, 2–22. https://doi.org/10.1021/ie403245p

Eustance, E., Badvipour, S., Wray, J.T., Sommerfeld, M.R., 2016. Biomass productivity of two Scenedesmus strains cultivated semi-continuously in outdoor raceway ponds and flat-panel photobioreactors. J. Appl. Phycol. 28, 1471–1483. https://doi.org/10.1007/s10811-015-0710-6

Fernandez, F.G., Sevilla, J.M., Molina-Grima, E., 2012. Principles of Photobioreactor Design, in: Posten, C., Walter, C. (Eds.), Microalgal Biotechnology: Potential and Production. De Gruyter, pp. 151–178.

Fritz, H.M., Hager, W.H., 1998. Hydraulics of Embankment Weirs. J. Hydraul. Eng. 124, 963–971. https://doi.org/10.1061/(ASCE)0733-9429(1998)124:9(963)

Gifuni, I., Pollio, A., Safi, C., Marzocchella, A., Olivieri, G., 2019. Current Bottlenecks and Challenges of the Microalgal Biorefinery. Trends Biotechnol. 37, 242–252. https://doi.org/10.1016/j.tibtech.2018.09.006

Goldsack, D.E., Franchetto, R., 1977. The viscosity of concentrated electrolyte solutions. I. Concentration dependence at fixed temperature. Can. J. Chem. 55, 1062–1072. https://doi.org/10.1139/v77-148

Gordon, J.M., Polle, J.E.W., 2007. Ultrahigh bioproductivity from algae. Appl. Microbiol. Biotechnol. https://doi.org/10.1007/s00253-007-1102-x

Green, D.W., Perry, R.H., 2008. Perry's Chemical Engineers' Handbook, 8th ed. McGraw-Hill Companies, Inc.

Griffiths, M.J., Harrison, S.T.L., 2009. Lipid productivity as a key characteristic for choosing algal species for biodiesel production. J. Appl. Phycol. 21, 493–507. https://doi.org/10.1007/s10811-008-9392-7

Grobbelaar, J.U., 2012. Microalgae mass culture: The constraints of scaling-up. J. Appl. Phycol. 24, 315–318. https://doi.org/10.1007/s10811-011-9728-6

Grobbelaar, J.U., 2009. Upper limits of photosynthetic productivity and problems of scaling. J. Appl. Phycol. 21, 519–522. https://doi.org/10.1007/s10811-008-9372-y

Grobbelaar, J.U., Nedbal, L., Tichý, V., 1996. Influence of high frequency light/dark fluctuations on photosynthetic characteristics of microalgae photoacclimated to different light intensities and implications for mass algal cultivation. J. Appl. Phycol. 8, 335–343. https://doi.org/10.1007/BF02178576

Hadiyanto, H., Elmore, S., Van Gerven, T., Stankiewicz, A., 2013. Hydrodynamic evaluations in high rate algae pond (HRAP) design. Chem. Eng. J. 217, 231–239. https://doi.org/10.1016/j.cej.2012.12.015

Hakim, S.S., Azimi, A.H., 2017. Hydraulics of Submerged Triangular Weirs and Weirs of Finite-Crest Length with Upstream and Downstream Ramps. J. Irrig. Drain. Eng. 143, 06017008. https://doi.org/10.1061/(asce)ir.1943-4774.0001207

Hallman, A., 2007. Algal transgenics and biotechnology. Transgenic Plant J. 1, 81–98.

Han, L., 2015. Recirculation zone developing downstream of an expansion in a shallow open-channel flow. PhD Thesis. National Institute of Applied Sciences of Lyon.

Henderson, F.M., 1966. Similitude and Models, in: Open Channel Flow. Macmillan Publishing Company, N.Y., pp. 488–513.

Holthuijsen, L.H., 2007. Linear Wave Theory (Coastal Waters), in: Waves in Oceanic and Coastal Waters. Cambridge University Press, pp. 197–242. https://doi.org/10.1017/CBO9780511618536

Hoque, A., Aoki, S., 2005. Distributions of void fraction under breaking waves in the surf zone. Ocean Eng. 32, 1829–1840. https://doi.org/10.1016/J.OCEANENG.2004.11.013

Hreiz, R., Sialve, B., Morchain, J., Escudié, R., Steyer, J.-P., Guiraud, P., 2014. Experimental and numerical investigation of hydrodynamics in raceway reactors used for algaculture. Chem. Eng. J. 250, 230–239. https://doi.org/10.1016/J.CEJ.2014.03.027

Huang, J., Qu, X., Wan, M., Ying, J., Li, Y., Zhu, F., Wang, J., Shen, G., Chen, J., Li, W., 2015. Investigation on the performance of raceway ponds with internal structures by the means of CFD simulations and experiments. Algal Res. 10, 64–71. https://doi.org/10.1016/j.algal.2015.04.012

Huang, Z.C., Hsiao, S.C., Hwung, H.H., Chang, K.A., 2009. Turbulence and energy dissipations of surf-zone spilling breakers. Coast. Eng. 56, 733–746. https://doi.org/10.1016/j.coastaleng.2009.02.003

Janssen, M., 2016. Microalgal Photosynthesis and Growth in Mass Culture. Adv. Chem. Eng. 48, 185–256. https://doi.org/10.1016/bs.ache.2015.11.001

Kannan, D.C., Venkat, D., 2019. An open outdoor algal growth system of improved productivity for biofuel production. J. Chem. Technol. Biotechnol. 94, 222–235. https://doi.org/10.1002/jctb.5768

Kapoor, K.L., 2019. Ionic Equilibria, in: A Textbook of Physical Chemistry: States of Matter and Ions in Solution. McGraw Hill Education (India) Private Limited, pp. 231–405.

Khan, M.I., Shin, J.H., Kim, J.D., 2018. The promising future of microalgae: Current status, challenges, and optimization of a sustainable and renewable industry for biofuels, feed, and other products. Microb. Cell Fact. https://doi.org/10.1186/s12934-018-0879-x

Klinthong, W., Yang, Y.H., Huang, C.H., Tan, C.S., 2015. A Review: Microalgae and their applications in CO<inf>2</inf> capture and renewable energy. Aerosol Air Qual. Res. https://doi.org/10.4209/aaqr.2014.11.0299

Kraus, N.C., Smith, E.R., Kraus, N.C., (U.S.), C.E.R.C., Station., U.S.A.E.W.E., States., U., 1990. Laboratory study on macro-features of wave breaking over bars and artificial reefs / by Ernest R. Smith, Nicholas C. Kraus. Available from National Technical Information Service, Vicksburg, Miss. : https://doi.org/10.5962/bhl.title.48327

Kubar, A., Cheng, J., Guo, W., Kumar, S., Song, Y., 2020. Development of a single helical baffle to increase CO2 gas and microalgal solution mixing and Chlorella PY-ZU1 biomass yield. Bioresour. Technol. 307, 123253. https://doi.org/10.1016/j.biortech.2020.123253

Kumar, K., Mishra, S.K., Shrivastav, A., Park, M., Yang, J.-W., 2015. Recent Trends in the Mass Cultivation of Algae in Raceway Ponds. Renew. Sustain. Energy Rev. 51, 875–885.

Kumar, S., Cheng, J., Guo, W., Ali, K.A., Song, Y., 2019. Self-rotary propellers with clockwise/counterclockwise blades create spiral flow fields to improve mass transfer and promote microalgae growth. Bioresour. Technol. https://doi.org/10.1016/j.biortech.2019.121384

Lahav, O., Morgan, B., Loewenthal, R., 2001. Measurement of pH, alkalinity and acidity in ultra-soft waters. Water SA 27, 423–432. https://doi.org/10.4314/wsa.v27i4.4954

Laws, E.A., Berning, J.L., 1991. A Study of the Energetics and Economics of Microalgal Mass Culture with the Marine Chlorophyte Tetraselmis suecica: Implications for Use of Power Pkant Stack Gases. Biotechnol. Bioeng. 37, 936–947.

Lee, Y.K., 2016. Microalgae Cultivation Fundamentals, in: Bux, F., Chisti, Y. (Eds.), Algae Biotechnology: Products and Processes. Springer International Publishing, pp. 1–19.

Leman, A., Holland, M., Tinoco, R.O., 2018. Identifying the dominant physical processes for mixing in full-scale raceway tanks. Renew. Energy 129, 616–628. https://doi.org/10.1016/j.renene.2018.05.087

Li, Y., Zhang, Q., Wang, Z., Wu, X., Cong, W., 2014. Evaluation of power consumption of paddle wheel in an open raceway pond. Bioprocess Biosyst. Eng. 37, 1325–1336. https://doi.org/10.1007/s00449-013-1103-3

Liffman, K., Paterson, D.A., Liovic, P., Bandopadhayay, P., 2013. Comparing the energy efficiency of different high rate algal raceway pond designs using computational fluid dynamics. Chem. Eng. Res. Des. 91, 221–226. https://doi.org/10.1016/j.cherd.2012.08.007

Lohman, E.J., Gardner, R.D., Pedersen, T., Peyton, B.M., Cooksey, K.E., Gerlach, R., 2015. Optimized inorganic carbon regime for enhanced growth and lipid accumulation in Chlorella vulgaris Luisa Gouveia. Biotechnol. Biofuels 8, 1–13. https://doi.org/10.1186/s13068-015-0265-4

López, A.R., Rodríguez, S.B., Vallejo, R.A., García, P.G., Macías-Sánchez, M.D., Díaz, M.G., Librán, R.G., Acero, F.J.F., 2019. Sustainable cultivation of Nannochloropsis gaditana microalgae in outdoor raceways using flue gases for a complete 2-year cycle: a Circular Economy challenge. J. Appl. Phycol. 31, 1515–1523. https://doi.org/10.1007/s10811-018-1710-0

Madadi, M.R., Hosseinzadeh Dalir, A., Farsadizadeh, D., 2013. Control of undular weir flow by changing of weir geometry. Flow Meas. Instrum. 34, 160–167. https://doi.org/10.1016/j.flowmeasinst.2013.09.003

Masojidek, J., Koblizek, M., Torzillo, G., 2004. Photosynthesis in Microalgae, in: Richmond, A. (Ed.), Handbook of Microalgal Culture: Biotechnolohy and Applied Phycology. Blackwell Science, pp. 20–39.

Masojídek, J., Ranglová, K., Lakatos, G.E., Benavides, A.M.S., Torzillo, G., 2021. Variables governing photosynthesis and growth in microalgae mass cultures. Processes 9.

https://doi.org/10.3390/pr9050820

Massey, B., 2006. Flow with a Free Surface, in: Mechaniscs of Fluids. Taylor & Francis, pp. 414–483.

Mehta, S.K., Gaur, J.P., 2005. Use of algae for removing heavy metal ions from wastewater: Progress and prospects. Crit. Rev. Biotechnol. https://doi.org/10.1080/07388550500248571

Melville, W.K., 1996. The Role of Surface-Wave Breaking in Air-Sea Interaction. Annu. Rev. Fluid Mech. 28, 279–321. https://doi.org/10.1146/annurev.fl.28.010196.001431

Mendoza, J.L., Granados, M.R., de Godos, I., Acién, F.G., Molina, E., Banks, C., Heaven, S., 2013a. Fluid-dynamic characterization of real-scale raceway reactors for microalgae production. Biomass and Bioenergy 54, 267–275. https://doi.org/10.1016/j.biombioe.2013.03.017

Mendoza, J.L., Granados, M.R., de Godos, I., Acién, F.G., Molina, E., Heaven, S., Banks, C.J., 2013b. Oxygen transfer and evolution in microalgal culture in open raceways. Bioresour. Technol. 137, 188–195. https://doi.org/10.1016/j.biortech.2013.03.127

Millero, F.J., 1995. Thermodynamics of the carbon dioxide system in the oceans. Science (80-.). 59, 661–677.

Molina-Grima, E., 1999. Microalgae, Mass Culture Methods, in: Flickinger, M.C., Drew, S.W. (Eds.), Encyclopedia of Bioprocess Technology: Fermentation, Biocatalysis and Bioseparation. John Wily & Sons Inc.

Montgomery, D.C.A.S.U., 2013. Two-Level Fractional Factorial Designs, in: Design and Analysis of Experiments. John Wiley & Sons, pp. 320–376.

Moroney, J. V., Somanchi, A., 1999. How do algae concentrate CO2 to increase the efficiency of photosynthetic carbon fixation? Plant Physiol. 119, 9–16. https://doi.org/10.1104/pp.119.1.9

Mukaro, R., Govender, K., McCreadie, H., 2013. Wave Height and Wave Velocity Measurements in the Vicinity of the Break Point in Laboratory Plunging Waves. J. Fluids Eng. 135, 061303. https://doi.org/10.1115/1.4023659

Munson, B., Young, D., Okiishi, T., Huebsch, W., 2009. Open Channel Flow, in: Fundamentals of Fluid Mechanics. Wiley and Sons, pp. 554–591.

Musgrave, E., 2017. Investigating the performance of paddlewheels used in microalgae raceways for the production of biomass. University of Southampton Research Repository.

Musgrove, E., Heaven, S., 2014. Investigating the hydrodynamic performance of carbonation sumps in High Rate Algal Pond (HRAP)raceways using computational fluid dynamics (CFD). Biofuels 5, 723–739. https://doi.org/10.1080/17597269.2015.1024387

Ohtsu, I., Yasuda, Y., Gotoh, H., 2001. Hydraulic condition for undular-jump formations. J. Hydraul. Res. 39, 203–209. https://doi.org/10.1080/00221680109499821

Olaizola, M., 2000. Commercial production of astaxanthin from Haematococcus pluvialis using 25,000-liter outdoor photobioreactors. J. Appl. Phycol. 499–506.

Oswald, W.J., 2003. My sixty years in applied algology. J. Appl. Phycol. 15, 99–106. https://doi.org/10.1023/a:1023871903434

Packer, M.A., Harris, G.C., Adams, S.L., 2016. Food and Feed Application of Algae, in: Bux, F., Chisti, Y. (Eds.), Algae Biotechnology: Products and Processes. Springer International Publishing, pp. 217–247.

Pedersen, O., Colmer, T.D., Sand-Jensen, K., 2013. Underwater photosynthesis of submerged plants - Recent advances and methods. Front. Plant Sci. 4. https://doi.org/10.3389/fpls.2013.00140

Price, G.D., Badger, M.R., Woodger, F.J., Long, B.M., 2008. Advances in understanding the cyanobacterial CO2-concentrating- mechanism (CCM): Functional components, Ci transporters, diversity, genetic regulation and prospects for engineering into plants, in: Journal of Experimental Botany. pp. 1441–1461. https://doi.org/10.1093/jxb/erm112

Pritchard, P.J., Leylegian, J.C., 2011. Fox and McDonald's Introduction to Fluid Mechanics, Eigth. ed. John Wiley & Sons, Inc.

Pulz, O., Gross, W., 2004. Valuable products from biotechnology of microalgae. Appl. Microbiol. Biotechnol. https://doi.org/10.1007/s00253-004-1647-x

Putt, R., Singh, M., Chinnasamy, S., Das, K.C., 2011. An efficient system for carbonation of high-rate algae pond water to enhance CO2 mass transfer. Bioresour. Technol. 102, 3240–3245. https://doi.org/10.1016/J.BIORTECH.2010.11.029

Richardson, J.F., Harker, J.H., Backhurst, J.R., 2002. Absorption of Gases, in: Coulson and

Richardson's Chemical Engineering: Particle Technology and Separation Processes Volume 2. Elsevier, pp. 656–717.

Rivas-Interián, R.M., Guillén-Francisco, J.A., Sacramento-Rivero, J.C., Zitlalpopoca-Soriano, Á.G., Baz-Rodríguez, S.A., 2019. Concentration effects of main components of synthetic culture media on oxygen transfer in bubble column bioreactors. Biochem. Eng. J. 143, 131–140. https://doi.org/10.1016/j.bej.2018.12.008

Russell, R.C.H., MacMillan, D.H., 1954. Waves and Tides, 2nd ed.

Scargiali, F., Busciglio, A., Grisafi, F., Brucato, A., 2013. Influence of viscosity on mass transfer performance of unbaffled stirred vessels, in: Chemical Engineering Transactions. pp. 1483–1488. https://doi.org/10.33032/CET1332248

Shukry, A., 1950. Flow Around Bends in an Open Flume. Trans. Am. Soc. Civ. Eng. 115, 751–779.

Simon, E.J., Dicky, J.L., Reece, J.B., 2019. Photosynthesis: Using light to make food, in: Cambell Essential Biology. Pearson, pp. 106–115.

Sompech, K., Chisti, Y., Srinophakun, T., 2012. Design of raceway ponds for producing microalgae. Biofuels 3, 387–397. https://doi.org/10.4155/bfs.12.39

Sumer, B.M., Guner, H.A.A., Hansen, N.M., Fuhrman, D.R., Fredsøe, J., 2013. Laboratory observations of flow and sediment transport induced by plunging regular waves. J. Geophys. Res. Ocean. 118, 6161–6182. https://doi.org/10.1002/2013JC009324

Sunamura, T., Okazaki, S., 1996. Breaker Types and Wave Reflection Coefficient: Laboratory Relationships. J. Coast. Res. 12, 240–245.

Sutherland, D.L., Howard-Williams, C., Turnbull, M.H., Broady, P.A., Craggs, R.J., 2015. Enhancing microalgal photosynthesis and productivity in wastewater treatment high rate algal ponds for biofuel production. Bioresour. Technol. 184, 222–229. https://doi.org/10.1016/J.BIORTECH.2014.10.074

Ting, F.C.K., Kirby, J.T., 1996. Dynamics of surf-zone turbulence in a spilling breaker. Coast. Eng. 27, 131–160. https://doi.org/10.1016/0378-3839(95)00037-2

Veron, F., Melville, W.K., Lenain, L., 2009. Measurements of ocean surface turbulence and wave-turbulence interactions. J. Phys. Oceanogr. 39, 2310–2323. https://doi.org/10.1175/2009JPO4019.1

Wallingford, H.R., n.d. Tables for the Hydraulic Design of Pipes, Sewers and Channels, Volume 1, 7th ed. Thomas Telford Services.

Wang, Y., Stessman, D.J., Spalding, M.H., 2015. The CO2 concentrating mechanism and photosynthetic carbon assimilation in limiting CO2: How Chlamydomonas works against the gradient. Plant J. 82, 429–448. https://doi.org/10.1111/tpj.12829

Webb, P., 2019. Waves, in: Introduction to Oceanography. Simple Book Publishing, pp. 231–250.

Weggel, J.R., 2015. Maximum Breaker Height for Design, in: Coastal Engineering Proceedings. pp. 419–432. https://doi.org/10.1061/9780872620490.024

Weissman, J.C., Tillett, D.M., Goebel, R.P., 1989. Design and operation of an outdoor microalgae test facility. Microbial Products, Inc., Vacaville, CA (USA), Golden, CO. https://doi.org/10.2172/7024835

White, F., 2015. Open-Channel Flow, in: Fluid Mechanics. Mcgraw-Hill Education, pp. 701–756.

Wiltshire, K., Boersma, M., Meyer, B., 2003. Grazer-induced changes in the desmid Staurastrum. Hydrobiologia 491, 255–260. https://doi.org/10.1023/A:1024474827107

Wood, I.R., 2018. Free Surface Air Entrainment on Spillways, in: Air Entrainment in Free-Surface Flows. A.A. Balkema, pp. 55–84. https://doi.org/10.1201/9781315137049

Wu, S., Rajaratnam, N., 1996. Submerged Flow Regimes of Rectangular Sharp-Crested Weirs. J. Hydraul. Eng. 122, 412–414. https://doi.org/10.1061/(ASCE)0733-9429(1996)122:7(412)

Yang, S.-Q., Tan, S.K., Wang, X.-K., 2012. Mechanism of secondary currents in open channel flows. J. Geophys. Res. Earth Surf. 117, n/a-n/a. https://doi.org/10.1029/2012JF002510

Yang, Z., Cheng, J., Li, K., Zhou, J., Cen, K., 2016. Optimizing gas transfer to improve growth rate of Haematococcus pluvialis in a raceway pond with chute and oscillating baffles. Bioresour. Technol. 214, 276–283. https://doi.org/10.1016/j.biortech.2016.04.107

Zeebe, R.E., Wolf-Gladrow, D., 2001. CO2 in Seawater: Equilibrium, Kinetics, Isotopes, Volume 65 1st Edition. Elsevier Science.

Zhang, Q., Xue, S., Yan, C., Wu, X., Wen, S., Cong, W., 2015. Installation of flow deflectors and wing baffles to reduce dead zone and enhance flashing light effect in an open raceway pond. Bioresour. Technol. 198, 150–156. https://doi.org/10.1016/j.biortech.2015.08.144

Zhang, T.Y., Hu, H.Y., Wu, Y.H., Zhuang, L.L., Xu, X.Q., Wang, X.X., Dao, G.H., 2016. Promising solutions to solve the bottlenecks in the large-scale cultivation of microalgae for biomass/bioenergy production. Renew. Sustain. Energy Rev. 60, 1602–1614. https://doi.org/10.1016/j.rser.2016.02.008

Zheng, Q., Xu, X., Martin, G.J.O., Kentish, S.E., 2018. Critical review of strategies for CO2 delivery to large-scale microalgae cultures. Chinese J. Chem. Eng. 26, 2219–2228. https://doi.org/10.1016/J.CJCHE.2018.07.013

Appendix A:

A.1 Summary of references to online dataset

All relevant data and calculations can be found in the linked datasets on Zivahub (https://figshare.com/s/00ec7e5192c6be962de8). Four data sets are documented, named Raceway 1, Raceway 2, Raceway 3 and Raceway 4, respectively. Table A-1 below gives a consolidated list of the specific references to calculations that was made throughout this thesis.

Table A-1: Summary of the references to the datasets used throughout this thesis

Page	Description	ZivaHub Dataset
11	Empirical equations used to calculate the equilibrium constants in Equation 2-16 - Equation 2-19	Raceway 2
17	Error propagation performed on the k_La data of Burke (2016)	Raceway 2
39	Excel sheet used to model conductivity data through Equation 3-2 to determine the Peclet number	Raceway 1
40	Scilab code used to calculate k_La	Raceway 2
42	Validation of the empirical curves created by Shukry (1950) to calculate the bend loss coefficient in open channels	Raceway 2
42	Sample calculation to determine the bend loss coefficient for a system with a slope in the channel (20 cm slope)	Raceway 2
43	Calculating the error in the theoretical energy demand through error prorogation from the error in circulation time and fluid depth	Raceway 2
44	Scilab code used to iteratively solve the Colebrook-White formula and estimate the error in the friction coefficient	Raceway 2
45	Details of the light intensity throughout the raceway pond	Raceway 4
56	Calculating the wave length of the pulse created by the paddlewheel	Raceway 1
56	Calculating the depth at which the wave will break based on Equation 2-22 and Equation 2-23	Raceway 1
57	Calculating the desired slope angle for Slope PW based on the Iribarren number	Raceway 1
59	Calculations to show the mixing time and k_La when the control is operated at the same energy expenditure as with Slope PW	Raceway 2
61	Calculating the relationship between motor frequency and paddlewheel RPM for each configuration	Raceway 1
72	Inverse relation between the mixing time and dispersion coefficient	Raceway 1
84	Comparison in the hydrodynamics between the two raceways used for the cultivation experiments	Raceway 1
84	Calculations showing that no statistically significant differences were found between the two raceways	Raceway 1
88	Comparison between measuring the productivity up to the drop in pH or up to a concentration of 0.6 g L^{-1}	Raceway 4
89	Microscope images of the protozoan flagellate observed in one of the cultivation runs	Raceway 4

A.2 Framework for propeller system

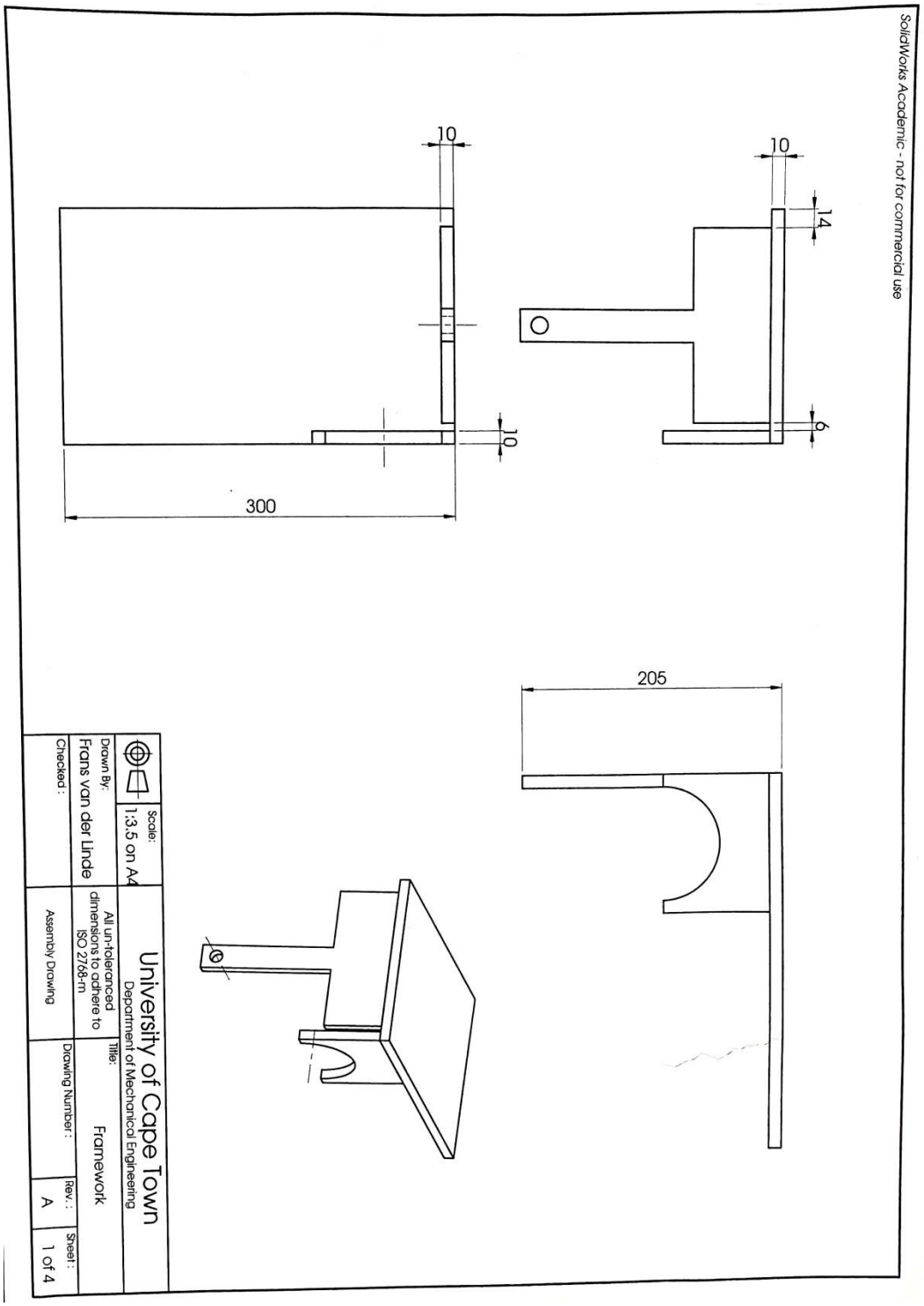

Figure A-1: SolidWorks drawing of the propeller framework design